ROBUST THERMAL ERROR MODELING AND COMPENSATION FOR CNC MACHINE TOOLS

by

Jie Zhu

A dissertation submitted in partial fulfillment
of the requirements for the degree of
Doctor of Philosophy
(Mechanical Engineering)
in The University Of Michigan
2008

Doctoral Committee:

Professor Jun Ni, Co-Chair
Professor Albert J. Shih, Co-Chair
Professor S. Jack Hu
Professor Nickolas Vlahopoulos
Associate Research Scientist Reuven R. Katz

To my family

ACKNOWLEDGEMENTS

I have learned many things since I began my journey toward my Doctoral degree; some things I realized early while other things I have only recently come to understand. Among the most important things I have learned along my journey are persistence, humbleness and diligence. I would not have been able to make any of these advancements without the help of many individuals, to whom I am deeply indebted and with whom I am very grateful.

I would like to express my most sincere gratitude to my advisor, Professor Jun Ni, for his continuous support, guidance and encouragement throughout my graduate study. Without him, I would never have had the chance to begin, continue, or complete my research. I also appreciate the invaluable assistance provided by Professor Albert J. Shih, who has taught me how to be a better researcher and helped me to cope with the difficulties I have encountered during my research.

I am grateful to Professor Nickolas Vlahopoulos for devoting his precious time to reviewing this dissertation and providing me with detailed and useful feedback. Finally, I want to thank Professor S. Jack Hu and Dr. Reuven Katz for agreeing to join my committee in lieu of the unexpected absence of some of my original committee members. Additionally, I am indebted to Professor Hu for helping me to gain valuable experience as a teaching assistant.

TABLE OF CONTENTS

DEDICATION ..... **ii**
ACKNOWLEDGEMENTS ..... **iii**
LIST OF TABLES ..... **vii**
LIST OF FIGURES ..... **viii**
LIST OF APPENDICES ..... **xii**

CHAPTER 1 INTRODUCTION **1**
1.1 Problem Statement 1
1.2 Research Objectives 3
1.3 Dissertation Outline 4

CHAPTER 2 LITERATURE REVIEW **6**
2.1 Basic Machine Tool Error Reduction 6
2.1.1 Error Sources 6
2.1.2 Error Reduction Methods 7
2.2 Geometric Error Compensation 8
2.2.1 Kinematic Error Synthesis Model 9
2.2.2 Geometric Error Calibration 10
2.2.3 Error Compensation Algorithm 14
2.3 Thermal Error Compensation 15
2.3.1 Thermal Error Identification 17
2.3.2 Thermal Error Modeling 19
2.3.3 Temperature Sensor Placement 22

CHAPTER 3 ROBUST MACHINE TOOL THERMAL ERROR MODELING THROUGH THERMAL MODAL ANALYSIS 24

3.1 Introduction 24

3.2 Thermal Modal Analysis 27

3.2.1 Thermal Modes 27

3.2.2 Mode Truncation 30

3.3 Robust Thermal Error Modeling 31

3.3.1 Temperature Sensor Placement 31

3.3.2 Thermal Error Modeling 32

3.4 Numerical Simulation for Simple Thermal Deformation Shapes 33

3.4.1 Temperature Sensor Placement Based on Thermal Modal Analysis 35

3.4.2 Comparison of Temperature Sensor Placement Schemes 39

3.4.3 Thermal Error Modeling and Robustness Verification 42

3.5 Experimental Validation 48

3.6 Summary 52

CHAPTER 4 THERMAL ERROR COMPENSATION STRATEGY BASED ON THERMAL LOOP ANALYSIS 53

4.1 Introduction 53

4.2 Thermal Loop Analysis 55

4.2.1 Framework of Thermal Loop Analysis 58

4.2.2 Structural Loop and Thermal Loop 59

4.2.3 Thermal Loop Decomposition and Modeling 61

4.3 Numerical Illustration 63

4.4 Experimental Verification 70

4.4.1 Thermal Loop Decomposition 70

4.4.2 Thermal Modal Analysis for Each Thermal Link 73

4.4.3 Thermal Loop Reassembly 85

4.5 Summary 88

CHAPTER 5 ASSESSMENT OF ROTARY AXIS GEOMETRIC ERRORS BY USING TELESCOPIC MAGNETIC BALL BAR 89
5.1 Introduction 89
5.2 Rotary Axis Calibration Strategy 93
5.2.1 Algorithm Derivation 93
5.2.2 Estimation Methods 101
5.3 Numerical Simulation 101
5.3.1 Sensitivity Analysis of R_x 103
5.3.2 Sensitivity Analysis of Dimensional Variations 105
5.4.3 Classification of Error Patterns 106
5.4 Experimental Demonstration 110
5.5 Summary 113

CHAPTER 6 CONCLUSIONS AND FUTURE WORK 114
6.1 Conclusions 114
6.2 Recommendations for Future Work 116

APPENDICES 118
BIBLIOGRAPHY 152

LIST OF TABLES

Table 3.1 Parameters and material properties of simplified machine elements. 35
Table 4.1 The HTMs for the numerical illustration of the thermal loop analysis. 65
Table 4.2 Thermal deformation parameters for each thermal link. 67
Table 4.3 Parameters of normal distribution for residual errors. 87
Table 5.1 Accuracy specifications of the rotary table..... 102
Table 5.2 Error component estimation results. 111
Table 5.3 Comparison of the estimation results by using l_2 and l_∞ norm methods..... 112

LIST OF FIGURES

Figure 3.1 Basic thermal deformation shapes. (a) Thermal elongation and (b) thermal bending. 34

Figure 3.2 First four thermal modes with temperature fields and time constants for the thermal elongation. (a) Mode I, (b) Mode II, (c) Mode III, and (d) Mode IV. 36

Figure 3.3 First four thermal modes with temperature fields and time constants for the thermal bending. (a) Mode I, (b) Mode II, (c) Mode III, and (d) Mode IV. 37

Figure 3.4 Time constant and weight distribution for the thermal elongation. (a) Time constant and (b) weight distribution. 38

Figure 3.5 Time constant and weight distribution for the thermal bending. (a) Time constant and (b) weight distribution. 38

Figure 3.6 Temperature sensor placements. (a) Thermal elongation and (b) thermal bending. 39

Figure 3.7 Temperature sensor placement schemes comparison. (a) Thermal elongation and (b) thermal bending. 42

Figure 3.8 Heat flux input for numerical simulation. 43

Figure 3.9 Thermal error modeling results for the thermal expansion of (a) the thermal elongation and (b) the thermal bending. 43

Figure 3.10 Thermal error modeling results for (a) the thermal deflection and (b) the slope angle of the thermal bending. 44

Figure 3.11 Extrapolation examination of the thermal error model for the expansion of the thermal elongation. 45

Figure 3.12 Extrapolation examination of the thermal error model for the expansion of the thermal expansion. 45

Figure 3.13 Extrapolation examination of the thermal error model for (a) the deflection and (b) the slope angle of the thermal bending. 46

Figure 3.14 Heat flux input for frequency sensitivity examination. (a) T = 20 min, (b) T = 40 min, and (c) T = 10 min. 46

Figure 3.15 Frequency sensitivity examination for the thermal elongation. (a) T = 20 min, (b) T = 40 min, and (c) T = 10 min. 47

Figure 3.16 Frequency sensitivity examination for the thermal bending. (a) T = 20 min, (b) T = 40 min, and (c) T = 10 min. 47

Figure 3.17 Experimental setup for spindle thermal expansion test. 48
Figure 3.18 Experiment results of Test 1. (a) Spindle speed, (b) temperature variations. 49
Figure 3.19 Measured and modeled results of the spindle experiment..... 49
Figure 3.20 Spindle speed, measured and predicted thermal errors for robustness verification. (a) Test 2 and (b) Test 3. 50
Figure 3.21 Temperature variations after each test. (a) Test 1, (b) Test 2, and (c) Test 3. 51
Figure 3.22 Weight distributions of the first three temperature modes. (a) Sensor 1, (b) Sensor 2, and (c) Sensor 3..... 52
Figure 4.1 Framework of the thermal loop analysis 58
Figure 4.2 Representative structural loops. (a) Open frame and (b) closed frame. 60
Figure 4.3 Representative thermal links with thermal deformation and HTMs. (a) Thermal elongation and (b) thermal bending..... 61
Figure 4.4 Schematic 2D layout of the reconfigurable machine tool. (a) Nominal configuration: 0 Deg, (b) reconfiguration 1: –10 Deg, and (c) reconfiguration 2: 10 Deg. 64
Figure 4.5 Thermal loop analysis for the machine tool in the numerical illustration. 65
Figure 4.6 Thermal deformations of thermal links. (a) Link 0, (b) link 1, (c) link 2, and (d) Link 3. 66
Figure 4.7 Thermal errors of the moving axis. (a) X-axis and (b) Y-axis. 68
Figure 4.8 Volumetric errors within the working space for the nominal configuration. .. 69
Figure 4.9 Volumetric errors within the working space for the reconfigurable configurations. (a) Reconfiguration 1: –10 Deg, and (b) reconfiguration 2: 10 Deg. 69
Figure 4.10 CAD model of Sodick AQ55L EDM machine (Courtesy of Sodick Inc.). ... 71
Figure 4.11 Disassembly of Sodick AQ55L EDM machine..... 72
Figure 4.12 Weight distributions of thermal modes for the *Z*-axis unit (thermal link 3). 74
Figure 4.13 Temperature field distribution of dominant thermal modes for the *Z*-axis unit (thermal link 3). (a) Mode 1, (b) Mode 3, and (c) Mode 4. 74
Figure 4.14 Weight distributions of thermal modes for the *X*-axis unit (thermal link 2). 75
Figure 4.15 Temperature field distribution of dominant thermal modes for the *X*-axis unit (thermal link 2). (a) Mode 1, (b) Mode 2, and (c) Mode 5. 75
Figure 4.16 Weight distributions of thermal modes for the *Y*-axis unit (thermal link 1). 76
Figure 4.17 Temperature field distribution of dominant thermal modes for the *Y*-axis unit (thermal link 1). (a) Mode 1, (b) Mode 2, and (c) Mode 4. 76
Figure 4.18 Weight distribution of thermal modes for the Base unit (thermal link 0). 77

Figure 4.19 Temperature field distribution of dominant thermal modes for the Base unit (thermal link 0). (a) Mode 1, (b) Mode 4, and (c) Mode 6. 77

Figure 4.20 Temperature sensor placement scheme for Sodick AQ55L EDM machine.. 78

Figure 4.21 Geometrie and thermal errors of *Z*-axis unit. (a) Geometric and thermal errors and (b) Geometric errors..... 80

Figure 4.22 Thermal error model training I for *Z*-axis unit. (a) Thermal error model, (b) residual errors, and (c) temperature vairations. 80

Figure 4.23 Thermal error model training II for *Z*-axis unit. (a) Thermal error model, (b) residual errors, and (c) temperature vairations. 81

Figure 4.24 Geometrie and thermal errors of *X*-axis unit. (a) Geometric and thermal errors and (b) Geometric errors..... 82

Figure 4.25 Thermal error model training for *X*-axis unit. (a) Thermal error model, (b) residual errors, and (c) temperature vairations. 82

Figure 4.26 Geometrie and thermal errors of *Y*-axis unit. (a) Geometric and thermal errors and (b) Geometric errors..... 83

Figure 4.27 Thermal error model training for *Y*-axis unit. (a) Thermal error model, (b) residual errors, and (c) temperature vairations. 83

Figure 4.28 Modeling and measurement of linear positioning accuracy along *XY*-plane face diagonal. (a) Error modeling and verification, (b) temperature variation for *X*-axis, and (c) temperature variation for *Y*-axis. 85

Figure 4.29 Modeling and measurement of linear positioning accuracy along body diagonal. (a) Error modeling and verification, (b) temperature variation for *X*-axis, (c) temperature variation for *Y*-axis, and (d) temperature variation for *Z*-axis. 86

Figure 4.30 Histograms of linear positioning accuracy for (a) face diagonal before compensation (b) face diagonal after compensation, (c) body diagonal before compensation, and (d) body diagonal after compensation..... 87

Figure 5.1 Error components induced by the rotational motion. 94

Figure 5.2 Schematic setup for rotary table calibration. 94

Figure 5.3 Modified rotary axis calibration setups. 99

Figure 5.4 Rotary table to be calibrated (Courtesy of Aerotech. Inc.)..... 102

Figure 5.5 Socket with known dimensions for the calibration setup. 103

Figure 5.6 Sensitivity analysis of R_x. 104

Figure 5.7 Sensitivity analysis of dimensional variation of setup parameters..... 105

Figure 5.8 Error patterns of error components D_x and D_y. (a) Positive D_x and D_y and (b) negative D_x and D_y. 107

Figure 5.9 Error patterns of error components D_z. (a) Positive D_z and (b) negative D_z. 107

Figure 5.10 Error patterns of error components E_x and E_y. (a) Positive E_x and E_y and (b) negative E_x and E_y. 108

Figure 5.11 Error patterns of error components H_x and H_y. (a) Positive H_x and positive H_y, (b) positive H_x and negative H_y, (c) negative H_x and positive H_y, and (d) negative H_x and negative H_y. 109

Figure 5.12 Polar plots of the collected data for two calibration setups with (a) short TMBB and (b) long TMBB. 111

Figure 5.13 Plots of residual errors by using (a) l_2 and (b) l_∞ norm methods. 112

LIST OF APPENDICES

A Kinematic Error Synthesis Modeling..... 119
B Machine Tool Error Budget and Its Application..... 124
C Five-Axis Machine Tool Classification 144
D Temperature Sensor Locations for the Sodick AQ55L EDM Machine..... 150

CHAPTER 1

INTRODUCTION

1.1 Problem Statement

Machine tools with three translational axes have shown the ability to fabricate a large variety of products with relatively simple geometry to a satisfactory accuracy. However, thermal errors are still one of the main factors affecting the machine accuracy. In addition, in order to machine workpieces with complex shapes, such as impeller blades, engine blocks, etc, five-axis machine tools are preferred due to the excellence of simultaneously positioning and orienting the tool with respect to the workpiece. Nevertheless, current five-axis machine tools still cannot provide the same consistency and accuracy as their three-axis counterparts. This, aside from the cost, prevents the wider acceptance and utilization of five-axis machine tools despite many superior characteristics.

Major barriers hindering the development and practical implementation of five-axis precision machining specifically include:

(1) Inaccurate and non-robust prediction model for thermal errors. Thermal errors have become the major contributor to the inaccuracy of machine tools. Time-variant thermal errors are more elusive to model than geometric errors. The robustness of the thermal error model under various working conditions depends on the thoroughness of

the training process and the length of characterization time. A model estimated under one working condition may not be applicable under other working conditions.

(2) Insufficient pragmatic application of thermal error compensation on five-axis machine tools. Optimal sensor location determination, thermal deformation mode analysis and dynamic thermal error model derivation have been developed and demonstrated for machine components and simple machine tools. But there is still no significant breakthrough for production machines with complicated structures due to the lack of a generalized thermal error compensation strategy, which is more than a merely concept-proving method. In addition, thermal error compensation of five-axis machine tools is usually circumvented because of the intricate algorithms.

(3) Lack of systematic analysis and methodological study on five-axis machine tools from the accuracy perspective. Introduction of rotary axes fundamentally alters the machine's kinematic structure, thus limiting the application of analytical methods developed for three-axis machines to five-axis machine tools. The overall accuracy is determined by the interaction of a number of error terms in the kinematic chain of a five-axis machine. But the influence of the major components is still difficult to reveal.

(4) Inadequate error identification and calibration approaches. There is still no efficient calibration method to identify the complete error components due to inherent structure imperfection and relative movements of a five-axis machine tool. Traditional laser interferometer or ball bar system has been proved to be competent for linear axis calibration, but the existing algorithms do not work efficiently for rotary axes. Such error components as squareness errors between the linear axes and parallelism errors between linear and rotary axes are even more challenging.

It is worth noting that the issues of five-axis machine tools are not a straight extension from the three-axis machine areas. With the introduction of rotary axes, orientations of the tools become as important as tool positions, which are not considered for three-axis machines. Besides, mutual interaction between the five axes is totally different from independent movement of traditional machines with three orthogonal linear axes. Lastly, numerical calculation complexity significantly increases for tool path generation, post-processing, compensation algorithm development, and so on in five-axis machining.

1.2 Research Objectives

The objective of this research is to develop a systematic methodology to improve the accuracy of five-axis machine tools from design, testing until practical application stages. To achieve the ultimate research goal, the following tasks are proposed:

(1) To apply the innovative thermal modal analysis. Thermal modal analysis is exploited for the temperature sensor placement strategy and thermal error modeling. Finite element analysis (FEA) is utilized to examine the essence of thermal process of machine tool elements. Numerical simulation and practical experiments are carried out to illustrate the existence and feasibility of the thermal modal analysis in reality.

(2) To propose the thermal loop analysis. A machine tool is decomposed into several thermal links, which are separately analyzed based on the thermal modal analysis, along the thermal loop. The overall thermal errors are obtained through vectorial summation. This methodology associated with the thermal modal analysis constructs an innovate framework, facilitating the application of thermal error compensation to various machine

tools.

(3) To develop an efficient rotary axis calibration and compensation methodology. Error components induced by rotational motion can be identified by an inverse kinematic analysis. The formulation and mathematical rationale behind this method is investigated. Effective geometric error calibration algorithm is derived to improve the positioning accuracy of a five-axis machine tool.

The major contributions of this research include the practical application of thermal modal analysis to machine tool elements, the development of an innovative thermal loop, the proposal of a generalized thermal error compensation framework and the identification and measurement of geometric error components of rotary axis for five-axis machine tools.

1.3 Dissertation Outline

This dissertation contains six Chapters. Chapter 2 is the literature review of machine tool error compensation techniques. The basic steps and procedures of error compensation methods are summarized. The existing geometric and thermal error compensation approaches are surveyed and compared in details.

In Chapter 3, the innovative thermal modal analysis is revisited and modified for the practical application. The essence of thermal deformation process of machine tools is revealed by the thermal modal analysis. Hence, the number of temperature sensors could be well controlled, and the locations be appropriately decided. Thermal error models thus derived are insensitive to the training conditions.

Chapter 4 attempts to present a thermal loop analysis for the further enhancement the thermal error compensation results associated with the thermal modal analysis of

machine tool elements. A complete methodology of the thermal loop analysis, including the identification of thermal loops, decomposition and recombination of machine tools, and the prediction of overall thermal errors based on the thermal error model of each thermal link will be developed.

Chapter 5 is devoted to the development of the calibration approach for rotary axis through the inverse kinematics analysis. The error components induced by the movement of rotary axis will be measured by using a telescopic magnetic ball bar. Based on the calibration results, geometric error compensation could be implemented on five-axis machine tools to substantially improve the machining accuracy.

Chapter 6 summarizes the research work and provides recommendations for future work.

CHAPTER 2

LITERATURE REVIEW

2.1 Basic Machine Tool Error Reduction

2.1.1 Error Sources

Machined part accuracy is essentially determined by machine tool performance from the point of view of compliance to tolerance, surface definition, etc. Accuracy is one of the most important performance measures, the ability to control errors to optimize performance while maintaining cost is crucial in the machine tool industry.

In general, there are two basic categories of errors, quasi-static errors and dynamic errors. Quasi-static errors are errors in the machine, fixturing, tooling, and workpiece that occur relatively slowly (Slocum, 1992). Sources of this type of errors include geometric errors, kinematic errors, thermal errors, cutting force induced errors, etc. Geometric errors are defined as errors in the form of individual machine components. Kinematic errors are caused by misaligned components in the trajectory. Thermal errors are induced by thermo-elastic deformations due to internal and external heat sources of a machine tool. As heat generation at contact points is unavoidable, thermal errors are one of the most difficult error sources to completely eliminate.

Dynamic errors are, on the other hand, primarily caused by structural vibration, spindle error motion, controller errors, etc. They are more dependent on the particular

operating conditions of the machine. Overall, quasi-static errors account for about 70 percent of the total errors of a machine (Bryan, 1990).

2.1.2 Error Reduction Methods

Error avoidance and error compensation are the two basic approaches to improve the machine tool accuracy (Ni, 1997). The general approach to apply error avoidance is to build an accurate machine during its design and manufacturing stage so that the error sources could be kept to a minimum extent. Good rules of thumb such as reasonable assignment of stiffness, proper addition of damping, careful selection of materials, symmetrical structure design, and the like are extensively adopted. Error avoidance by the refinement of a machine from its basic structure or the control of working environment is generally accepted as the most desirable way to eliminate errors. This approach, however, has two inevitable drawbacks. On the one hand, it is impossible to eliminate all the errors solely by design and manufacturing techniques; on the other hand, the machining costs rise exponentially as the level of precision requirement is tightened.

Unlike error avoidance, no attempts are made to avoid errors for error compensation. Rather, errors are allowed to manifest themselves, and then be measured and corrected. As the accuracy of a machine tool is affected by various error sources, error compensation places more emphasis on the interactive impact rather than individual errors. The basic idea of error compensation does not aim at reducing the absolute value of errors, but the effects of these errors on the machining accuracy and final dimensions of produced parts. Error compensation gains its importance because design and operating specifications are either difficult to realize or subtly contradictory to each other.

Moreover, compensation is considered as an efficient method for periodic machine accuracy enhancement during the machine utilization over the years.

Nevertheless, there also exist limitations in error compensation techniques. The degree to which machining accuracy can be achieved by error compensation is highly dependent on the repeatability of the machine itself and the method selected to demonstrate the interconnection between different errors. The former is closely related to the design and fabrication of the machine, in other words, error avoidance approach sets the bottom line of the performance improvement that can be obtained through error compensation. The latter highly depends on the insight into the influences of errors on the machining accuracy, which could not be easily embraced in mathematical models.

2.2 Geometric Error Compensation

Geometric errors (Ramesh et al., 2000a) are extant in a machine on account of its basic design, the inaccuracies built-in during assembly and as a result of the components used on the machine. These factors affecting geometric errors include surface straightness, surface roundness, bearing preload, etc. Geometric errors have various components like linear positioning error, straightness and flatness of movement of the axis, backlash error, etc. Geometric errors are especially significant with medium-size and large-size machine tools where rigid machine structures are difficult to achieve. Kinematic errors are mainly concerned with the relative motion errors of several moving machine components that need to move in accordance with precise functional requirements. These errors are particularly significant during the combined motion of different axes. Kinematic errors include squareness and parallelism of axes with respect

to their ideal locations between each other. Literally, kinematic errors in a well-designed and manufactured machine should be very repeatable.

Compensation for geometric and kinematic errors has been widely realized in machine tools and coordinate measuring machines (CMMs) to effectively improve the machine tool accuracy (Zhang et al., 1985; Donmez et al., 1986; Belforte et al., 1987; Duffie and Malmberg, 1987; Balsamo et al., 1990; Chen et al., 1993; Lo et al., 1995; Mou et al., 1995a and 1996b; Weck et al., 1995; Chen and Ling, 1996; Barakat et al., 2000; Wang et al., 2002; Harris and Spence, 2004; Raksir and Parnichkun, 2004; Choi et al., 2004). In spite of the vast amount of literature reported on the error compensation techniques, the underlying approaches are basically similar. Kinematic error modeling, error measurement and calibration, and error compensation methods are the three basic building blocks.

2.2.1 Kinematic Error Synthesis Model

The development of kinematic models based on the machine structure is one of the key steps for an efficient error compensation strategy. Investigators have addressed the error modeling problem from different perspectives. Early researchers utilized trigonometric relationships (Leete, 1961) and vector chain representation (Schultschik, 1977) to model kinematic errors. Currently, homogeneous transformation matrix (HTM) based error synthesis method (Hocken et al., 1977) has been widely recognized and employed to build kinematic error models since it easily accommodates various error components. Rigid body kinematics and small angle approximation are two basic assumptions (Ferreira and Liu, 1986). Denavit-Hartenberg (D-H) convention (Denavit

and Hartenberg, 1954), first introduced to describe the robotic configuration, is another commonly used method to derive kinematic models (Paul, 1981). Derivations of kinematic error models for five-axis machine tools have also been conducted and reported (Kim and Kim, 1991; Soons et al., 1992; Lin and Ehmann, 1993; Kiridena and Ferreira, 1993; Srivastava et al., 1995). The inclusion of two rotary axes brings additional orientation errors besides the positioning errors of the existing three linear axes, and motivates new calibration methods for the measurement of rotation induced errors.

2.2.2 Geometric Error Calibration

Calibration is the process of establishing the relationship between a measuring device and the units of measure. This is done by comparing a devise or the output of an instrument to a standard having known measurement characteristics. The national standard, ASME B5.54-1992, provides procedures for the performance evaluation of CNC machining centers by using different kinds of instruments, such as laser interferometers, electronic levels, capacitance gages, etc. In addition, it facilitates performance comparison between machines under specified environmental requirements.

Error calibration methods can be categorized into direct and indirect methods (Ramesh et al., 2000a). The direct error measurement is performed by measuring and modeling each error component independently. The indirect error estimation is realized by measuring volumetric errors or produced part dimensions with some type of artifacts or reference standards and estimating error components based on inverse kinematics. The direct method requires familiarity with measurement equipment and operator

expertise, while the indirect method needs complex mathematical derivation, but much simpler devices for data acquisition.

Direct Calibration Method

The advantage of using the direct method is that it gives direct evidence of mechanical accuracy of a machine tool or its axis. Each error component is measured by conventional equipment such as laser interferometer, autocollimator or electronic level.

Weck and Bibring (1984) comparatively described the calibration instruments and algorithms used to measure geometric error components for three-axis machine tools at that time. Sartori and Zhang (1995) also summarized the available equipment and approaches as a benchmark. Most methods therein were intended to measure single error component of a moving axis at a time. Because of this, it is very tedious and laborious to calibrate a machine.

To simplify the calibration procedures, Zhang et al. (1988) developed an approach to measure the overall 21 error components of a three-axis machine by measuring the linear displacement errors along 22 lines within the working space. Chen et al. (2001) improved this method by reducing the number of measurement lines to 15. Laser vector measurement is another efficient calibration technique. Wang (2000) and Janeczko et al. (2000) proposed this approach for the measurement of the volumetric positioning errors of a machine tool. This method is able to measure the linear displacement errors and straightness errors simultaneously, rather than once an error component by using laser interferometer. However, the limitations and constraints of vector or sequential diagonal methods were pointed out by Chapman (2003). To justify the laser vector measurement

technique, Svoboda (2006) conducted a series of tests and concluded that this method does not work properly if the magnitude of the linear displacement error is large.

On-line geometric error calibration is also proposed and implemented by many researchers. Ni et al. (1991) developed a multi-degree-of-freedom measuring (MDFM) system for CMM geometric errors. Based on the MDFM system, Ni and Wu (1993) presented a hybrid on-line and off-line measurement technique for volumetric error compensation. When implemented on a 3-axis machine, up to 15 geometric error components were measured simultaneously on-line and the remaining 6 components needed to be calibrated off-line. Huang and Ni (1995) utilized three MDFM systems, one for each moving axis of a CMM, to develop an on-line error compensation algorithm. Mico et al. (2005) proposed an on-line measurement system in the mechanization process of a designed machine tool for high-speed machining applications. The measurement system was based on the integration and optimization of the Michelson-Morley interferometer configuration. Spindle probes (Pahk et al., 1996; Choi et al., 2004; Kwon et al., 2006; Cho et al., 2006) are extensively employed to enhance the machined part accuracy as well. The machining process is iteratively intercepted for on-machine measurement, and the measurement results are thus exploited to predict the geometric errors. Lim et al. (2007) developed an on-machine optical measurement device based on non-contact optical method.

Some other instruments were also proposed for error calibration. Umetsu et al. (2005) utilized a laser tracking system to calibrate a CMM. Chen et al. (1999) presented an auto-alignment laser interferometer system for the measurement of geometric errors.

Indirect Calibration Method

Indirect calibration method uses artifacts or ball bars to estimate geometric errors of machine tools and CMMs. Generally speaking, error components are not directly measured, but computed through inverse kinematics analysis or other mathematical relationship between the measured errors and error components. Indirect calibration method usually requires more derivations and calculation, and the calibration accuracy is not as high as the direct calibration method.

Artifacts, as a standard reference with known dimensions, are employed to obtain the geometric errors on the basis of comparison. Zhang and Zang (1991) used a 1-D array ball to measure the machine geometric errors. Kruth et al. (1994) proposed a squareness error measurement method by using a single properly sized artifact. Mou et al. (1995a and 1995b) proposed an adaptive error correction method using a feature-based analysis technique. The information from pre-process characterization, process-intermittent gauging, and post-process inspection were integrated to automatically improve machine performance. Chen and Ling (1996) used artifacts to model the positioning and contouring errors. Balsamo et al. (1997) reviewed the use of ball plate based techniques for CMM parametric errors determination and concluded that the low cost, ease to use and the insensitivity to pre-existing error compensation schemes are the main advantages of the ball pate. Zhang and Fu (2000) utilized a grid plate to calibrate an optical CMM with a pre-calibrated axis. Barakat et al. (2000) proposed a calibration method by measuring a commercial ring gauge in a structured lattice in the work volume of a CMM. De Aquino Silva and Burdekin (2002) presented a space frame of tetrahedral form for the rapid performance assessment of CMMs.

The application of ball bars to measure geometric errors is basically through a circular test. Bryan (1982a and 1982b) designed the magnetic ball bars and developed the principles and operations to collect the positioning errors. This technique gives rapid and precise indications of the two or three dimensional accuracy of a machine. Knapp (1983) developed a circular test to evaluate the geometric accuracy of three-axis machines. Kunzmann and Waldele (1983) used a fixed ball bar to estimate the linear displacement errors and squareness error of a CMM. The impact of those error sources on the positioning errors of the CMM was formulated and estimated. Kakino et al. (1987) measured the motion errors of NC machine tools and diagnosed of their origins by using the telescopic magnetic ball bar. By detecting the relative distance between the two balls, the motion errors during circular interpolation motion were measured. Suh and Lee (2000) obtained the machine errors by using a ball bar in a contouring test and incorporated the results in the CAM to optimize the tool path accuracy. Overall speaking, the calibration methods by using ball bars allow the measurement of numerous quasi-static and dynamic parameters through circular tests, and thus have been extensively used for the accuracy inspection of three-axis machine tools (Kakino et al., 1993).

2.2.3 Error Compensation Algorithm

In order to realize the error compensation technique in the machine tools and CMMs, the tool end position along the trajectory must be continuously adjusted by additional compensatory values in machine control cycles. Encoder feedback signal interception and origin shift method are the two common approaches (Ni, 1997).

Encoder feedback signals can be intercepted by an external computer for real-time

error compensation. The computer calculates the volumetric error of a machine and inserts or removes the equivalent number of pulses of the quadrature signals. The servo system will therefore adjust the positions of the moving slides in real-time. The advantage of this technique is that it requires no extra module of CNC controller software. It can be applied to any CNC machine, including some old types of CNC machines, with position feedback of machine axes. However, specially developed electronic devices are needed to insert quadrature signals into the servo loops. These insertions are sometimes very tricky and require extreme caution in such a way that they do not interfere with the feedback signals of a machine.

Another way to compensate for errors in real-time is the origin shift method. In this method, the amounts by which the machine axes need to be moved to compensate for the errors are sent to the CNC controller to shift the reference origins of the control system through an I/O interface, and then added to the command signals for the servo loop automatically. To achieve real-time error compensation effectively in the commercial application, all error origins have to be addressed in a timely fashion.

2.3 Thermal Error Compensation

The thermal error is one of the most significant factors influencing the machine tool accuracy (Bryan, 1990). With the improvement of machine tool positioning accuracy and machining performances, thermal errors become even more significant.

Most machine tools are unavoidably subject to continuously varying operating conditions. The internally generated heat and environment temperature gradient render the machine tool exposed to complex and changing temperature distributions. As

mentioned by Bryan (1990), there are six main thermal error sources: (1) heat generated from the cutting process, (2) by the machine energy loss, (3) hydraulic oil, coolant, and cooling systems, (4) room environment, (5) people, and (6) thermal memory from previous environment. The thermal deformation errors thus caused are even more difficult to quantify and predict if the complicated structure of a machine tool is taken into account.

Thermal errors can be divided into two categories, position independent thermal errors (PITE) and position dependent thermal errors (PDTE) (Chen et al., 1993). PITE change as a function of temperature but not the axis position. The effect of PITE on component accuracy is strongly dependent on the rate of change of the PITE relative to the time taken to produce a part. PDTE change as a function of axis position as well as temperature. They effectively alter the linear positioning of the machine. To simplify the problem and determine the most suitable thermal error compensation techniques, it is useful to differentiate these two kinds of thermal errors.

Researchers have been investigating the influences of thermal errors on the machine tool accuracy and seeking solutions to reduce these errors for decades. Special approaches pertaining to the thermal error avoidance include: (1) reducing and relocating heat sources (Donaldson and Thompson, 1986), (2) rearranging the machine tool structure to achieve thermal robustness (Spur et al., 1988), and (3) using materials that have strong thermal stiffness (Suh and Lee, 2004). Controlling the environmental temperature is also helpful in reducing thermal errors, because daily environment temperature fluctuation is one of the major heat disturbances. For the implementation of thermal error compensation, besides the common approach of moving machine slides

through sending compensatory signals to CNC controller, artificially controlled heat sources on machine tool structures are employed to offset the thermal bending effects, thus eliminating the thermal errors (Sata et al., 1975; Hatamura et al., 1993; Fraser et al., 1999c).

2.3.1 Thermal Error Identification

Thermal error identification is one of the crucial steps for a successful thermal error modeling and compensation. There are two basic error identification categories: workspace measurement approach and error synthesis approach (Yang, 2002).

In workspace measurement approach, the required compensation values are determined by making direct measurements of the thermal errors between the tool tip and workpiece during machining (Yandayan and Burdekin, 1997). Normal machining process is usually stopped and a probe is used to measure a datum or reference point on the machine; error maps are then generated associated with different machine temperature status and axis positions.

Chen (1996b) developed a quick setup and multiple-error measurement system with on-line probes. Measurements were performed at several selected points, and the thermal errors at any location of the working zone were interpolated in between. Direct measurement is very effective in correcting slowly changing thermal errors, but has the disadvantages of requiring potentially expensive additional measurement equipment and intruding into the machining process, thus reducing the production efficiency.

In error synthesis approach, the resultant thermal errors at the tool tip are computed by combining the measurement of the distortion of each individual machine element along the kinematic chain of a machine tool. This method gives the

comprehensive evidence of the accuracy of each machine element, but is generally time-consuming.

A laser interferometer and non-contact capacitance sensors are usually used to directly measure the thermal errors, such as the linear and angular errors of moving axis under changing temperature fields and the thermal expansion of the rotating spindle (Donmez et al., 1986; Chen et al., 1993; Lo et al., 1995). Because there are many thermal error components to be measured separately, the labor-intensive calibration procedures must be repeated several times. In addition, the interactive impact between the thermal error sources is sometimes ignored. Reference artifacts or gauges with known dimensions are also exploited for the thermal error identification. Error components are inversely estimated based on the comparison of the measurement results and the reference values (Ziegert and Kalle, 1994; Li et al, 1997; Kim and Chung, 2004). A large number of equation derivations and parameter estimation make this method relatively complicated. The derived relationship between the machine error components and the aggregate thermal errors might not be able to accurately predict the dimensional accuracy of the finished parts.

"Part-oriented" identification techniques were developed to relate the part-feature errors of a part family with machine tool errors. Mou et al. (1995a and 1995b) presented a feature-based analysis technique to relate the dimensional and form errors of manufactured features to the machine tool thermal errors. This approach dealt with mathematic models and measurements closely related to the real parts. This method is applicable for the mass or batch production, where the machine tools are dedicated to a

particular part family. Therefore, only a limited number of part-feature related machine tool errors are important and need to be identified.

2.3.2 Thermal Error Modeling

For most thermal error compensation systems, mathematical models are necessary to relate the thermal errors to other variables that are easier to measure. Although the use of variables such as spindle speed (Li et al, 1997; Lim and Meng, 1997) and strain gauges measurement (Hatamura et al., 1993) have been reported in the literature, temperature measurements at certain key positions on the machine tool structures are most widely utilized. Consequently, mathematical models describing the relationships between the thermal errors and the temperature measurements become essentially important. Various thermal error models underlining the thermo-elastic relationship have been investigated and applied for the thermal error compensation. They are categorized into two groups: time independent static models and time dependent dynamic models (Yang, 2002).

For time independent static model, only current temperature measurements are taken as the model inputs. Donmez et al. (1986) derived a polynomial function of the temperature rise at the spindle bearings to predict the spindle tilt-up error of a turning machine. Chen and Chiou (1995) compared the thermal error modeling effects by using multiple regression analysis (MRA) and artificial neural network. In recent years, different types of neural network have been employed in the thermal error modeling (Veldhuis and Elbestawi, 1995), including cerebellar model articulation controller (CMAC) neural network (Yang et al., 1996), fuzzy ARTMAP neural network (Srinivasa and Ziegert, 1997), and the like. Ramesh et al. (2003a and 2003b) utilized the Bayesian network and support vector machine (SVM) model to classify the thermal errors

depending on the operation conditions and develop the mapping of the thermal errors with the machine tool temperature profile.

For time dependent dynamic models, time is either explicitly taken as the model inputs (Kim and Cho, 1997) or implicitly inferred by including previous temperature measurement. Janeczko (1989) observed that the spindle thermal expansion has a lagging characteristic compared with the collected temperature at certain sensor locations, so an exponential function, including time constant and expansion length, was developed to estimate spindle thermal expansion errors. Moriwaki (1998) experimentally determined the transfer functions between the spindle rotation speeds and thermal displacement, and between the air temperature and thermal displacement, respectively. Convolution was used to determine the time domain thermal deformation based on the linear system assumption, and model adaptation was performed for different spindle speeds.

Fraser et al. (1998a, 1998b, 1999a, 1999b and 1999c) proposed a generalized modeling approach to model the thermal-elastic relationship. Inverse heat conduction problem (IHCP) was resolved to identify the heat sources from temperature reading and then system model was derived to predict thermal deformation according to these heat sources. The generalized model for the thermal deformation process and generalized transfer functions of the dynamic thermal deformation process in the *S*-domain were determined for the purpose of control system design.

Wang et al. (1998) presented a systematic methodology for the thermal error correction of a machine tool. The thermal deformation was modeled using the grey system theory to dynamically predict the thermal errors. Unfortunately, some short-term

dynamics of the system were lost due to the properties of Accumulated Generating Operation (AGO). Therefore, the model obtained under one particular operating condition was not robust under other conditions.

Yang and Ni (2003) proposed an Output Error (OE) model to describe the dynamic nature of machine tool thermal errors by considering the time series of both temperature inputs and thermal deformation outputs for model estimation. This approach significantly improved the accuracy and robustness of thermal error models. Yang and Ni (2005a) presented a recursive model adaption mechanism based on the Kalman filter technique with multiple-sampling horizons to update the thermal error model during continuous changes of manufacturing conditions such as system reconfiguration or performance degradation over a long period.

The abovementioned approaches are empirical and highly dependent on the model training conditions. Numerical methods, such as the finite difference method (FDM) and the finite element method (FEM) are also utilized for the development of thermal error models. The numerical methods are powerful tools in simulating the practical heat transfer and thermo-elastic processes, where analytical solutions to temperature fields and thermal deformations are prohibited due to the complexity of machine tool structures.

Attia and Kops (1981a) approximated the thermal behaviors and deformations of a machine tool structure in response to the effect of fixed joints using the FEM. Moriwaki (1988) used the FDM to predict and compensate for the thermal deformations of a hydrostatically supported precision spindle. Lingard et al. (1991) analyzed the temperature perturbation effects on a high precision CMM using the FEM. Jedrzejewski

and Modrzycki (1992) applied the FEM to optimize the thermal behavior of a machine tool under various service conditions.

The absolute accuracy of the numerical methods is limited by several complex uncertainty factors, such as geometrical dimensions, boundary conditions, and machine joints. However, the limitations with respect to the reliability of quantitative results cannot reduce the impact of numerical methods on the qualitative evaluation of machine tool accuracy (Weck et al, 1995). The FEM is capable of making important contributions in deciding the initial temperature sensor locations for the subsequent thermal error modeling (Bryan, 1990).

2.3.3 Temperature Sensor Placement

For those thermal error models with temperature as inputs, the locations of temperature sensors play a vital role in determining the accuracy, efficiency and robustness of the derived models. Generally speaking, to put a large number of temperature sensors onto the machine structure can improve the accuracy and robustness of the thermal error model. Balsamo et al. (1990) initially used nearly 100 temperature sensors to predict the thermal deformations of a CMM.

However, it is always an engineering concern to reduce the number of temperature sensors. Some researchers chose the variables based on their experiences with the potential heat sources and machine tool thermal deformations (Donmez et al., 1986; Moriwaki, 1988). Correlation coefficients between thermal errors and temperature variables were exploited to select highly correlated temperature variables for modeling (Kurtoglu, 1990). Chen et al. (1996b) used a standard step-wise regression method to

find better linear models with multiple temperature variables. The most strongly correlated temperature variables were first included; then one temperature variable was either added or subtracted at a time based on the statistical significance evaluation of that variable. Lo et al. (1999) used an objective function formulated by a modified model adequacy criterion based on the Mallow's C_p to select the temperature variables.

In most researches, complete information of the dynamic characteristics of the temperature fields and the thermal errors is not considered in determining the temperature sensor locations. If temperature sensors are not placed within the significant sensing areas of a machine tool structure, the resultant thermal error models cannot be robust under various operating conditions. Ma (2001) proposed an optimization method to locate temperature sensors. The basic rule for selecting optimal sensor locations is that the smaller the frequency of the thermal load is, the farther the sensor should be mounted away from the heat source. This method is theoretically appealing, but has not yet been applied and validated through practical experiments. Therefore, it is still necessary to develop a systematic methodology for optimizing the temperature sensor locations so that the waste of time and resources can be reduced.

CHAPTER 3

ROBUST MACHINE TOOL THERMAL ERROR MODELING THROUGH THERMAL MODAL ANALYSIS

\

3.1 Introduction

The importance of enhancing machine tool accuracy has been well recognized in both industry and academia in the past few decades due to the increasing demands for products with better quality and tighter tolerances while still maintaining the high productivity. The machine tool accuracy directly determines the dimensional accuracy of machined products. The most significant factor influencing the machine tool accuracy is the thermal error, which accounts for about 50% of the total machine tool errors (Bryan, 1990). Internal and external heat sources can cause thermal deformations in machine tool structures far beyond the acceptable dimensional tolerances of common machined products.

A large number of researches have been carried out to investigate the influences of thermal errors and thus to reduce these errors on machine tools for decades. Examples of successful thermal errors reduction with the aid of error compensation techniques have been demonstrated in both research laboratories and industrial facilities (Donmez et al., 1986; Balsamo et al., 1990; Chen et al., 1993; Mou et al., 1995a and 1995b; Srinivasa and Ziegert, 1996; Yang et al., 1999). However, the accuracy and robustness of the thermal

error models are still considered as the major barriers which have to be removed before the widespread applications of thermal error compensation are possible (Ni, 1997).

Some researchers concentrated on the development of thermal error models by using different modeling methodologies. Such methods include polynomial regression (Donmez et al., 1986; Chen et al., 1993), artificial neural networks (Chen, 1996a; Yang et al., 1996; Srinivasa and Ziegert, 1997; Mou, 1997; El Ouafi et al, 2000), and system identification (Wang et al. 2006; Yang and Ni, 2003, 2005a and 2005b). The locations of the temperature sensors are generally selected to be as close as possible to heat sources in most researches. Consequently, either the deficient number or the improper locations of the temperature sensors could undermine the effectiveness of the thermal error models. To resolve this problem, statistical methods are employed to choose temperature sensors at certain key positions from an excessive number of sensors mounted on the machine based on the ranked contributions to a specified measure (Kurtoglu, 1990; Lo et al. 1999; Lee and Yang, 2002). In general, an extensive amount of time and effort is required for the machine characterization, variable selection and model training to develop a machine tool thermal error model (Ni, 1997).

The abovementioned methods are mostly empirical and merely applied to single machines as a means of proving concept. In most cases they could not easily and cost-effectively be extended to machines of similar type or structural configuration. One of the main reasons is that the essence of the underlying thermal deformation process has been neglected. Very limited research has been conducted to reveal the importance of thermo-elastic relationship, especially for the machine tools. Lo (Lo, 1994) illustrated the hysteresis effects between the temperature and thermal deformation of a simplified

spindle model. Ma et al. (1999) provided an analytical description for the hysteresis effects and pointed out the dependence of temperature sensor locations on the frequency of the heat inputs due to the factors like machining cycles and daily shifts. Ma (2001) proposed a thermal deformation modal analysis to further explore the thermo-elastic relationship by using the finite element method (FEM). Similar to the dynamic modal analysis, a small number of significant modes are supposed to dominate the entire thermal deformation process. If temperature sensors are mounted on certain locations to capture these dominant modes, more accurate and robust thermal error models could be developed accordingly.

Fortunately, the topic of sensor placement has been widely investigated, giving rise to many schemes for the identification and control of dynamic systems. Shah and Udwadia (1978) proposed a sensor placement method by minimizing the trace of the covariance matrix associated with the structural parameters estimation. Salma et al. (1987) selected the sensor locations so that the modal kinetic energy of the response of the structure could be maximized. Carne and Dohrmann (1994) employed the minimization of the off-diagonal terms in the modal assurance matrix (MAC) as a measure of the utility of a sensor configuration. Papadimitriou et al. (2000) proposed to use the information entropy that is a measure of uncertainties in the model parameters for determining the optimal sensor placement. Kammer (1991) presented the effective independence (EfI) method based on the contributions of each sensor to the corresponding Fisher information matrix. The objective of this sensor placement strategy is to select sensor locations that render the target mode shape partitions as linearly independent as possible, and at the same time, maximize the signal strength of the target

modal responses within the sensor data. Those schemes could be modified to resolve the conceptually similar thermal deformation problems.

In this Chapter, a thermal error modeling method is presented to rationalize the thermal deformation process. The thermal behavior of a machine tool is fully assessed based on the thermal modal analysis. This provides an in-depth understanding of the magnitude and type of thermal errors existing in the machine tool. It also helps to identify the machine structural elements, which are significantly responsible for thermal errors. With this knowledge, the temperature sensor locations are decided. The entire thermal deformation process is simply represented by a small number of dominant thermal modes. Suitable thermal error models are then derived to describe the particular type of thermal errors. The validity of the thermal error models is verified through both simulation and experiments. This method is applicable to the machine tools with same structural configuration under similar working conditions because the essence of thermal deformation process has been physically underlined.

3.2 Thermal Modal Analysis

3.2.1 Thermal Modes

Finite element analysis (FEA) has been employed by some researchers to investigate the thermal errors of machine tools to consolidate the conventionally empirical modeling approaches (Moriwaki, 1988; Jedrzejewski et al., 1990; Attia and Fraser, 1999b). Finite element modal analysis is also used to analyze dynamics (Shah and Udwadia, 1978; Juang and Pappa, 1985; Salama et al., 1987; Kammer, 1991) and heat transfer problems (Coutinho et al., 1989; Dos Santos et al., 1990). However, finite

element modal analysis is seldom utilized to explore the essence of thermal-elastic problems in machine tools, even though the similar idea of decomposing a complicated system into simpler sub-systems without the loss of substantial characterization has been proposed. Matsuo et al. (1986) evaluated the steady-state temperature and the rate of temperature rise of a machine tool structure to shorten the machine warm-up period based on the modal analysis. Weck et al. (1995) expressed measured thermal errors in response to a step-like thermal load as a sum of two exponential functions, which were named modes.

To perform the thermal modal analysis, the finite element solution of heat transfer problem needs to be solved, which requires the integration of coupled differential equations of the form

$$[C_T]\{\dot{T}(t)\} + [K_T]\{T(t)\} = \{Q(t)\} \tag{3.1}$$

where $[C_T]$ is the heat capacity matrix, $[K_T]$ is the heat conductivity matrix, $\{T(t)\}$ is the nodal temperature vector, and $\{Q(t)\}$ is the nodal thermal load vector.

The eigen-problem (Ma, 2001) associated with Equation (3.1) is

$$[K_T][\Phi_T] = [C_T][\Phi_T][\Lambda] \tag{3.2}$$

where $[\Lambda]$ is a diagonal matrix composed of all the eigenvalues, λ_i, and $[\Phi_T]$ is the corresponding eigenvector matrix. Theoretically, λ_i is the reciprocal of the time constant

$$\lambda_i = \frac{1}{\tau_i} \tag{3.3}$$

where λ_i and τ_i are the *i*-th eigenvalue and time constant, respectively. The time constant describes how quickly the mode responds to thermal loads.

Similar to structural dynamic system, each mode includes one eigenvalue and eigenvector. The smallest eigenvalue, or the largest time constant, corresponds to the

lowest mode. The thermal modes, i.e., the time constants and the temperature field, are the intrinsic properties of a machine tool structure and its working conditions. They are independent of the magnitudes or the locations of thermal loads.

In the modal analysis, the eigenvector matrix $[\Phi_T]$ can be used as a transformation matrix to decouple Equation (3.1). Temperature $\{T(t)\}$ is then transformed into modal temperature $\{\theta(t)\}$

$$\{T(t)\} = [\Phi_T]\{\theta(t)\} \tag{3.4}$$

Substituting Equation (3.4) into Equation (3.1) and multiplying both sides by $[\Phi_T]^T$ gives

$$[\Phi_T]^T[C_T][\Phi_T]\{\dot{\theta}(t)\} + [\Phi_T]^T[K_T][\Phi_T]\{\theta(t)\} = [\Phi_T]^T\{Q(t)\} \tag{3.5}$$

where $[\Phi_T]^T[C_T][\Phi_T]$ is the modal heat capacity matrix, $[\Phi_T]^T[K_T][\Phi_T]$ is the modal heat conductivity matrix, and $[\Phi_T]^T\{Q(t)\}$ is the modal thermal load.

Since the eigenvectors are $[C_T]$ orthonormal, the modal heat conductivity and capacity matrices satisfy

$$[\Phi_T]^{\mathrm{T}}[C_T][\Phi_T] = [I] \tag{3.6}$$

$$[\Phi_T]^{\mathrm{T}}[K_T][\Phi_T] = [\Lambda] \tag{3.7}$$

Introducing Equations (3.6) and (3.7) into Equation (3.5) yields

$$\{\dot{\theta}(t)\} + [\Lambda]\{\theta(t)\} = [\Phi_T]^T\{Q(t)\} = \{\xi(t)\} \tag{3.8}$$

where $\{\xi(t)\}$ is the modal thermal load vector.

Equation (3.8) is decoupled and can be expressed as a set of single variable, first order differential equations

$$\dot{\theta}_i(t) + \frac{\theta_i(t)}{\tau_i} = \xi_i(t) \tag{3.9}$$

where $\xi_i(t)$ denotes the modal thermal load. If a step-like heat input is imposed, the solution to Equation (3.9) is

$$\theta_i(t) = \xi_i \cdot \tau_i(1 - e^{-\frac{t}{\tau_i}}) \tag{3.10}$$

Step input is widely used for the analysis of linear systems. The thermal load variation of a machine tool can also be approximated as a serial combination of step inputs. The overall temperature response is thus regarded as the superposition of these thermal modes.

In practice, the heat capacity matrix and the heat conductivity matrix are extracted by using MSC/NASTRAN DMAP (Direct Matrix Abstraction Program). The time constants and temperature field mode shapes are obtained by eigen-analysis.

3.2.2 Mode Truncation

One advantage of thermal modal analysis is that the entire thermal process of a machine tool can be represented by several dominant thermal modes. To do this, the weight of each mode is defined as

$$w_i = |\xi_i \cdot \tau_i| \tag{3.11}$$

where ξ_i and τ_i denote the modal thermal load and the time constant of each mode, respectively. The magnitude of the weight quantifies the significance of each mode. A small number of modes usually constitute a large percentage of the total weight. The thermal deformation process is then described by these dominant modes. The remaining insignificant modes are simply discarded.

3.3 Robust Thermal Error Modeling

3.3.1 Temperature Sensor Placement

Thermal modal analysis provides a systematic method to characterize the thermal behavior of a machine tool by using several dominant thermal modes. To capture these modes, temperature sensors have to be mounted on the machine tool. In simulation, it might be possible to compare the effects of the temperature collected at different locations based on certain mathematical model. In reality, however, it is always extremely time-consuming, and could sometimes become impractical. Some locations may not be accessible and others not appropriate for temperature sensor placement.

Guidelines are thus preferred to efficiently identify the potential sensor locations for developing the thermal error models, since temperature reading is generally not very sensitive to the location because of the smooth distribution of temperature field. Those guidelines are proposed based on the thermal modal analysis; therefore, it is physically meaningful. For each thermal mode, similar to structural dynamics analysis, it is always desirable to place the temperature sensors according to the following two rules:

(1) Close to the extreme values of the dominant temperature fields or,

(2) Close to the heat flux sources.

By doing this, the dominant thermal modes are acquired and the multicollinearity of the collected temperature is reduced. It is obvious that sensors should be mounted away from the nodes, zero magnitude, of the target mode; otherwise no useful information would be collected for that mode.

Another advantage of this strategy is cost-effectiveness. Once sensors are mounted on the machine tool structure it is difficult to remove them. The conventional

temperature sensor selection method, however, requires a large amount of sensors to be mounted in the first place to improve the accuracy and robustness of the thermal error models. The proposed method provides an alternate way to place temperature sensors. If the number of sensors is not adequate, in other words, the number of representative thermal modes is not able to fully describe the thermal deformation process, additional sensors would be mounted to capture more thermal modes. By doing this, the number of temperature sensors could be well controlled.

3.3.2 Thermal Error Modeling

Machine tool thermal errors are generally divided into two categories, position independent and position dependent (Chen et al., 1993). Position independent thermal errors, merely functions of temperature, include the thermal expansion of the spindle. Position dependent thermal errors are functions of both temperature and axial positions, such as linear positioning accuracy along an axis. In consequence, different model forms are utilized to describe those thermal errors respectively.

The regression model using a least squares estimation method is employed to describe the thermo-elastic relationship due to its simple structure and better extrapolation compared with other modeling methods such as artificial neural networks.

The formula for position independent thermal errors is in the form of

$$E(t) = \sum_{i=1}^{N} \beta_i \cdot T_i(t) = \boldsymbol{T} \cdot \boldsymbol{B} \tag{3.12}$$

where $E(t)$ denotes the thermal errors, $\boldsymbol{T} = [T_1(t), \cdots, T_N(t)]$ represents the temperature variation, t is time, and N is the number of temperature sensors.

The position dependent thermal errors are formulated as

$$E(x,t) = \sum_{i=1}^{N} [\beta_{0i} + \beta_{1i} \cdot P(x) + \beta_{2i} \cdot P^2(x) + \cdots] T_i(t) = \boldsymbol{T} \cdot \boldsymbol{B} \tag{3.13}$$

where $P(x)$ is the position of the corresponding thermal errors.

In Equations (3.12) and (3.13), thermal errors, $E(t)$ and $E(x,t)$, are in linear relationship with respect to temperature variation, $T(t)$, which guarantees the extrapolation ability as long as the models are consistent with the data and knowledge of the problem settings. Equations (3.12) and (3.13) can be rearranged in matrix form of

$$\vec{\boldsymbol{E}} = \boldsymbol{T} \cdot \boldsymbol{B} \tag{3.14}$$

The coefficient matrix $\boldsymbol{B}$ is then computed by the linear least squares estimation

$$\boldsymbol{B} = (\boldsymbol{T}'\boldsymbol{T})^{-1}\boldsymbol{T}'\vec{\boldsymbol{E}} \tag{3.15}$$

The robustness of the proposed approach will be justified from two aspects, namely, linear extrapolation and frequency sensitivity. Linear extrapolation is important since it could reduce the time for the machine characterization and model training. The significance of frequency sensitivity (Ma et al., 1999) is largely due to the periodicity of machine operation and environment conditions, which causes the thermal loads to follow certain cycles.

3.4 Numerical Simulation for Simple Thermal Deformation Shapes

Simplified machine components are numerically simulated to illustrate the proposed temperature sensor placement strategy and thermal error modeling. There are two basic thermal deformation shapes, thermal elongation and thermal bending, shown in Figure 3.1. Thermal errors are defined corresponding to these thermal deformation

shapes, expansion, ε, for thermal elongation; and expansion, ε, deflection, δ, and slope angle, θ, for thermal bending.

In the simulation, the heat input, $Q(t)$, is assumed to be generated at the fixed end. Thermal errors occur at the free end. Heat exchange exists between the machine element surfaces and the environment through convection. For the thermal elongation, the convection heat transfer coefficient, h, is assumed to be equal to $20\ \mathrm{W/m^2K}$ for all the surfaces. For the thermal bending, the convection heat transfer coefficients are assumed to be equal to $20\ \mathrm{W/m^2K}$ and $100\ \mathrm{W/m^2K}$ for the upper and lower surfaces, respectively. The remaining geometric parameters and material properties are listed in Table 3.1. Candidate temperature sensor locations are also indicated in Figure 3.1. There are nine candidate temperature sensor locations for the thermal elongation, whereas there are eighteen, nine each in the upper and lower surfaces, for the thermal bending.

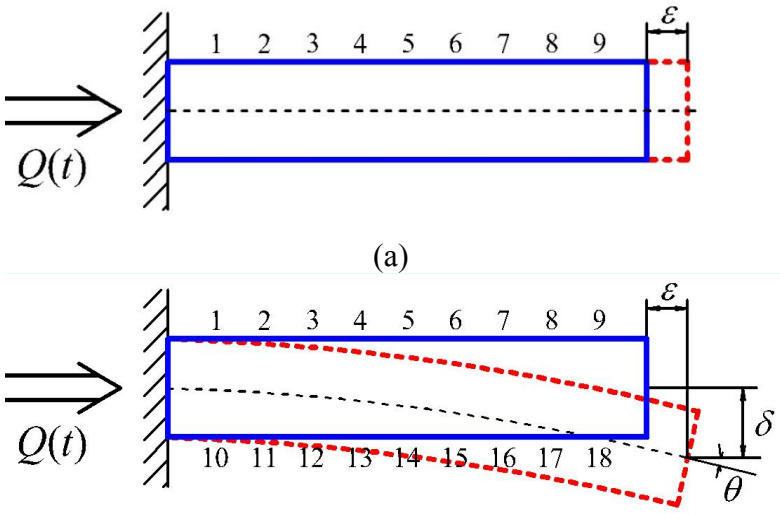

Figure 3.1 Basic thermal deformation shapes.
(a) Thermal elongation and (b) thermal bending.

Table 3.1 Parameters and material properties of simplified machine elements.

Heat conduction coefficient	k	60.5	$\mathrm{W/m \cdot K}$
Heat capacity	C_p	434	$\mathrm{J/kg \cdot K}$
Density	ρ	7.8×10^3	$\mathrm{kg/m^3}$
Thermal expansion coefficient	α	10.8	$\mathrm{\mu m/m \cdot K}$
Young's modulus	E	120	GPa
Poisson's ratio	υ	0.25	
Length	L	1.0	m
Area	A	0.0314	$\mathrm{m^2}$

3.4.1 Temperature Sensor Placement Based on Thermal Modal Analysis

In order to perform the thermal modal analysis, a finite element model for the simplified machine component was built. The machine component was divided into 22 elements. After applying the thermal modal analysis, the first four temperature field modes with the corresponding time constants are shown in Figures 3.2 and 3.3 for the thermal elongation and the thermal bending, respectively. The magnitude of temperature field for each thermal mode is normalized.

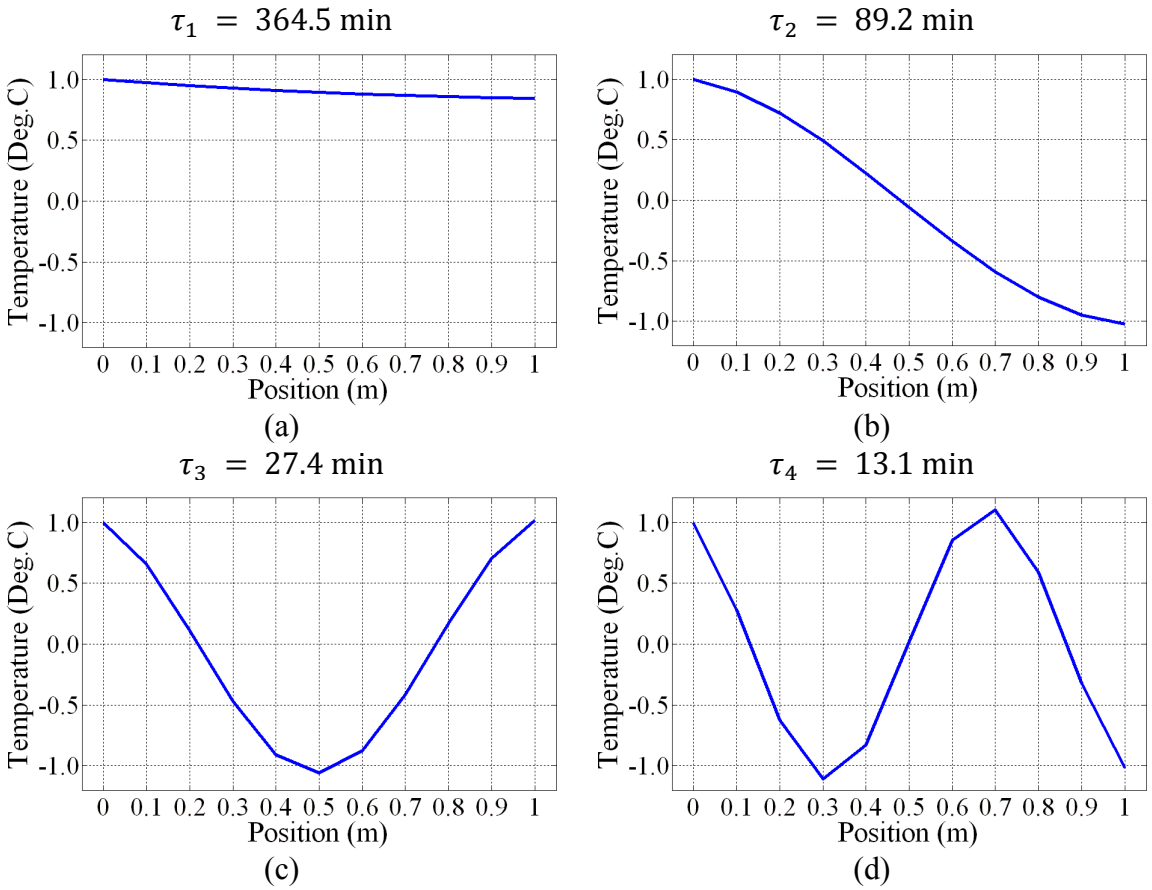

Figure 3.2 First four thermal modes with temperature fields and time constants for the thermal elongation. (a) Mode I, (b) Mode II, (c) Mode III, and (d) Mode IV.

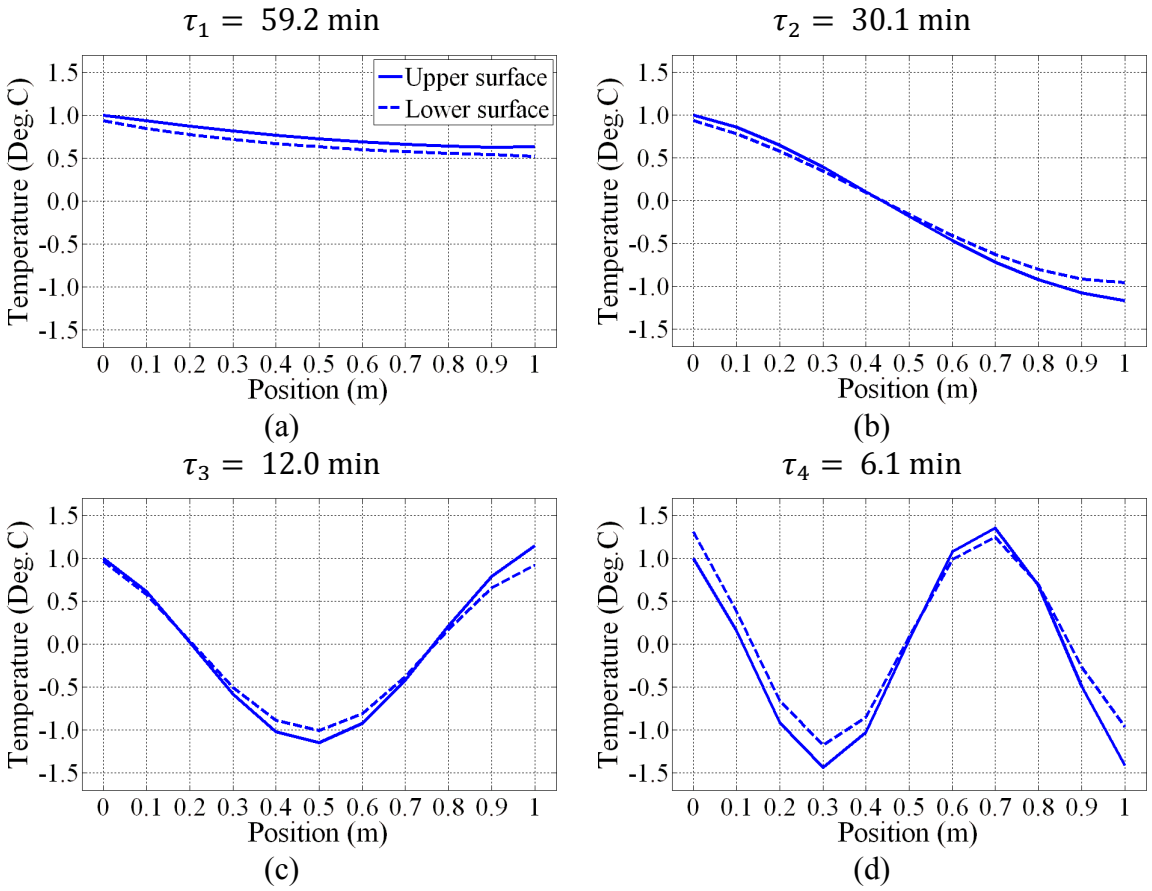

Figure 3.3 First four thermal modes with temperature fields and time constants for the thermal bending. (a) Mode I, (b) Mode II, (c) Mode III, and (d) Mode IV.

A step-like heat flux input was imposed to compute the modal thermal load and the weight of each mode. The time constants and weight distribution for the thermal elongation and the thermal bending are shown in Figures 3.4 and 3.5. As is expected, only a small number of thermal modes, which contribute more than 90% of the total weight, are significant.

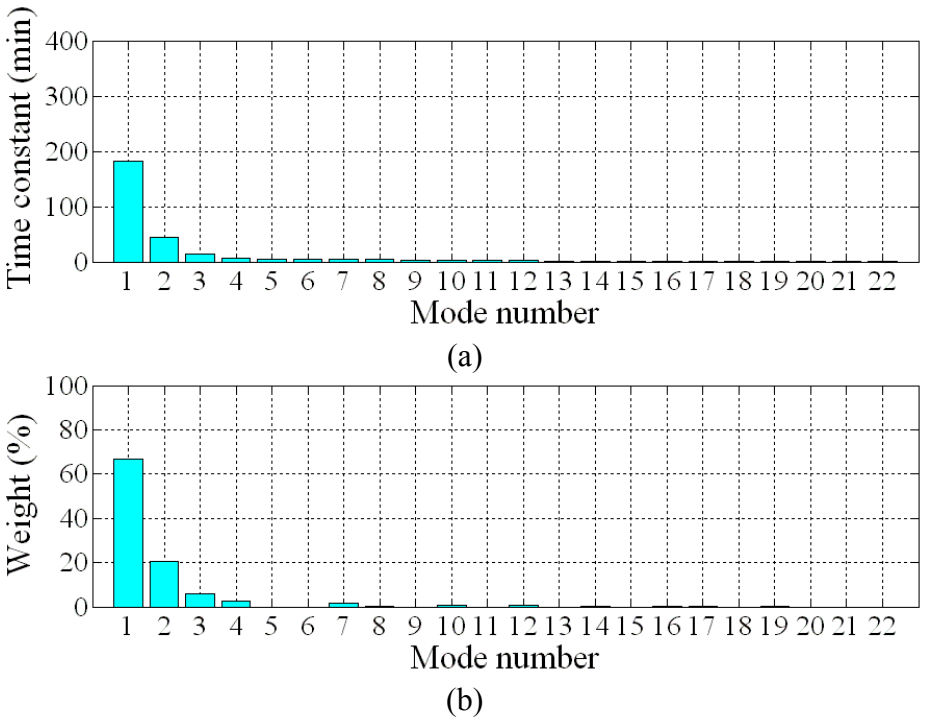

Figure 3.4 Time constant and weight distribution for the thermal elongation. (a) Time constant and (b) weight distribution.

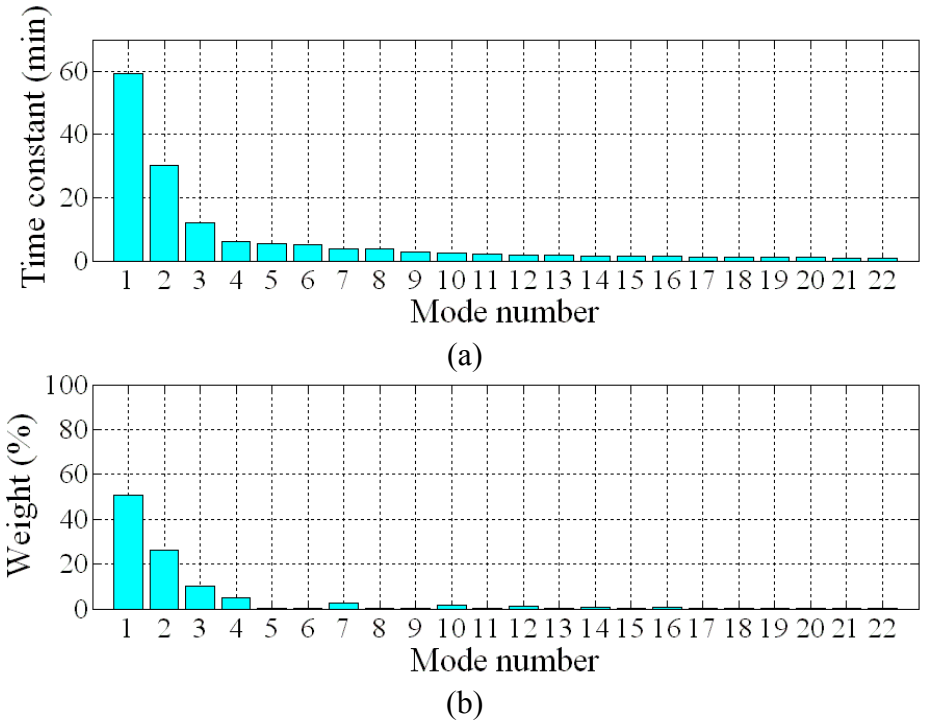

Figure 3.5 Time constant and weight distribution for the thermal bending. (a) Time constant and (b) weight distribution.

Temperature sensor locations are then decided according to the proposed temperature sensor placement scheme. Two temperature sensors were planned to be mounted for the thermal elongation shown in Figure 3.6(a). The locations of these two sensors depend on the first three temperature field mode shapes. One temperature sensor is placed at Position 5 for the thermal modes I and III and another one is at Position 1 for thermal mode II. Three temperature sensors were placed for the thermal bending shown in Figure 3.6(b). One temperature sensor is placed at Position 5 for thermal mode I, one temperature sensor is placed at Position 1 for thermal mode II, and one temperature sensor is placed at Position 10 for thermal mode III.

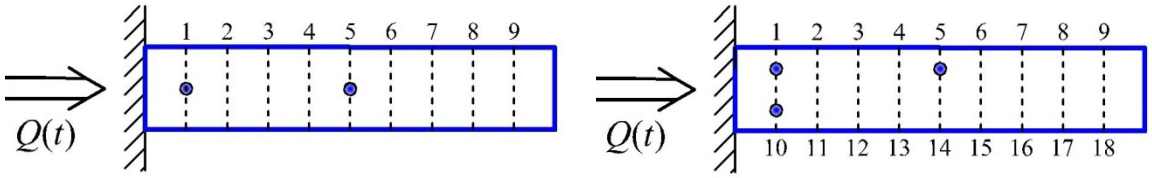

(a) (b)

Figure 3.6 Temperature sensor placements.
(a) Thermal elongation and (b) thermal bending.

3.4.2 Comparison of Temperature Sensor Placement Schemes

The proposed temperature sensor placement scheme is compared with other two commonly utilized methods, namely, Gaussian integration method (Krulewich, 1998) and exhaustive search method (Lo et al., 1995).

Gaussian Integration Method

In the Gaussian integration method (Buchanan and Turner, 1992), the temperature distribution of a machine tool is approximated by a high order polynomial. The thermal

errors are related to the integral of the temperature distribution. The locations of the temperature sensors are determined by the representative integration points, enabling the accurate computation of the integral of the temperature distribution. In the mathematical form

$$e = \int_S \alpha \cdot T(s) ds \approx \sum_{i=1}^{N} \beta_i T(x_i) \tag{3.16}$$

where e denotes the thermal error, S represents the integral domain over the temperature field, $T(s)$ is the temperature distribution, $T(x_i)$ is the temperature at the integration points decided based on the Gaussian integration method, N is the number of the temperature sensors, and β_i is the coefficient. The number of terms in the summation of Equation (3.16) is determined by the order of the approximated polynomial for the temperature distribution. In general, a higher order polynomial function results in a more accurate thermal error model, but requiring more temperature sensors.

Temperature sensor placement schemes based on the thermal modal analysis and Gaussian integration method do not require the information of the thermal errors. This significantly simplifies the selection of temperature sensor locations and the number of temperature sensors. Gaussian integration method is rigorous and systematic from the mathematic perspective, yielding satisfactory results for simple temperature distribution. However, this method becomes tremendously impractical for the machine tool with complex structure, because the analytical expression for the temperature distribution is almost unattainable and the integration point selection for the Gaussian integration higher than one dimension is mathematically intricate.

Exhaustive Search Method

Exhaustive search method is relatively more accurate than the abovementioned two methods, because the modeling results of all the possible temperature sensor locations are estimated and compared exhaustively. For the numerical simulation, this method is feasible though laborious, since both temperature data and thermal errors could be obtained through the simulation. However, compromise must be made in deciding the temperature sensor locations when multiple thermal errors are taken into consideration.

In practical, this method is difficult because it is impossible to acquire the entire temperature distribution and thermal errors, and then to compare the influence of different temperature sensor locations. The simplified exhaustive search method is commonly preferred. A huge number of temperature sensors are first mounted on the machine tool, and then a small portion is selected based on certain statistical measure. The exhaustive search method is presented here as a yardstick of the goodness of the proposed thermal modal analysis based temperature sensor placement scheme.

Temperature Sensor Placement Schemes Comparison

The temperature sensor placement schemes based on the thermal modal analysis, Gaussian integration method, and exhaustive search method for the thermal elongation and the thermal bending are summarized in Figure 3.7.

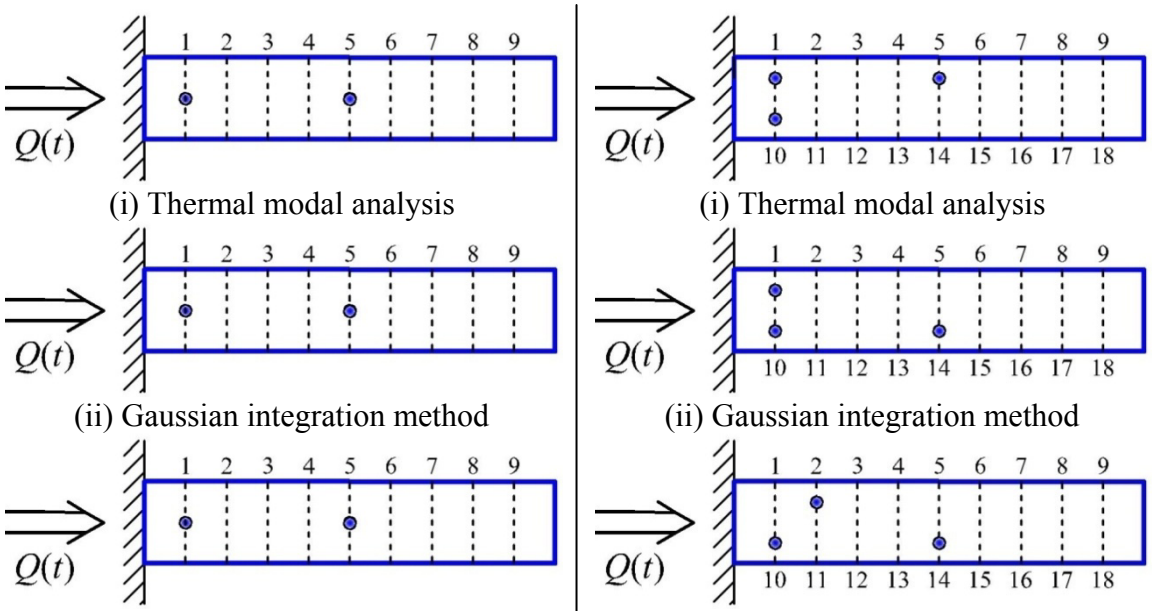

Figure 3.7 Temperature sensor placement schemes comparison.
(a) Thermal elongation and (b) thermal bending.

For the thermal elongation, all three methods give rise to the same temperature sensor placement scheme. For the thermal bending, the resultant sensor placement schemes are slightly different; but as mentioned previously, temperature sensors within certain range play the similar role and thus do not make much difference. Consequently, the sensor placement scheme based on the thermal modal analysis is still acceptable for the thermal bending.

3.4.3 Thermal Error Modeling and Robustness Verification

A numerically simulated heat flux input, $Q(t)$, is shown in Figure 3.8. Initially the simplified machine element was at the uniform temperature of 20 ℃. The temperature variation at the proposed temperature sensor locations and the thermal errors at the free end were collected.

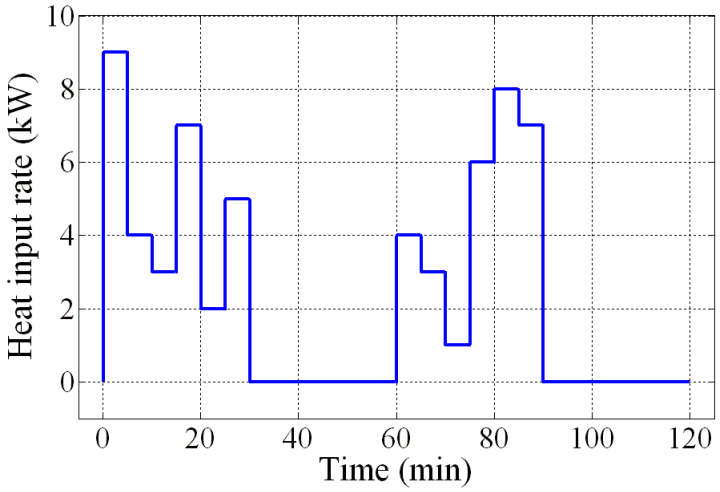

Figure 3.8 Heat flux input for numerical simulation.

Thermal Error Modeling

The thermal error models were derived to describe the relationship between temperature variation $T(t)$ and thermal errors based on Equation (3.12). Figure 3.9 summarizes the thermal error models and modeling results for the thermal expansion, ε, of the thermal elongation and thermal bending, respectively.

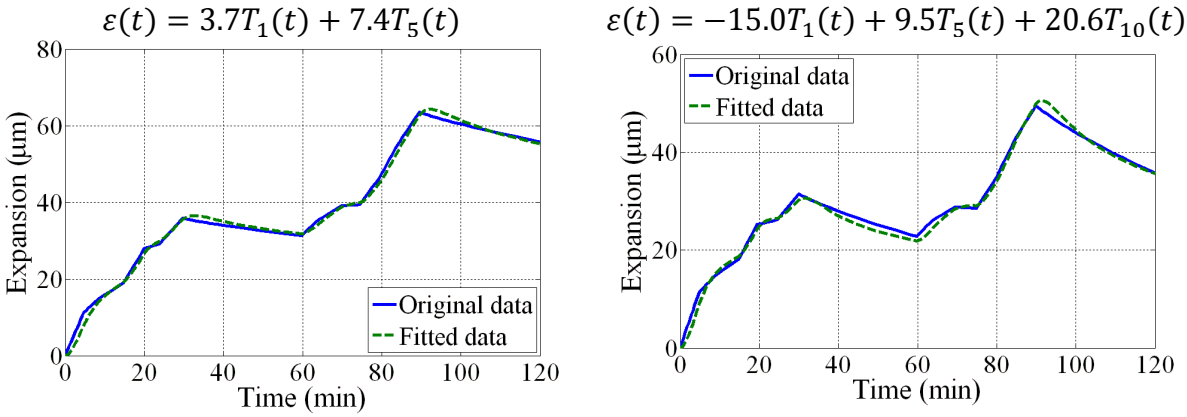

(a) (b)

Figure 3.9 Thermal error modeling results for the thermal expansion of (a) the thermal elongation and (b) the thermal bending.

The thermal error modeling results for the drift, δ, and the slope angle, θ, of the thermal bending are illustrated in Figure 3.10, as well as the thermal error models.

$\delta(t) = -8.1T_1(t) - 2.3T_5(t) + 7.6T_{10}(t)$ $\theta(t) = -2.0T_1(t) - 0.9T_5(t) + 1.9T_{10}(t)$

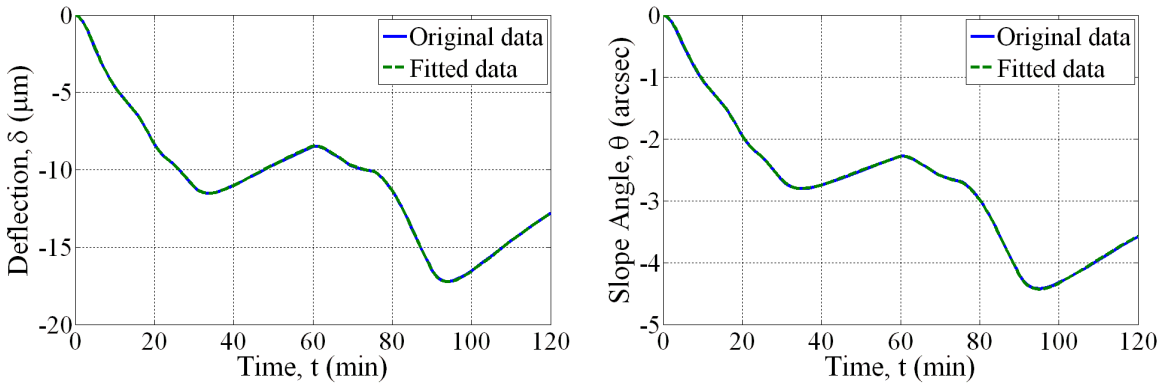

Figure 3.10 Thermal error modeling results for (a) the thermal deflection and (b) the slope angle of the thermal bending.

It is obvious that excellent agreement has been achieved between the simulation and modeling results.

Robustness Investigation

- **Linear Extrapolation**

In order to examine the robustness of the proposed thermal error modeling, two tests were separately conducted. In the first test for linear extrapolation, which spanned two hours, the first hour of data was used for model training and the remaining hour of data was used for model verification. Results are compared in Figures 3.11 for the expansion of the thermal elongation and in Figures 3.12 and 3.13 for the thermal errors of the thermal bending. Though the modeling results deviate slightly from the simulation

results in the second hour, the derived thermal error model is reasonably robust in the sense of linear extrapolation.

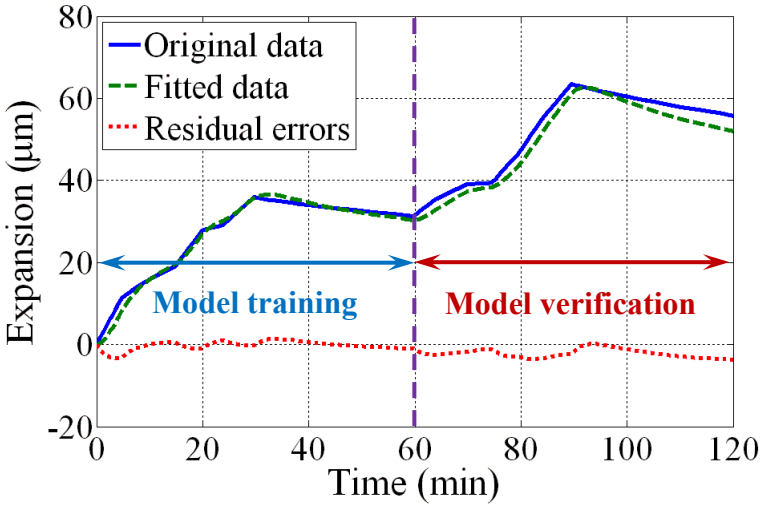

Figure 3.11 Extrapolation examination of the thermal error model for the expansion of the thermal elongation.

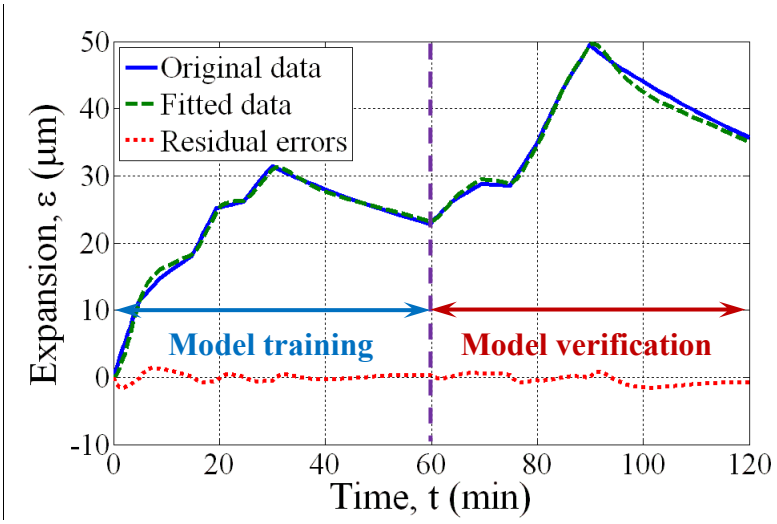

Figure 3.12 Extrapolation examination of the thermal error model for the expansion of the thermal expansion.

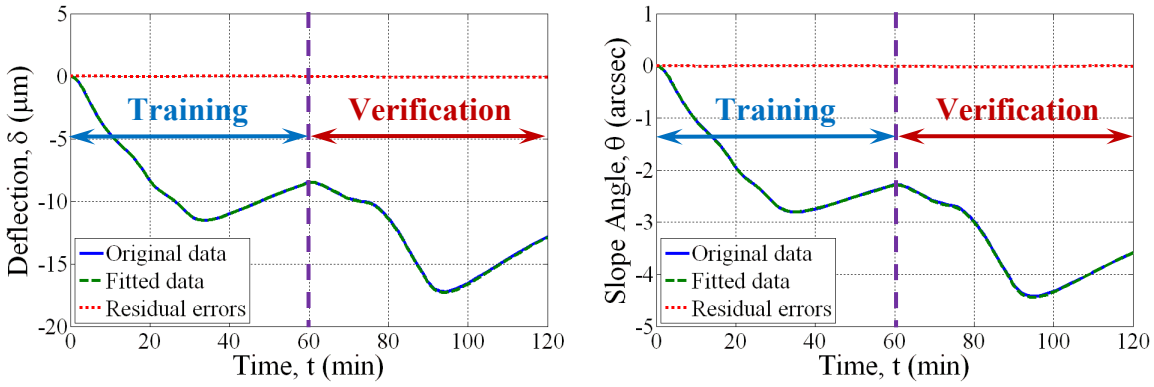

(a) (b)

Figure 3.13 Extrapolation examination of the thermal error model for (a) the deflection and (b) the slope angle of the thermal bending.

- **Frequency Sensitivity**

Machine elements are often subjected to some kind of cyclic variations due to the production schedules, environmental conditions, etc. To this end, in the second test, frequency sensitivity is examined with the generated heat inputs of different frequencies. One heat input with a period of 20 min, shown in Figure 3.14(a), was used to train the model, whereas two additional heat inputs with the period of 10 min and 40 min, shown in Figures 3.14(b) and 3.14(c), were used for verification. Figures 3.15 and 3.16 illustrate the modeling and verification results for the thermal elongation and thermal bending, respectively.

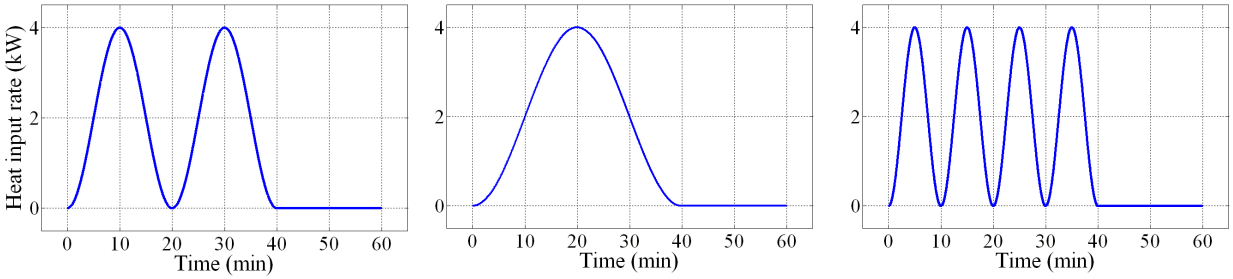

(a) (b) (c)

Figure 3.14 Heat flux input for frequency sensitivity examination. (a) $T = 20$ min, (b) $T = 40$ min, and (c) $T = 10$ min.

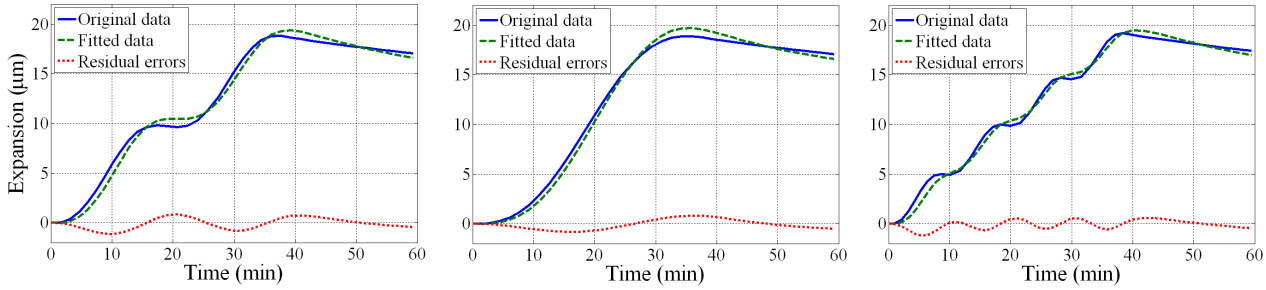

(a) (b) (c)

Figure 3.15 Frequency sensitivity examination for the thermal elongation. (a) $T = 20$ min, (b) $T = 40$ min, and (c) $T = 10$ min.

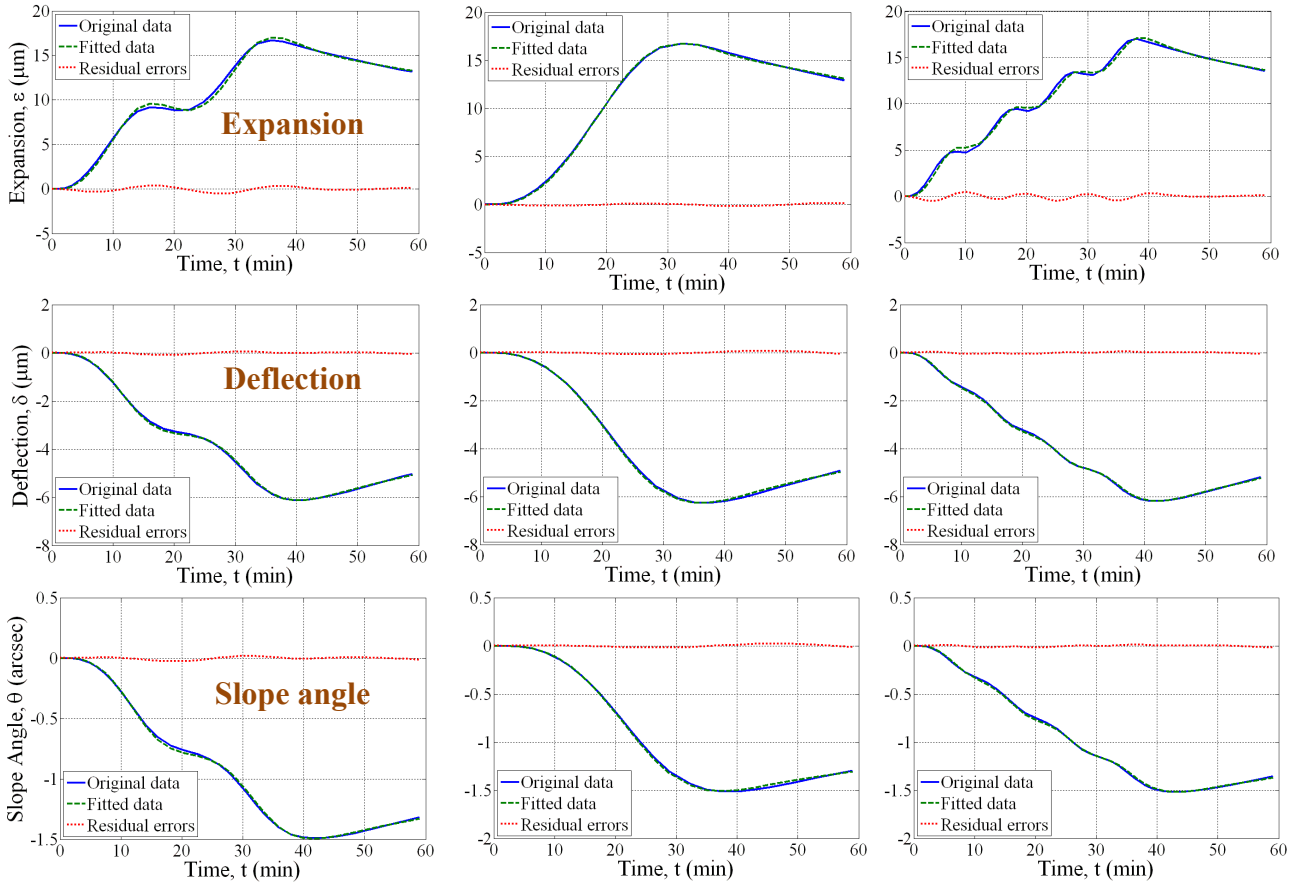

(a) (b) (c)

Figure 3.16 Frequency sensitivity examination for the thermal bending. (a) $T = 20$ min, (b) $T = 40$ min, and (c) $T = 10$ min.

It is obvious that that the derived thermal error model is robust to the frequency variation of the heat input for different kinds of thermal errors in both thermal elongation and thermal bending. The above two robustness examination indicates that the proposed

temperature sensor locations have captured the essence of the entire thermal deformation process.

3.5 Experimental Validation

The proposed thermal modeling method is validated on a spindle of a horizontal machining tool. Figure 3.17 shows the experimental setup, where the spindle is driven by an AC motor and spindle analyzer was used to measure the thermal expansion of the spindle tip. Three temperature sensors were mounted for the collection of temperature data based on the thermal elongation of the simplified machine component.

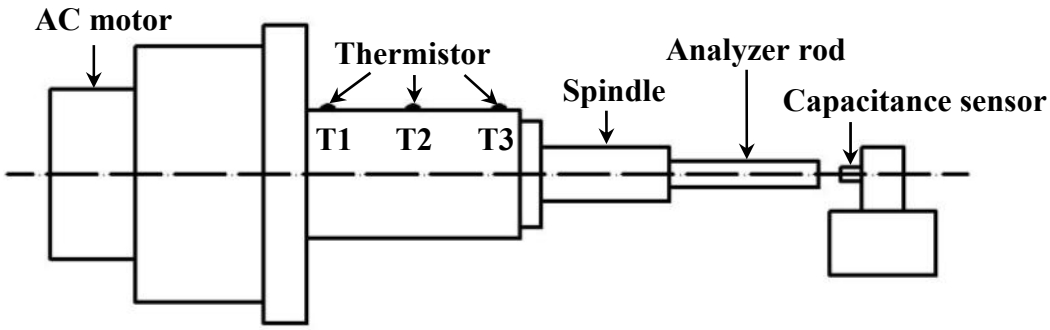

Figure 3.17 Experimental setup for spindle thermal expansion test.

One test was carried out at the programmed spindle speed as shown in Figure 3.18(a). Figures 3.18(b) illustrates the temperature variations. Temperature readings of sensors #1 and #2 were utilized for the thermal error model training. The measured thermal expansion and the modeling results are compared in Figure 3.19 as well as the residual errors.

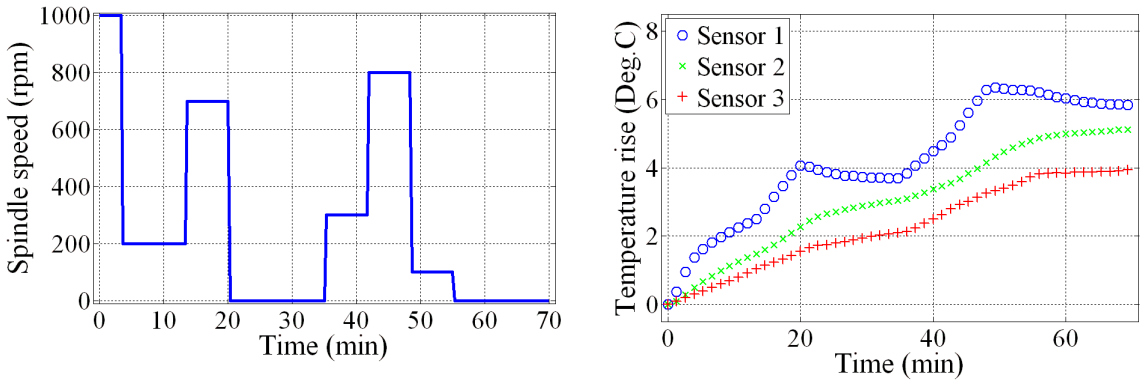

(a) (b)

Figure 3.18 Experiment results of Test 1. (a) Spindle speed, (b) temperature variations.

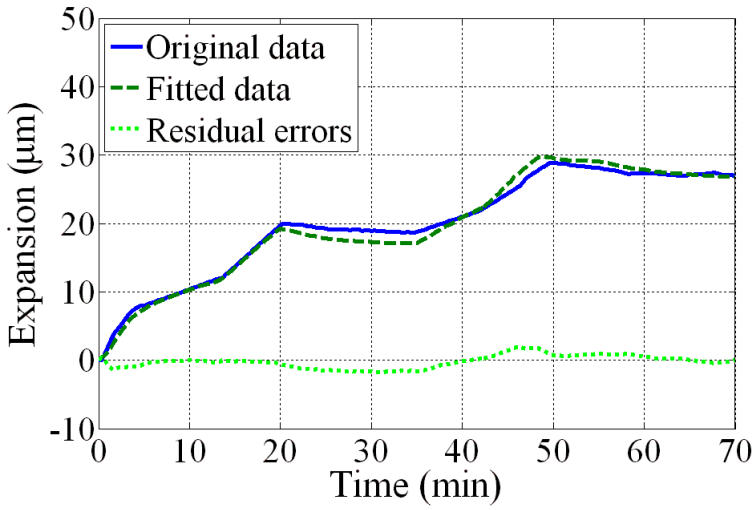

Figure 3.19 Measured and modeled results of the spindle experiment.

Another two sets of tests were conducted to investigate the robustness of the derived thermal error model. The spindle speed variations are shown in Figure 3.20. The only difference of spindle speeds between the verification and training tests is that the duration of warm-up period is shorten or elongated by 50%. The trained model by the first test was used to predict the thermal errors in the two verification tests. The measured and predicted thermal errors are also shown in Figure 3.20.

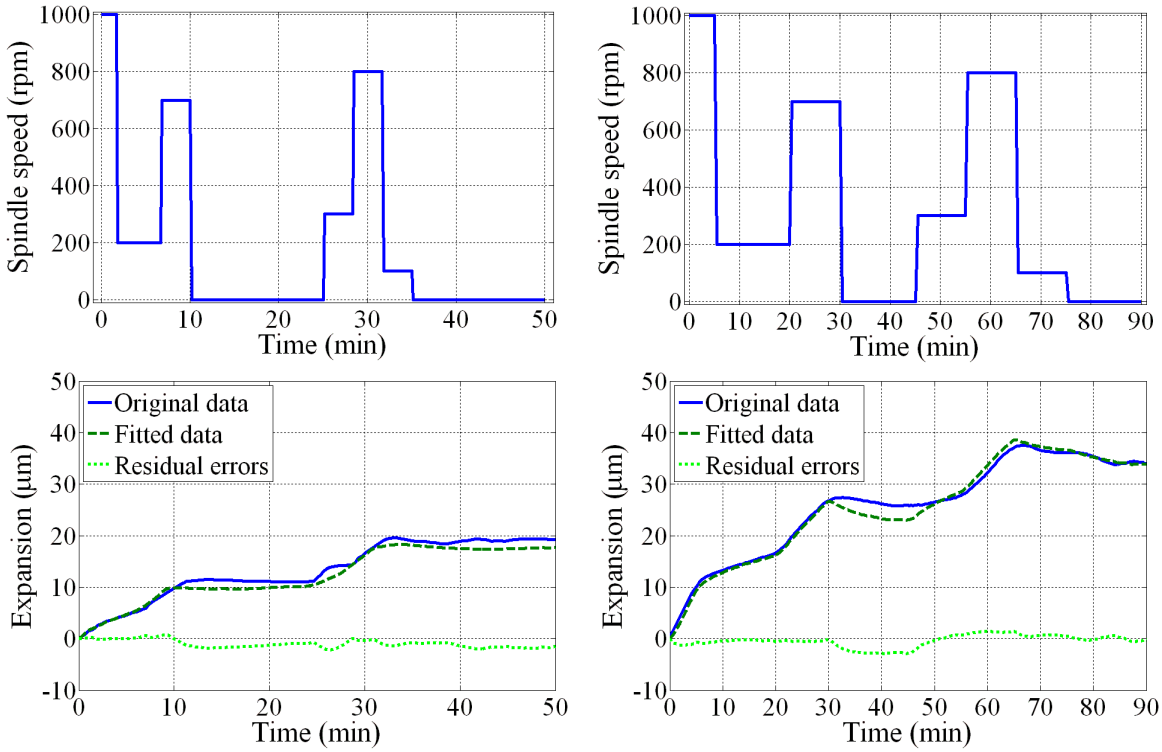

Figure 3.20 Spindle speed, measured and predicted thermal errors for robustness verification. (a) Test 2 and (b) Test 3.

It can be seen from the experimental results that most of the spindle expansion can be described by the derived model. During the cool-down periods, however, the discrepancy between the measured and predicted thermal errors are larger compared with the warm-up periods. The reason might be that the FEA of the spindle model is simplified without taking into account the inner structure of the spindle. The heat source is not merely from the heat generated by the AC motor, but from the friction of the spindle bearings as well. It is believed that a more detailed CAD model would enhance the FEA results and the addition of temperature sensors to capture more thermal modes should also further improve the effectiveness of the thermal error model.

To illustrate the dominant thermal modes, the corresponding time constants were estimated by curve fitting. The temperature variations of the mounted sensors were collected after each test shown in Figure 3.21. A function of the following form

$$T(t) = A_1\left(1 - e^{-\frac{t}{\tau_1}}\right) + A_2\left(1 - e^{-\frac{t}{\tau_2}}\right) + A_3\left(1 - e^{-\frac{t}{\tau_3}}\right) \tag{3.17}$$

was used to fit the collected temperature data based on the assumption that only three modes dominate the thermal process. The time constants were estimated to be $\tau_1 = 363.6$ min, $\tau_2 = 61.7$ min, and $\tau_3 = 27.0$ min. The weight distribution of each mode for the three tests is shown in Figure 3.22. For each sensor, the ratios between the weights under different working conditions are relatively consistent, indicating that the temperature variation is always the combination of thermal modes with same proportions. This practically illustrates the existence and relative significance of thermal. Admittedly, the boundary conditions during warm-up and cool-down periods are slightly different, but the fact that several modes govern the thermal expansion process has been unveiled.

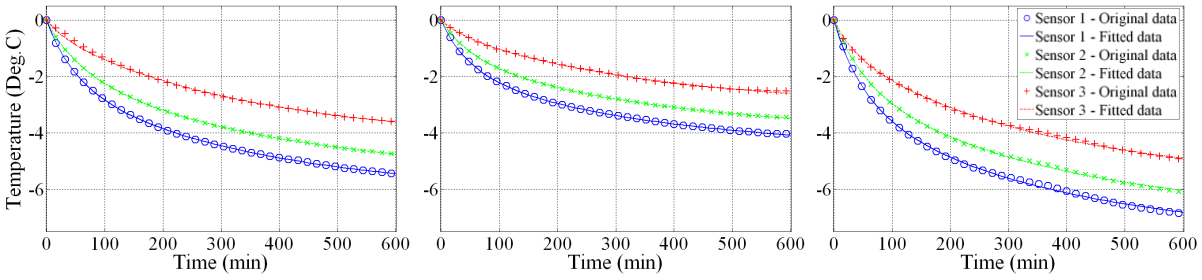

(a) (b) (c)

Figure 3.21 Temperature variations after each test. (a) Test 1, (b) Test 2, and (c) Test 3.

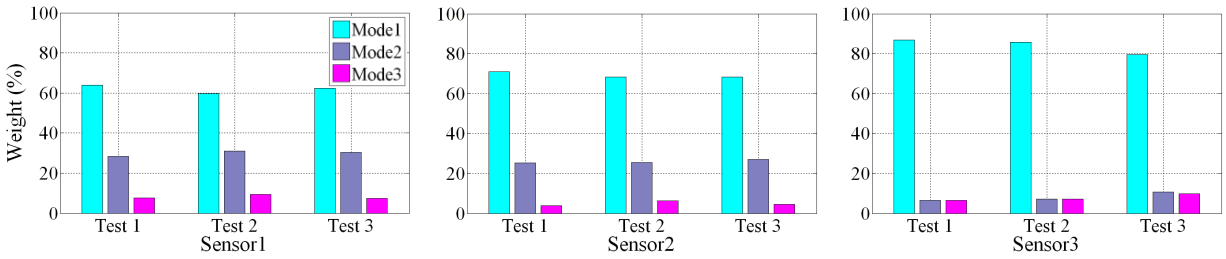

Figure 3.22 Weight distributions of the first three temperature modes. (a) Sensor 1, (b) Sensor 2, and (c) Sensor 3.

3.6 Summary

In this Chapter, a robust thermal error modeling strategy based on the thermal modal analysis was presented. Finite element analysis was utilized to determine the time constant, weight and temperature field of each thermal mode. Temperature sensors were then placed to capture the dominant thermal modes of thermal deformation process. By doing this, the essence of thermo-elastic relationship was acquired. Linear regression models were employed to describe both position independent and position dependent thermal errors. Numerical simulation and practical experiments were conducted to reveal the existence of thermal modes and the feasibility of the modeling method. The robustness of the thermal error models were also demonstrated in terms of linear extrapolation and frequency sensitivity

The proposed approach relates the theoretical thermal modal analysis to the conventionally empirical thermal error modeling methods, practically facilitating the thermal error compensation techniques. In addition, it provides an efficient and cost-effective temperature sensor placement scheme alternative. An excessive amount of time and efforts could be saved during the machine tool thermal error model training process. The accuracy of the derived models can be further enhanced by including additional significant thermal modes.

CHAPTER 4

THERMAL ERROR COMPENSATION STRATEGY BASED ON THERMAL LOOP ANALYSIS

4.1 Introduction

The dimensional accuracy of machined workpieces is highly dependent on the amount of machine tool errors (Hocken, 1980). Geometrical and kinematic errors, thermal errors, and dynamic errors are the major sources, which prevent the machine tools from achieving high accuracy. With the improvement of machine tool positioning accuracy, thermal errors currently become more significant in their contribution to the total errors (Ni, 1997). The heat generated by moving axes and machining processes create thermal gradients inside the machine tool structure, resulting in the thermal elongation and bending of machine tool elements, which substantially deteriorate the machine tool accuracy.

Thermal error compensation is one of the widely employed techniques to reduce the thermal errors due to its cost-effectiveness and ease-to-implement. Conventionally, temperature sensors are placed at a number of locations on the machine structure, and a model is then derived to calculate the thermal deformation from these temperature measurements (Donmez et al., 1986; Chen et al. 1993; Chen, 1996a). Engineering judgment and trial-and-error play an important part in deciding the number and

placement of required sensors. Moreover, the models describing the relationship between temperature and thermal deformation are usually derived empirically, which may cope well with training conditions, but cannot generally make accurate predictions under the operating conditions that have never been experienced. To improve the applicability and robustness of thermal error models, statistical approaches (Kurtoglu, 1990; Lo et al. 1995; Lee and Yang, 2002) and various modeling methods (Chen et al., 1996; Yang et al., 1996; Yang and Ni, 2003 and 2005a) are then utilized. However, as is summarized by Ni (1997), optimal sensor placement, lengthy machine characterization period and robust thermal error modeling are still the major barriers, restricting the more extensive applications of thermal error compensation techniques.

In order to resolve the abovementioned barriers, the machine tool thermo-elastic relationship must be profoundly investigated (Lo, 1994; Ma, 2001), thus obtaining insights into the essence of machine tool thermal behavior and providing theoretically potential solutions to the empirical model based thermal error compensation methods. In Chapter 4, an innovative thermal modal analysis has been proposed for the machine tool thermal error modeling. Machine tool thermal deformation is regarded to be dominated by a small number of dominant thermal modes. Temperature sensors are then placed to capture these dominant modes; and thermal error models are derived by linear regression to guarantee the robustness in terms of extrapolation and frequency sensitivity.

Though the effectiveness of thermal modal analysis has been demonstrated through simple machine tool element, an entire machine tool, consisting of several machine tool components, is generally too complicated to deal with. In addition, thermo-elastic behavior of machine tool joints is relatively subtle in mechanism; the assumption

of perfect thermal contact or insulation is usually not adequate. Furthermore, the advent of the Reconfigurable Machine Tool (RMT), which is designed for the rapid changes in productivity and in market demand, requires the characteristics such as modularity, interchangeability, etc., but still being cost-effective for the thermal error compensation system (Koren et al., 1999).

In this Chapter, a thermal loop analysis is proposed for the application of thermal error modeling and compensation of an entire machine tool. A systematic methodology is developed to quantify the volumetric errors through decomposition and reassembly of the machine tool. This approach could be further applied to a five-axis machine tool to compensate for the thermal errors, thus significantly enhancing the machining accuracy.

4.2 Thermal Loop Analysis

The basic idea of the thermal loop analysis is to decompose a machine tool into several machine elements as in the modular machine tool design. In general, it is more convenient to investigate the thermal behavior for these machine elements, such as the machine tool spindle, driving systems by ball-screw or linear motor, feedback devices, machine body structure, etc., rather than the machine tool as a whole. Moriwaki and Shamoto (1998) estimated the spindle thermal displacement based on the measurement of the rotational speed and ambient temperature. Bossmanns and Tu (1999) developed a finite difference model to characterize the heat generation, heat transfer and heat sinks of a high-speed motorized spindle. Yoshioka et al. (2006) proposed thermal deformation control by considering heat balance in the aerostatic spindle system. Following this work, Xu et al. (2007) simulated the spindle bearing thermal behavior of a grinding machine by

the finite element analysis. Zhao et al (2007) estimated the thermal deformation of a CNC machine tool spindle based on the sensitivity analysis.

Kim and Cho (1997) and Yun et al. (1999) proposed a modified lumped capacitance method, genius education algorithm and the finite element method for the modeling of thermal errors of the ballscrew and guide way system. Wu and Kung (2003) numerically analyzed the thermal deformation of a ballscrew feed drive system under different feedrates and preloads, and estimated the heat sources through inverse analysis. Kodera et al. (2004) developed an optical telemeter system for the real-time estimation of ballscrew thermal elongation. Kim et al. (2004) proposed a scheme to describe the typical thermal behavior of a machine tool equipped with linear motors; and showed that linear motor's cooling systems could significantly affect the thermal behavior of a machine tool.

Alejandre and Artes (2006) presented an approach to identify and estimate the non-linearities caused by the linear encoder to improve thermal error correction procedures. Huo et al. (2004) used the finite element analysis to describe the temperature distribution of an entire grinding machine tool structure. Suh and Lee (2004) investigated the thermal characteristics of composite sandwich structures for machine tool parts by both numerical simulation and experiments.

To certain extent, thorough understanding and accurate description of the thermal behavior of machine elements have been achieved compared with that of an entire machine tool. The major restriction for the thermal analysis of an entire machine tool is that the thermo-elastic behavior of machine tool structural joints has not been comprehensively clarified. A joint in a machine tool represents the contact between

elements with their contacting surfaces machined and characterized by a certain roughness and waviness. Attia and Kops (1979a, 1979b, 1980, 1981a, 1981b and 1993) showed that conduction is the only significant mode in the mechanism of heat transfer across the machine tool joint. The thermal deformation of structural elements in contact is affected significantly by the non-uniformity in the distribution of the thermal contact resistance. The contact resistance of the joint is further controlled by the contact configuration, the thickness of the interfacial gap and the thickness of the surface film. In addition, factors like external loading, surface texture and material properties of structural elements, contact pressure, thermal field and mechanical constraints have influences on the behavior of the machine tool joint as well.

Consequently, the assumption of perfect thermal contact or insulation does not always hold, considerably increasing the difficulty in accurately simulating the thermal behavior of the entire machine tool. In addition, most existing analysis of an entire machine tool merely concentrated on the nominal configuration, without considering various possible locations due to each moving axis (Jedrzejewski and Modrzycki, 1992; Fraser et al., 1998b and 1999b; Attia and Fraser, 1999a and 1999b; Yang and Ni, 2003; Kang et al., 2007). In order to account for the position dependent thermal errors, multiple simulations have to be carried out repeatedly, which is time-consuming and labor-intensive. The concept of thermal loop is therefore utilized to resolve the abovementioned obstacles. The procedures of the thermal loop analysis, including thermal loop decomposition, thermal error modeling for each thermal link and thermal loop reassembly are presented systematically in what follows.

4.2.1 Framework of Thermal Loop Analysis

The framework of the proposed thermal loop analysis is shown in Figure 4.1. There are three basic modules for this analysis, namely, thermal loop analysis, thermal modal analysis and robust thermal error modeling. Thermal modal analysis and robust thermal error modeling have been elaborated on in Chapter 4. The details of thermal loop analysis will be presented in this Chapter. This thermal loop analysis is capable of facilitating the thermal modal analysis and thermal error modeling of each machine element in a virtual machine tool design environment. In addition, by using this methodology, a potential modularity platform could be constructed for the comprehensive integration of machine components.

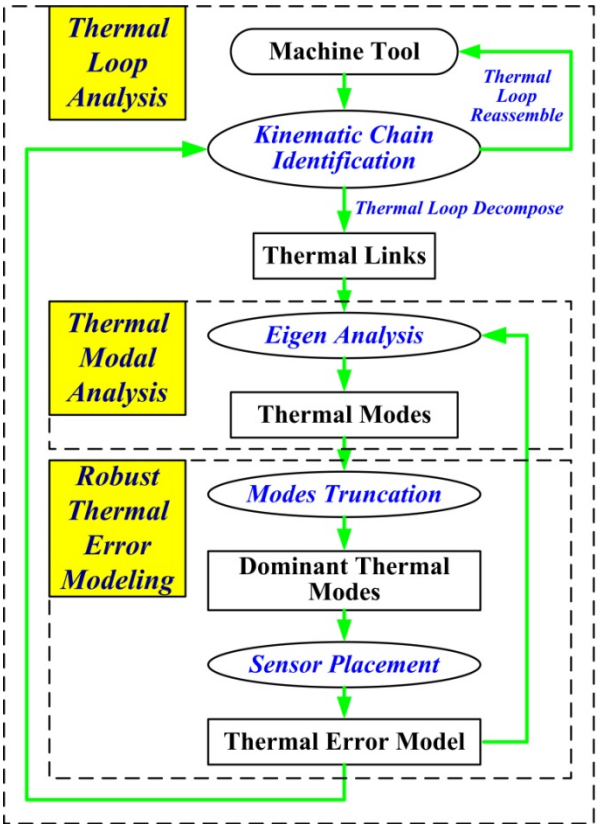

Figure 4.1 Framework of the thermal loop analysis

4.2.2 Structural Loop and Thermal Loop

A machine tool is an intricate system; in order to analyze the machine tool configuration, function of moving axes and operational stability, concepts of structural loop, thermal loop, metrology frame, etc. are proposed. Delbressine et al. (2006) developed a thermomechanical model to describe the thermal errors of a multi-axis machine tool based on the structural loop. Oiwa (2005) applied the compensation methods to improve moving accuracy of the parallel kinematics machine against temperature fluctuation and elastic deformations, and indicated that the measurement loop and force loop should be set apart because of the potential distortion of the metrology frame due to the imposed force.

Structural loop is defined as an assembly of mechanical components to maintain the relative position between specified objects (Schellekens et al., 1998). A typical pair of specified objects is a cutting tool and a workpiece; the structure loop includes the spindle shaft, the bearings and housing, the slide ways and frame, the drives, and the tool and work-holding fixtures. All mechanical components and joints in the propagation path from the drive to the point of reaction or the center of gravity must have a high stiffness to avoid deformations under changing loads. Figure 4.2 depicts two schematic structure loops, one for open frame configuration and the other for closed frame configuration (Slocum 1992).

Similar to the structural loop, a thermal loop is defined as a path across an assembly of mechanical components, which determines the relative position between specified objects under changing temperatures (Schellekens et al., 1998). Franse (1990)

mentioned that the thermal loop has both static and dynamic characteristics just like the structural loop.

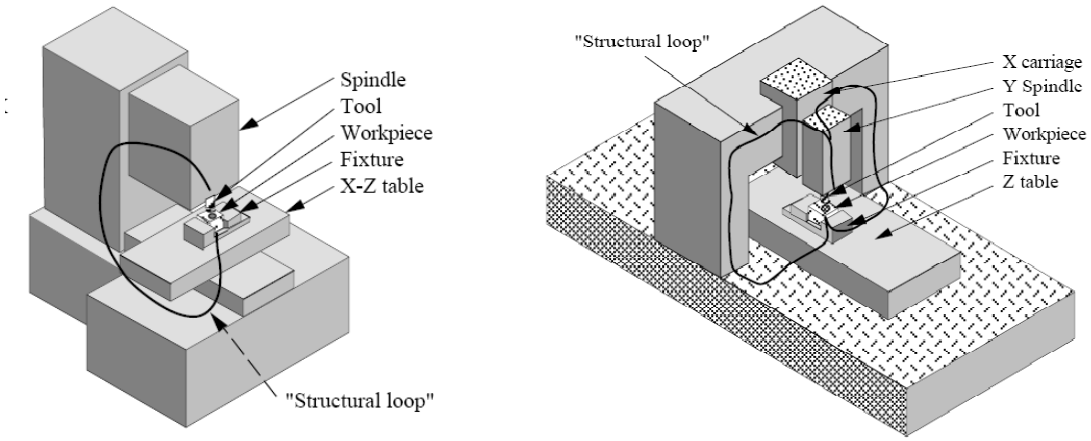

(a) (b)

Figure 4.2 Representative structural loops. (a) Open frame and (b) closed frame.

Split-up of machine tools in series or parallel paths is essentially helpful in recognizing good structural and thermal loop designs. Compared with closed frames, open frames are less structurally and thermally stable; and the lack of symmetry leads to undesirable bending moments and thermal gradients (Slocum, 1992).

The concept of the thermal loop is utilized to solidify the effectiveness and robustness of thermal error modeling and then improve the thermal error compensation efficiency. For a thermal loop, there are a series of thermal links from the cutting tool to workpiece; the resistance to temperature variation must be enhanced for each thermal link in the same manner as increasing the stiffness of the structural loop. In principle, a thermal loop should be kept as short as possible to minimize the influence of spatial thermal gradients.

4.2.3 Thermal Loop Decomposition and Modeling

The first step of the thermal loop analysis is to identify the thermal loop for a specific machine tool. The machine tool is then decomposed into several thermal links along the loop. Each thermal link, as an individual unit shown in Figure 4.3, corresponds to certain thermal deformation, either thermal elongation or thermal bending, and respectively contributes to the volumetric errors. For each thermal link with assumed length of L, the fixed and free ends represent the connecting joints with previous and subsequent thermal links along the thermal loop.

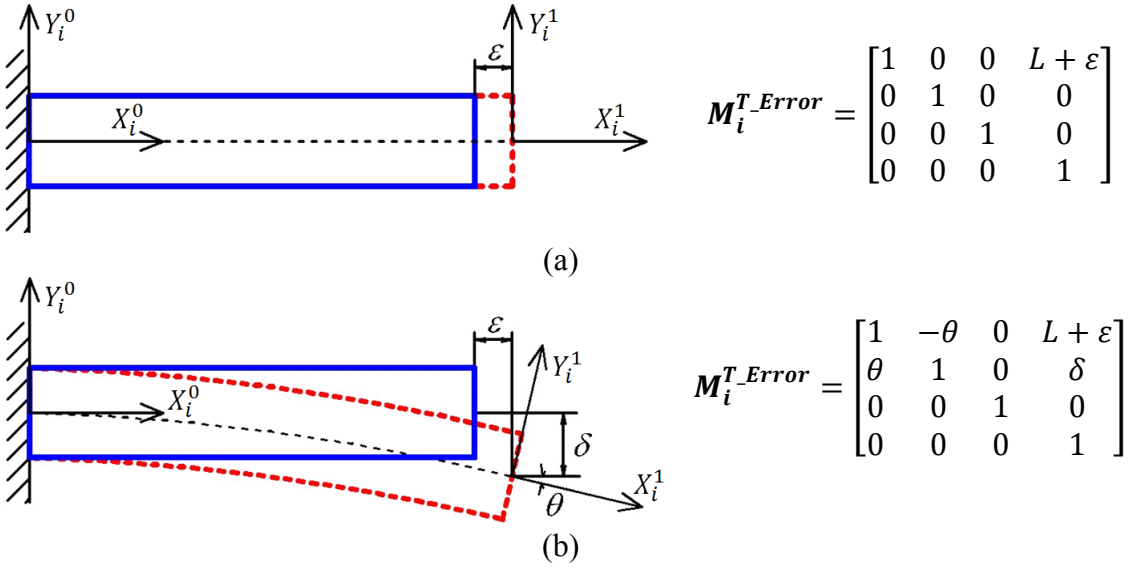

Figure 4.3 Representative thermal links with thermal deformation and HTMs. (a) Thermal elongation and (b) thermal bending.

The kinematic relationship between two connected links is described by the homogenous transformation matrix (HTM) between the assigned coordinate systems. Temperature sensor location and thermal error modeling of each thermal link is developed based on the thermal modal analysis. The overall dependence of the

volumetric errors on the thermal errors of each thermal link is finally established by vectorial addition and recombination of the thermal links in the thermal loop.

In order to account for the thermal errors of each thermal link, the established procedures for the volumetric error calculation, described in Appendix A, needs to be modified. Assume the kinematic chain, which indicates the kinematic relationship between the moving axes, of a machine tool to be

$$K_C = P_T K_{-m} \cdots K_{-1} G_R K_1 \cdots K_n T_L \tag{4.1}$$

where K_C denotes the kinematic chain, P_T, G_R and T_L are the part, ground and tool, and K_i, $i = -m, \cdots, -1, 1, \cdots n$, represents each machine element. For this configuration, there are m machine elements in the part branch (from P_T to G_R) and n machine elements in the tool branch (from G_R to T_L).

The HTM is employed to relate the thermal deformation of each thermal link and the thermal errors coupled with the geometric and kinematic errors due to the moving axes to the volumetric errors. The HTM from the tool coordinate system (TCS) to the part coordinate system (PCS) is expressed as

$$\boldsymbol{M_{PCS}^{TCS}} = \boldsymbol{M_{PCS}^{0}} \cdot \boldsymbol{M_{0}^{TCS}} = \left(\boldsymbol{M_{-0}^{T}} \cdot \boldsymbol{M_{-0}^{-1}} \cdot \cdots \cdot \boldsymbol{M_{-m}^{PCS}}\right)^{-1} \cdot \left(\boldsymbol{M_{0}^{T}} \cdot \boldsymbol{M_{0}^{1}} \cdot \cdots \cdot \boldsymbol{M_{n}^{TCS}}\right) \tag{4.2}$$

where $\boldsymbol{M_i^T}$ is added to indicate the thermal deformation of the specified thermal link, and $\boldsymbol{M_{i-1}^i}$ includes both thermal errors and geometric and kinematic errors induced by the moving axes. Volumetric errors, including positioning and orientation errors, can thus be obtained by using the HTMs for ideal and actual motions.

It is worth noting that thermal errors inevitably occur with the geometric and kinematic errors due to the time variant temperature gradients inside a machine tool. This portion of thermal errors can be conveniently embraced in the models for volumetric

errors as an addition of existing geometric and kinematic errors. However, the thermal errors induced by the thermal deformation of thermal links must be otherwise accounted for. That is the reason for the derivation of Equation (4.2), especially for the thermal loop analysis.

4.3 Numerical Illustration

In this Section, a simplified machine structure is simulated to demonstrate the proposed thermal loop analysis. Thermal errors are always time variant, and thus modeled as a function of time. But in this example, only thermal errors in the steady state are taken into account for the purpose of illustration. For a practical problem, the procedures must be repeated at each specified time interval.

Figure 4.4 shows the schematic 2D layout of this machine, which is conceptually similar to the arch-type Reconfigurable Machine Tool (Landers et al., 2001). Figure 4.4(a) represents the nominal configuration of this machine. The spindle unit can also be placed in two different locations, -10 Deg and 10 Deg with respect to the vertical axis for reconfigurable configurations 1 and 2, as depicted in Figures 4.4(b) and 4.4(c). In principle, this machine is capable of three-axis kinematics with one passive degree-of-freedom available for reconfiguration. The working space for each configuration is also indicated. The travel ranges for X-axis and Y-axis are 400 and 300 mm, respectively.

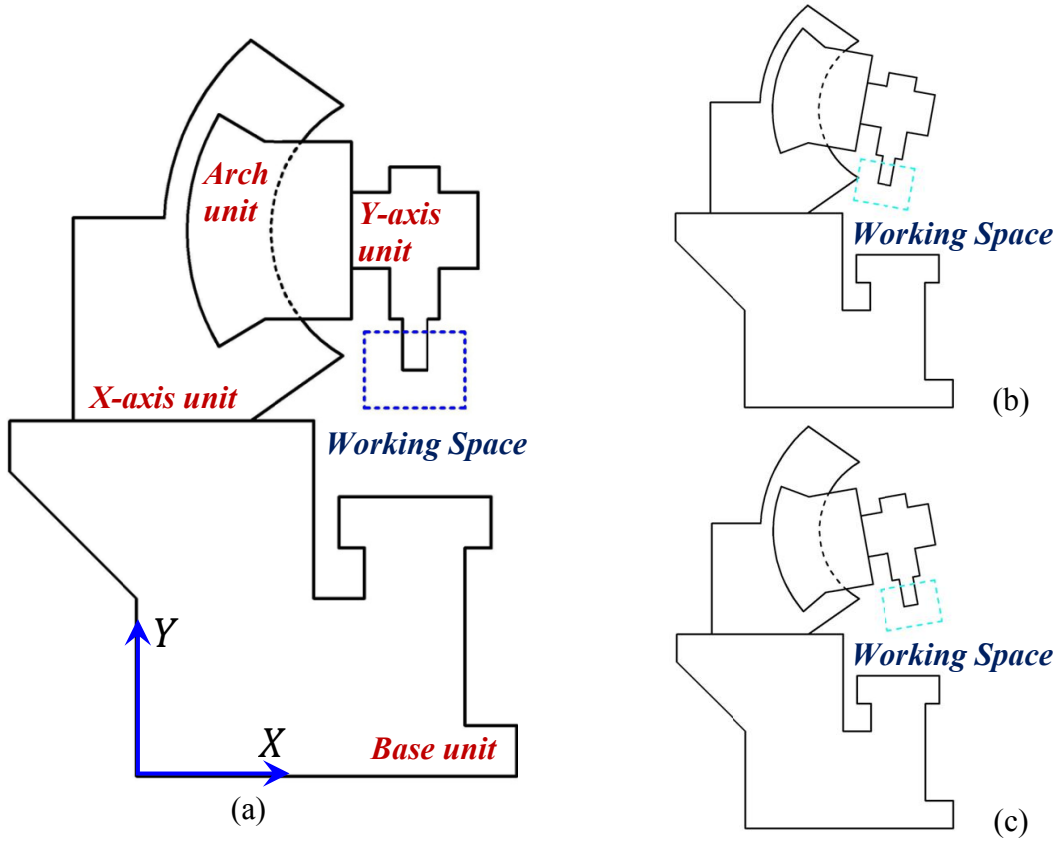

Figure 4.4 Schematic 2D layout of the reconfigurable machine tool. (a) Nominal configuration: 0 Deg, (b) reconfiguration 1: –10 Deg, and (c) reconfiguration 2: 10 Deg.

Through the thermal loop analysis, the machine tool is decomposed into four thermal links, which corresponds to the Base unit (link 0), *X*-axis unit (link 1), Arch unit (link 2), and *Y*-axis unit (link 3). The thermal loop is indicated in Figure 4.5 by the blue dotted line. For each link, two coordinates systems are assigned; the HTMs describing the thermal deformation of each link and the thermal errors between links according to the assigned coordinate systems are listed in Table 4.1.

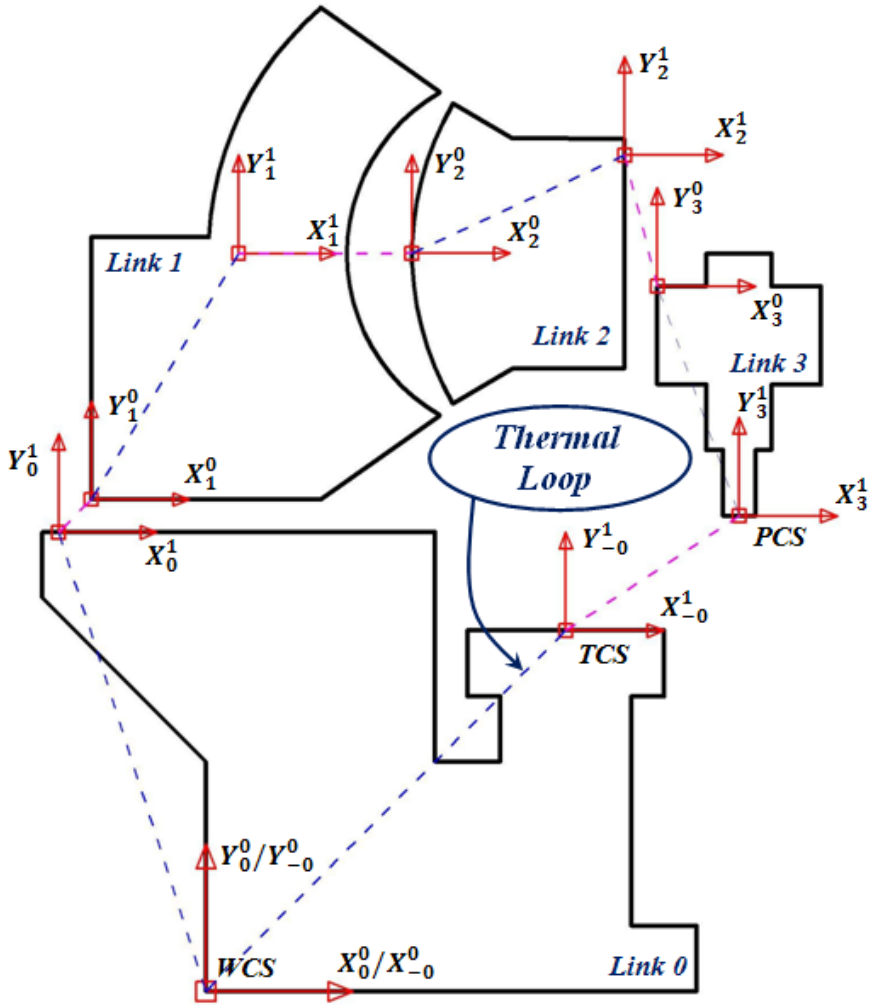

Figure 4.5 Thermal loop analysis for the machine tool in the numerical illustration.

Table 4.1 The HTMs for the numerical illustration of the thermal loop analysis.

	Link 0		Link 1	Link 2	Link 3
Link 0	$\boldsymbol{M_{-0}^T}$	N/A	N/A	N/A	N/A
	N/A	$\boldsymbol{M_0^T}$	$\boldsymbol{M_0^1}$	N/A	N/A
Link 1	N/A	$\boldsymbol{M_0^1}$	$\boldsymbol{M_1^T}$	N/A	N/A
Link 2	N/A	N/A	N/A	$\boldsymbol{M_2^T}$	$\boldsymbol{M_2^3}$
Link 3	N/A	N/A	N/A	$\boldsymbol{M_2^3}$	$\boldsymbol{M_3^T}$

The thermal deformation of each thermal link was separately simulated by using the finite element analysis. The heat sources were assumed to be the friction of moving axis. The simulated thermal deformation of each thermal link is shown in Figure 4.6.

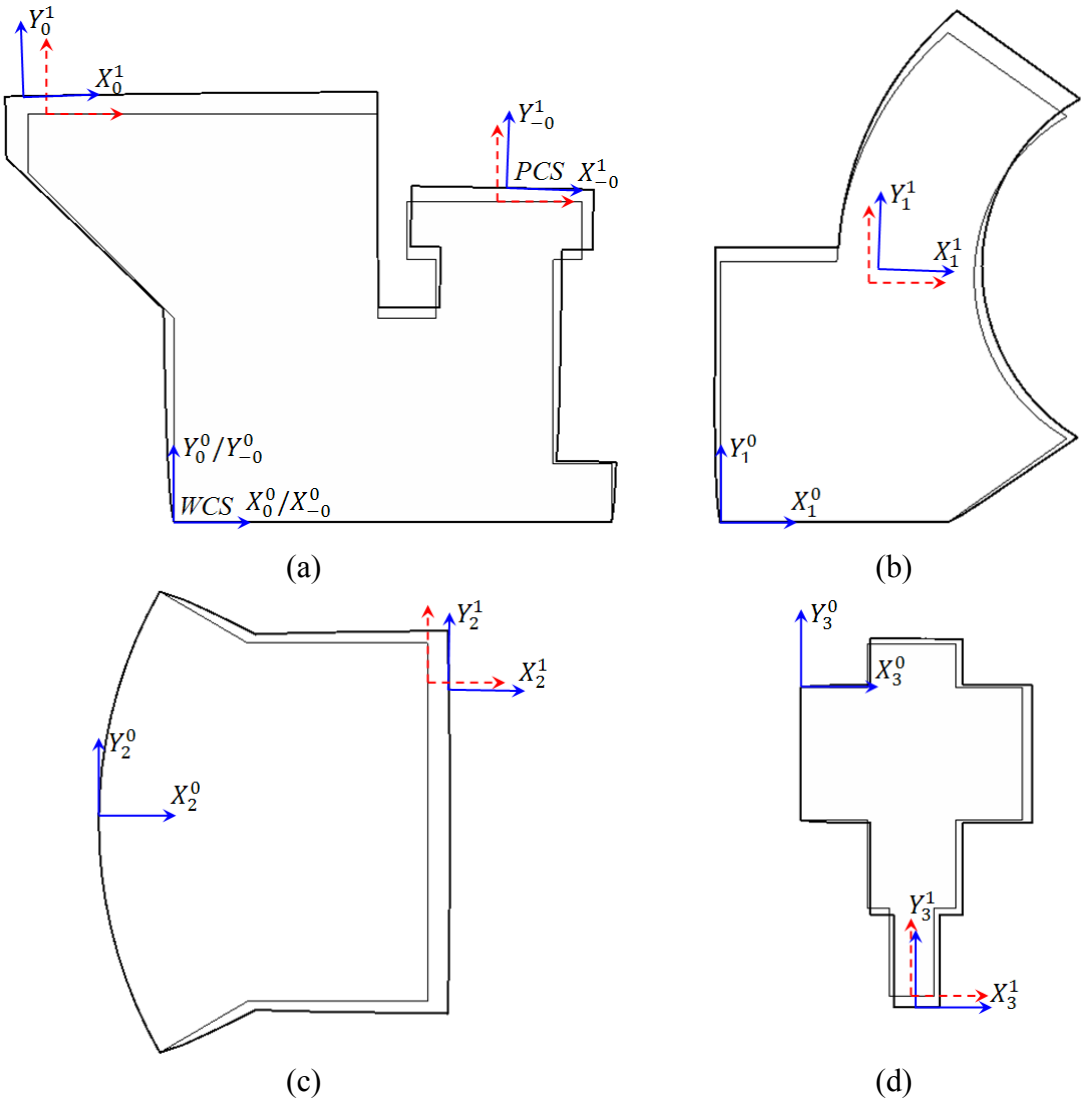

Figure 4.6 Thermal deformations of thermal links.
(a) Link 0, (b) link 1, (c) link 2, and (d) Link 3.

The corresponding thermal errors are summarized in Table 4.2, where ε, δ and θ indicate the expansion in X-axis, the deflection in Y-axis and the slope angle around Z-axis, respectively.

Table 4.2 Thermal deformation parameters for each thermal link.

	$\boldsymbol{M_{-0}^T}$	$\boldsymbol{M_0^T}$	$\boldsymbol{M_1^T}$			$\boldsymbol{M_2^T}$	$\boldsymbol{M_3^T}$
			-10 Deg	0 Deg	10 Deg		
ε (μm)	–74.38	27.14	10.99	8.53	7.83	41.39	11.18
δ (μm)	62.62	47.87	44.81	38.04	30.96	21.14	–22.83
θ (arcsec)	4.48	–20.43	–2.34	–48.17	–2.11	3.37	0.24

Figure 4.7 shows the position dependent thermal errors induced by each moving axis. $D_x(x)$, $D_y(x)$, $E_z(x)$ and $D_x(y)$, $D_y(y)$, $E_z(y)$ represent the linear errors and angular errors of X-axis and Y-axis, respectively. Because the origin position of each axis is assumed to be fixed, the thermal errors therefore either gradually increase or decrease due to the thermal expansion.

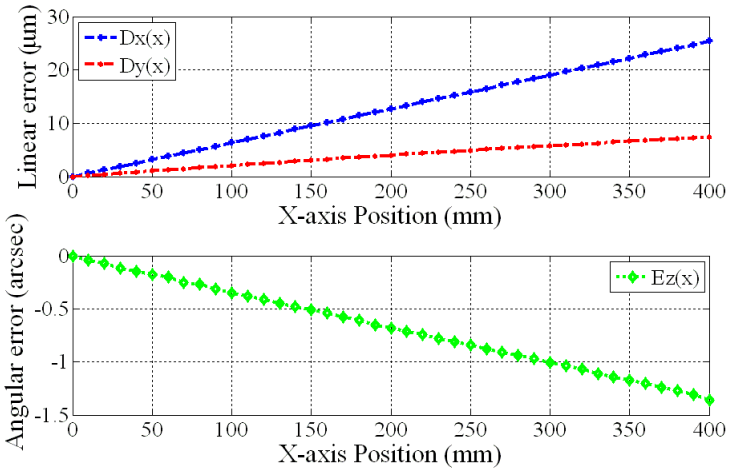

(a)

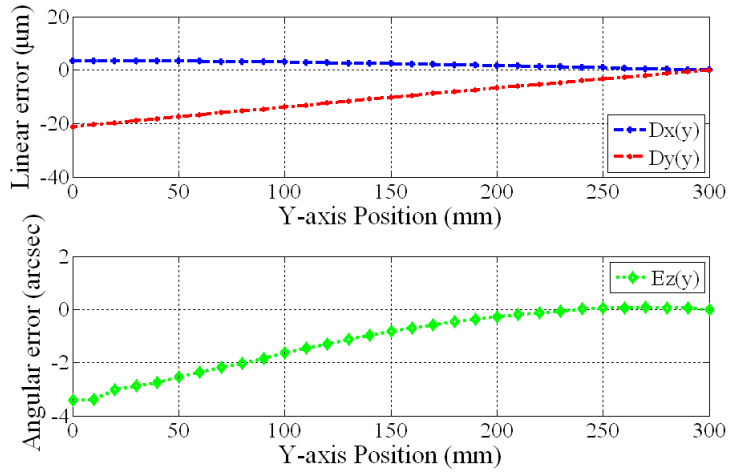

(b)

Figure 4.7 Thermal errors of the moving axis. (a) X-axis and (b) Y-axis.

These thermal errors summarized in Table 4.2 and Figure 4.7 are substituted into the HTMs shown in Figure 4.3; Equation (4.2) is then used to predict the volumetric errors, including both positioning and orientation errors within the working space. The results are shown in Figure 4.8 for the nominal configuration, where the linear and angular errors are amplified by factors of 10 and 1000 for the illustrative purpose. The grids and red dots indicate the ideal and actual locations of the tool tip. The line segments following the dots represent the actual tool orientation.

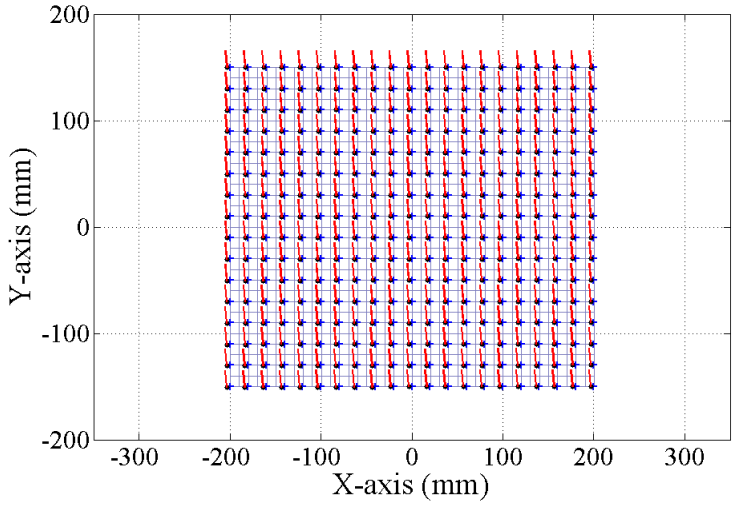

Figure 4.8 Volumetric errors within the working space for the nominal configuration.

The volumetric errors for the two reconfigurable configurations are shown in Figure 4.9. As is expected, the thermal loop analysis is able to predict the thermal errors of different configurations based on the results of the machine elements. This substantially facilitates the utilization of the finite element method in the thermal error analysis and compensation of machine tools, thus reducing the redundant simulation and calibration for the potential configurations.

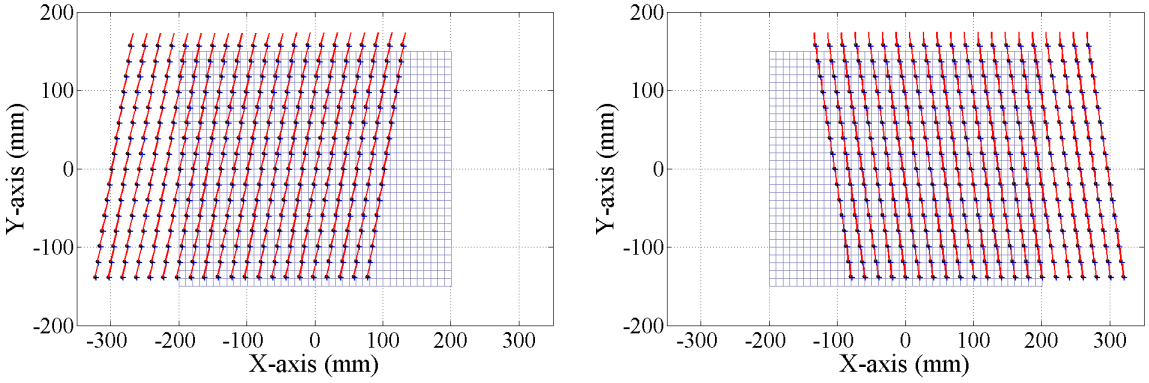

Figure 4.9 Volumetric errors within the working space for the reconfigurable configurations. (a) Reconfiguration 1: –10 Deg, and (b) reconfiguration 2: 10 Deg.

4.4 Experimental Verification

The thermal loop analysis is applied in this Section for the thermal error modeling and compensation of an EDM (electrical discharge machining) machine. The whole procedures including thermal loop decomposition and reassembly and thermal error modeling of each thermal link are presented. The effectiveness of the thermal loop analysis is verified through the comparison of the modeling and measurement results.

4.4.1 Thermal Loop Decomposition

Figure 4.10 shows the CAD model of a Sodick AQ55L EDM machine, which is a three-axis machine tool driven by linear motors with linear scales as the feedback devices for each axis. The main body and X and Y-axis are made of cast iron. The material of the Z-axis unit is ceramics. The travel ranges for X, Y, and Z-axis are 520, 360 and 320 mm, respectively.

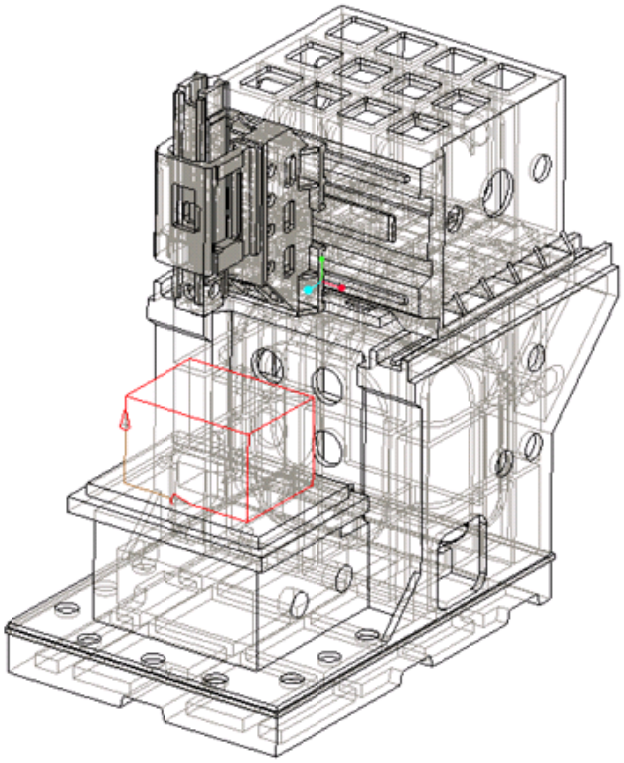

Figure 4.10 CAD model of Sodick AQ55L EDM machine (Courtesy of Sodick Inc.).

Based on the procedures of the proposed thermal loop analysis, the entire machine is decomposed into four major subassemblies (thermal links), the base (thermal link 0), the Y-axis unit (thermal link 1), the X-axis unit (thermal link 2) and the Z-axis unit (thermal link 3), as shown in Figure 4.11. Two coordinate systems are assigned to each thermal link for the prediction of thermal deformation at the tool tip.

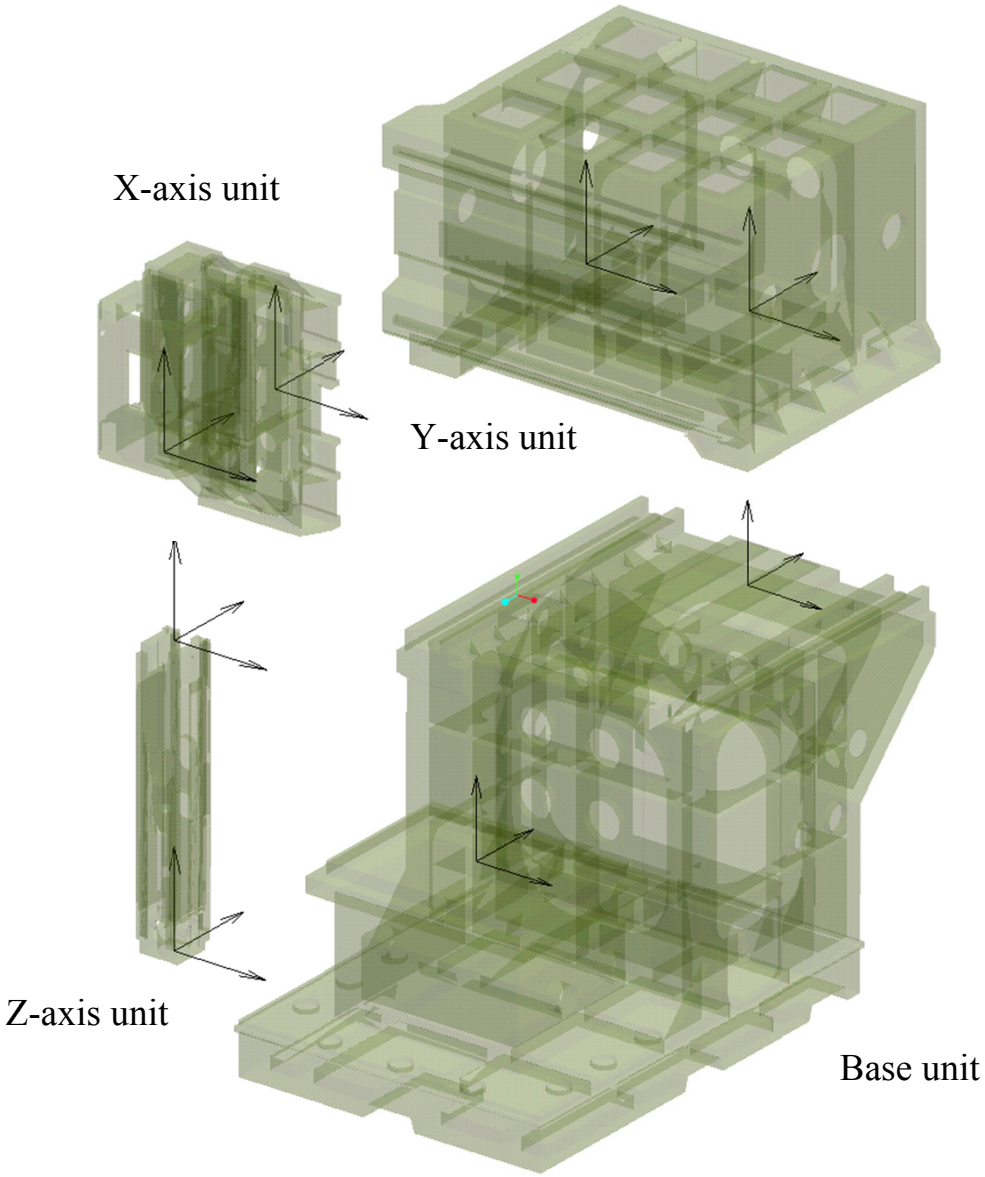

Figure 4.11 Disassembly of Sodick AQ55L EDM machine.

4.4.2 Thermal Modal Analysis for Each Thermal Link

Thermal modal analysis is performed for the determination of the dominant thermal modes and the thermal error modeling of each thermal link.

Temperature Sensor Placement

During the finite element analysis for each thermal link, the heat sources are assumed to be from the heat of the linear motor coils and the friction of bearings. The boundary conditions are assigned to give rise to relatively reasonable results in terms of the agreement between simulated and measured time constants. The weight distribution of thermal modes is estimated for the selection of the dominant thermal modes. Temperature sensors are then decided based on the plots of the corresponding temperature distribution fields.

The weight distributions and the first three dominant temperature distribution fields for each thermal link of the EDM machine are shown in Figures 4.12 to 4.19. It is obvious that several thermal modes govern the entire thermal process, which is desired because a small number of temperature sensors could be enough for an accurate and robust thermal error model of each thermal link. Due to the nature of temperature distribution fields, only temperature ranges are indicated in the plots.

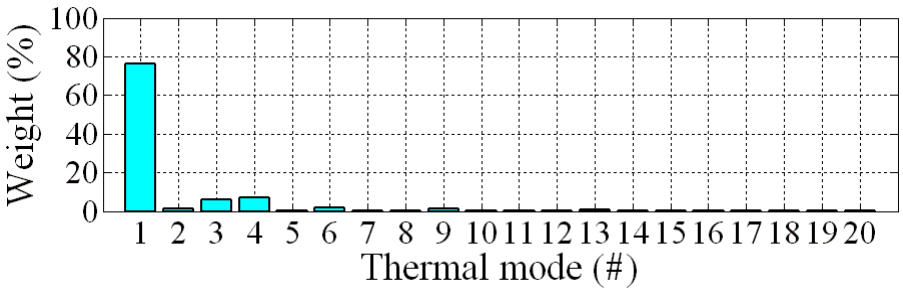

Figure 4.12 Weight distributions of thermal modes for the *Z*-axis unit (thermal link 3).

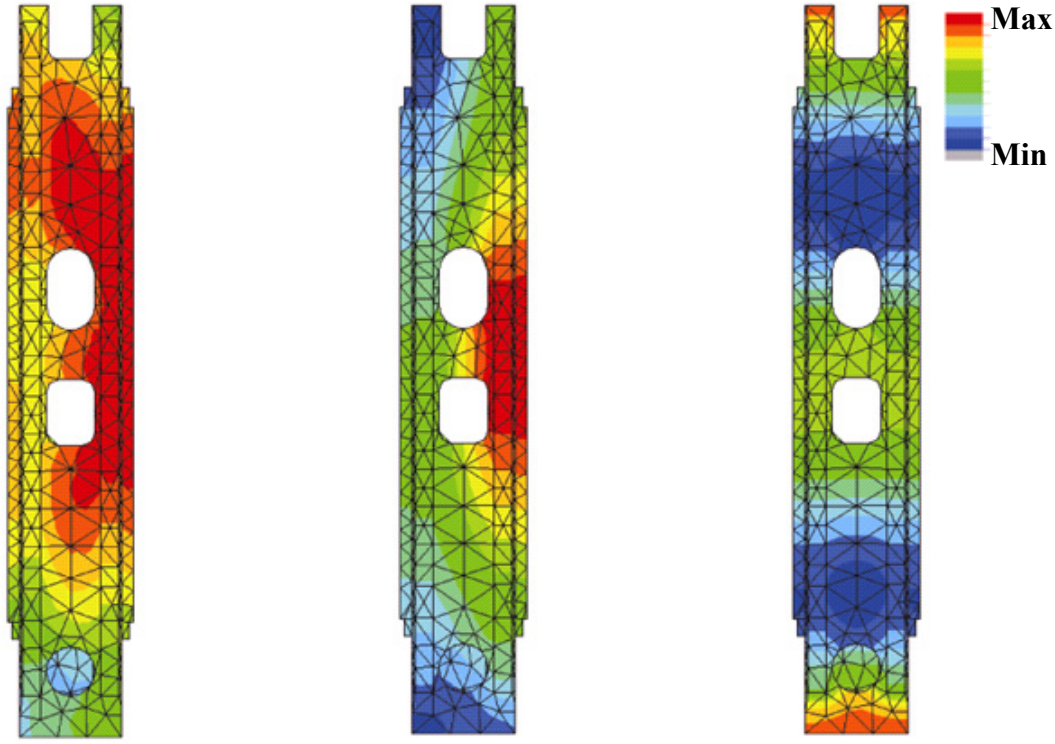

(a) (b) (c)

Figure 4.13 Temperature field distribution of dominant thermal modes for the *Z*-axis unit (thermal link 3). (a) Mode 1, (b) Mode 3, and (c) Mode 4.

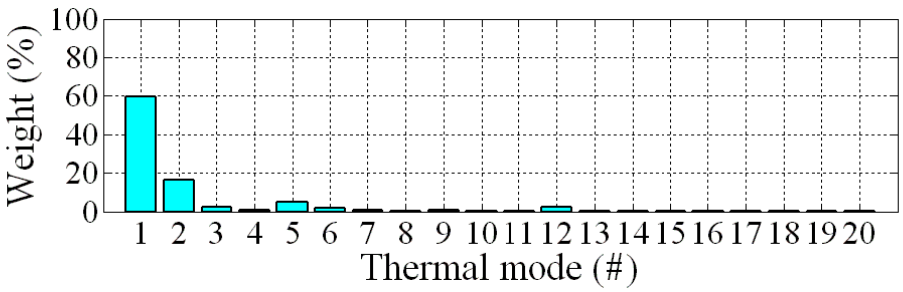

Figure 4.14 Weight distributions of thermal modes for the *X*-axis unit (thermal link 2).

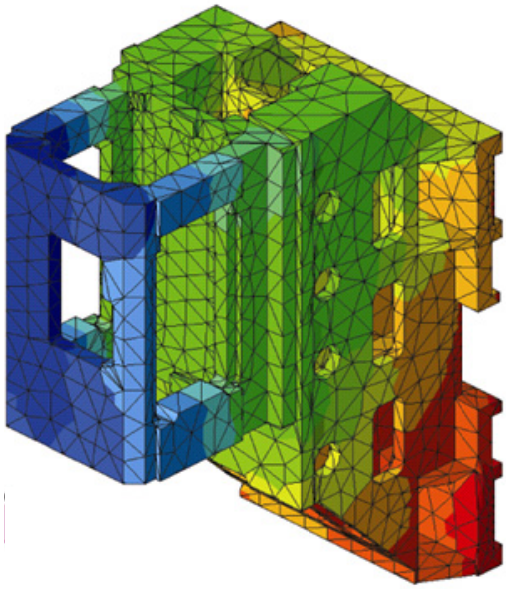

(a)

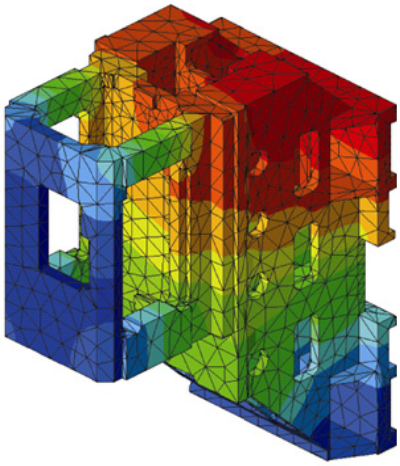

(b)

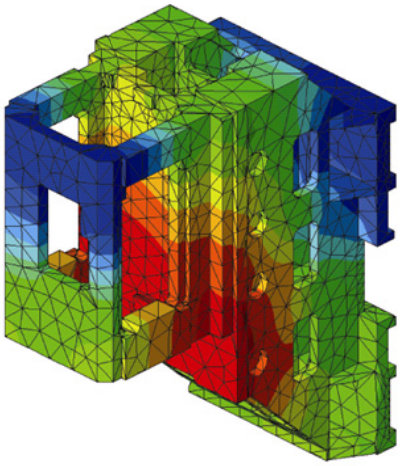

(c)

Figure 4.15 Temperature field distribution of dominant thermal modes for the *X*-axis unit (thermal link 2). (a) Mode 1, (b) Mode 2, and (c) Mode 5.

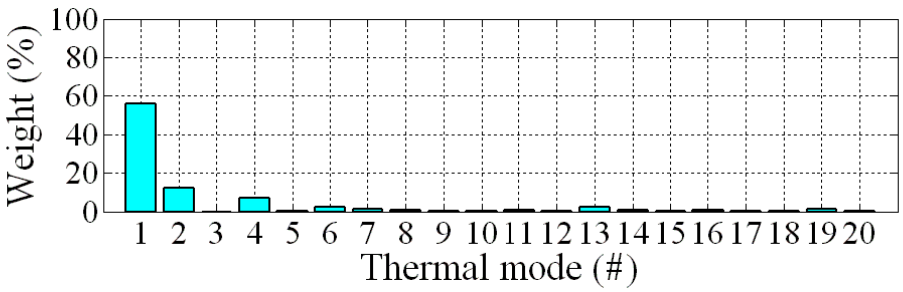

Figure 4.16 Weight distributions of thermal modes for the *Y*-axis unit (thermal link 1).

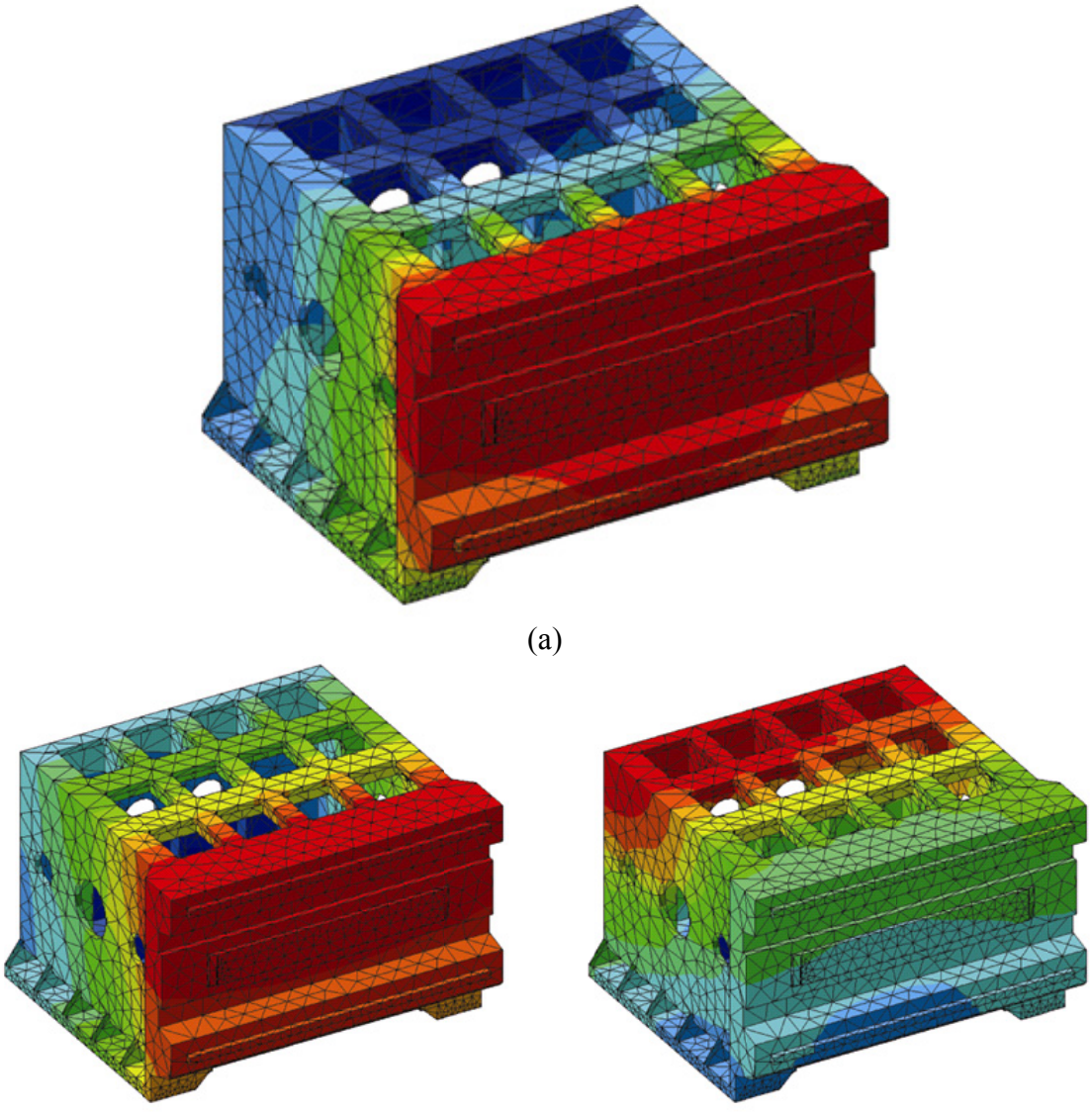

(a)

(b) (c)

Figure 4.17 Temperature field distribution of dominant thermal modes for the *Y*-axis unit (thermal link 1). (a) Mode 1, (b) Mode 2, and (c) Mode 4.

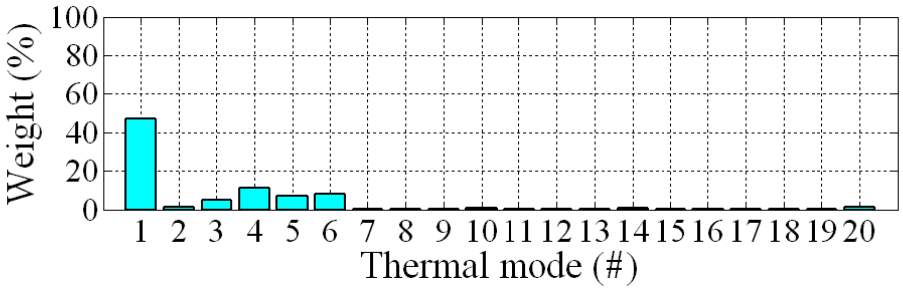

Figure 4.18 Weight distribution of thermal modes for the Base unit (thermal link 0).

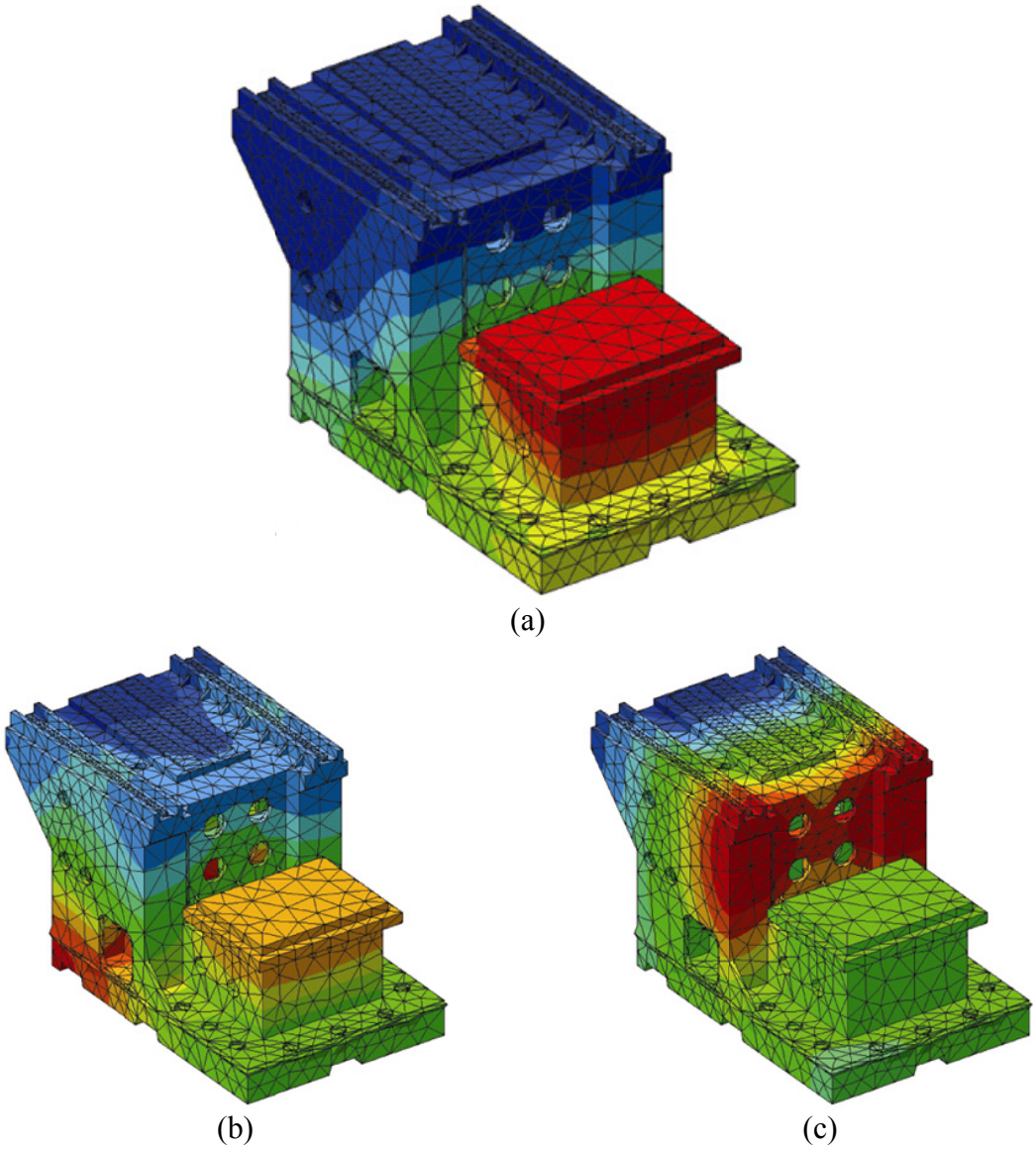

(a)

(b) (c)

Figure 4.19 Temperature field distribution of dominant thermal modes for the Base unit (thermal link 0). (a) Mode 1, (b) Mode 4, and (c) Mode 6.

Based on the temperature field distributions of the dominant modes for each thermal link, ten temperature sensors were mounted on the machine. These ten sensors are divided into several groups for the thermal error modeling of each thermal link. The locations of these temperature sensors are schematically illustrated in Figure 4.20. The detailed location for each temperature sensor is shown in the pictures in Appendix D.

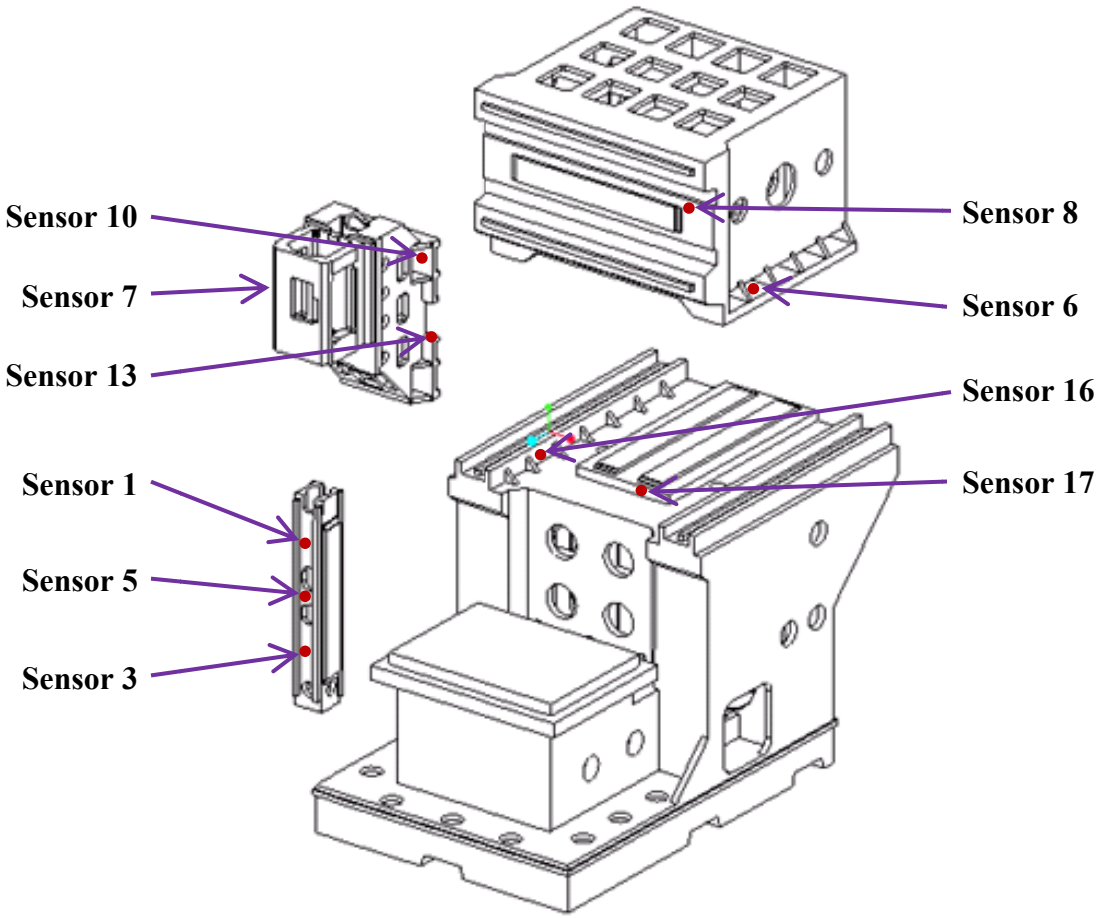

Figure 4.20 Temperature sensor placement scheme for Sodick AQ55L EDM machine.

Thermal Error Modeling

In order to derive the thermal models, each thermal link was warmed up separately, while maintaining the other thermal links unmoved. During the warming up,

that thermal link was programmed to move continuously. Thermal errors of each axis and the corresponding temperature sensor readings were collected.

For the thermal error modeling, a laser interferometer was used to measure the linear positioning accuracy along each axis. The measurement position interval is 16, 26 and 18 mm for Z, X and Y-axis, respectively. The measurement time interval is not constant, dependent on the span allowing a distinct temperature variation for the specific axis. The zero position of each axis was set according to the initial reading, and was not changed through the entire tests. Therefore, not only the position dependent thermal errors coupled with the geometric and kinematic errors but also the thermal deformation of each link itself along the measurement direction could be measured.

The collected overall errors including both geometric errors and thermal errors, the geometric errors, the thermal errors, the temperature variations, the thermal error modeling results, and the corresponding residual errors for each thermal link are shown in Figures 4.21 to 4.27.

For each axis, the measured thermal errors were first separated into geometric errors and thermal errors. The geometric errors are usually modeled by high-order polynomials. Thermal errors are modeled by the linear regression method described in Chapter 3.

Even though the temperature variation is not relatively significant due to the cooling system associated with linear motors, the thermal errors still contribute a notable portion compared with the geometric errors, especially for Z and X-axis.

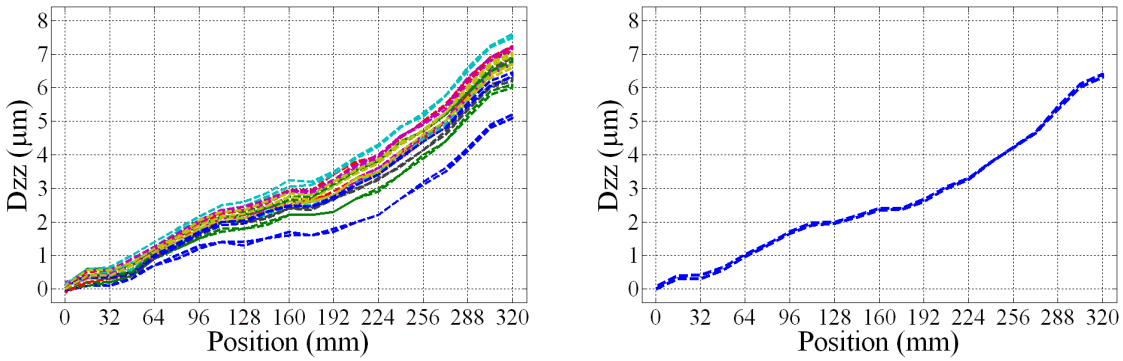

(a) (b)

Figure 4.21 Geometrie and thermal errors of *Z*-axis unit. (a) Geometric and thermal errors and (b) Geometric errors.

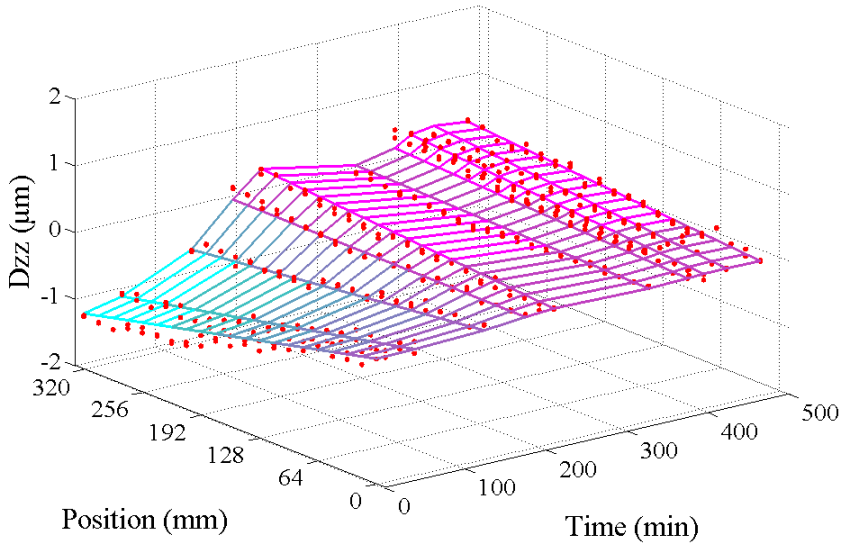

(a)

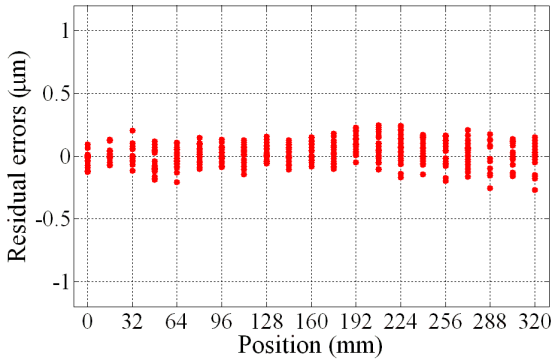

(b)

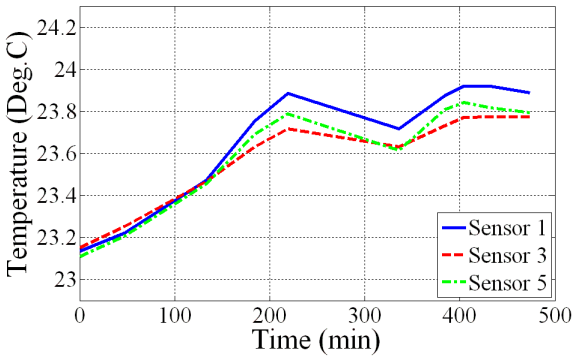

(c)

Figure 4.22 Thermal error model training I for *Z*-axis unit. (a) Thermal error model, (b) residual errors, and (c) temperature vairations.

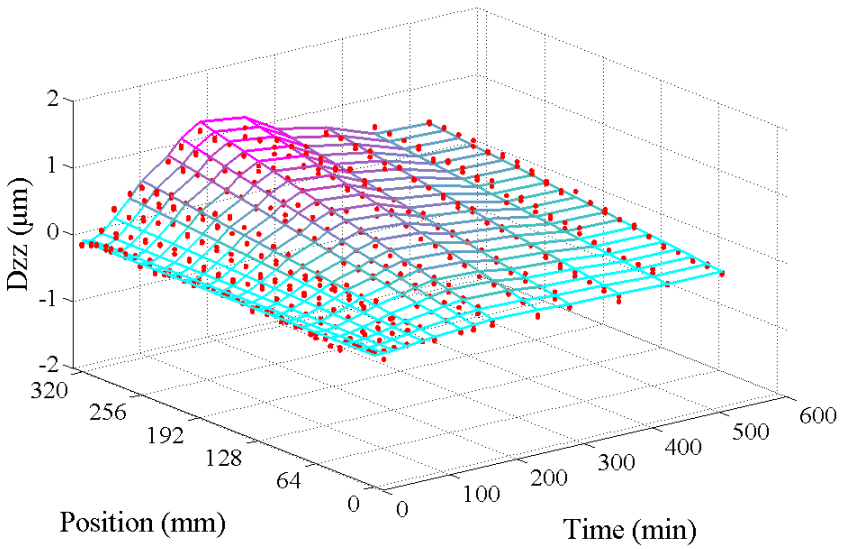

(a)

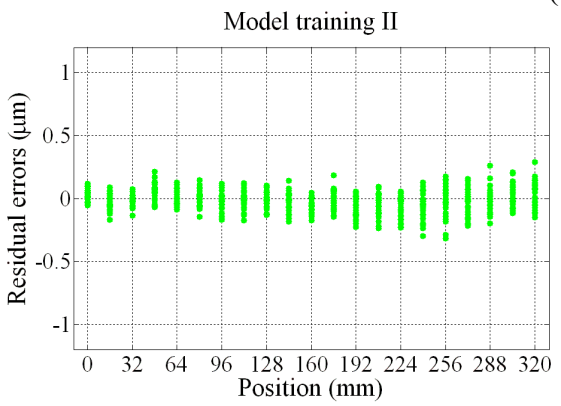

(b)

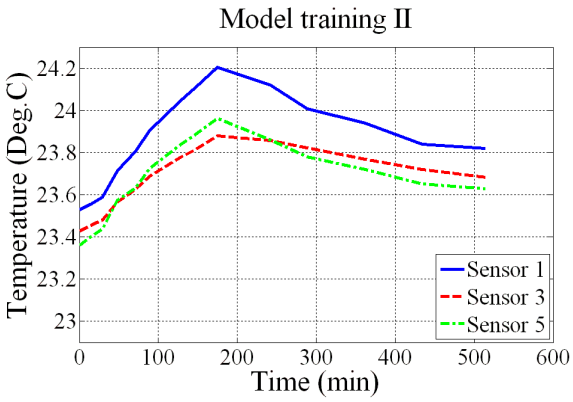

(c)

Figure 4.23 Thermal error model training II for *Z*-axis unit. (a) Thermal error model, (b) residual errors, and (c) temperature vairations.

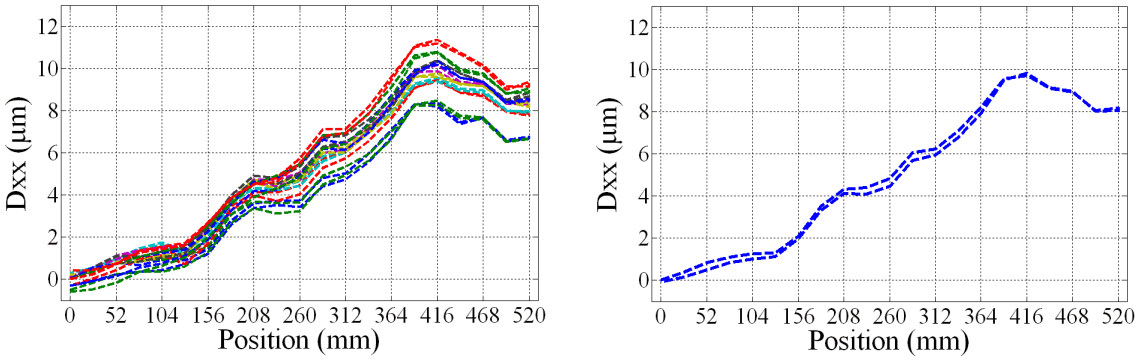

Figure 4.24 Geometrie and thermal errors of *X*-axis unit. (a) Geometric and thermal errors and (b) Geometric errors.

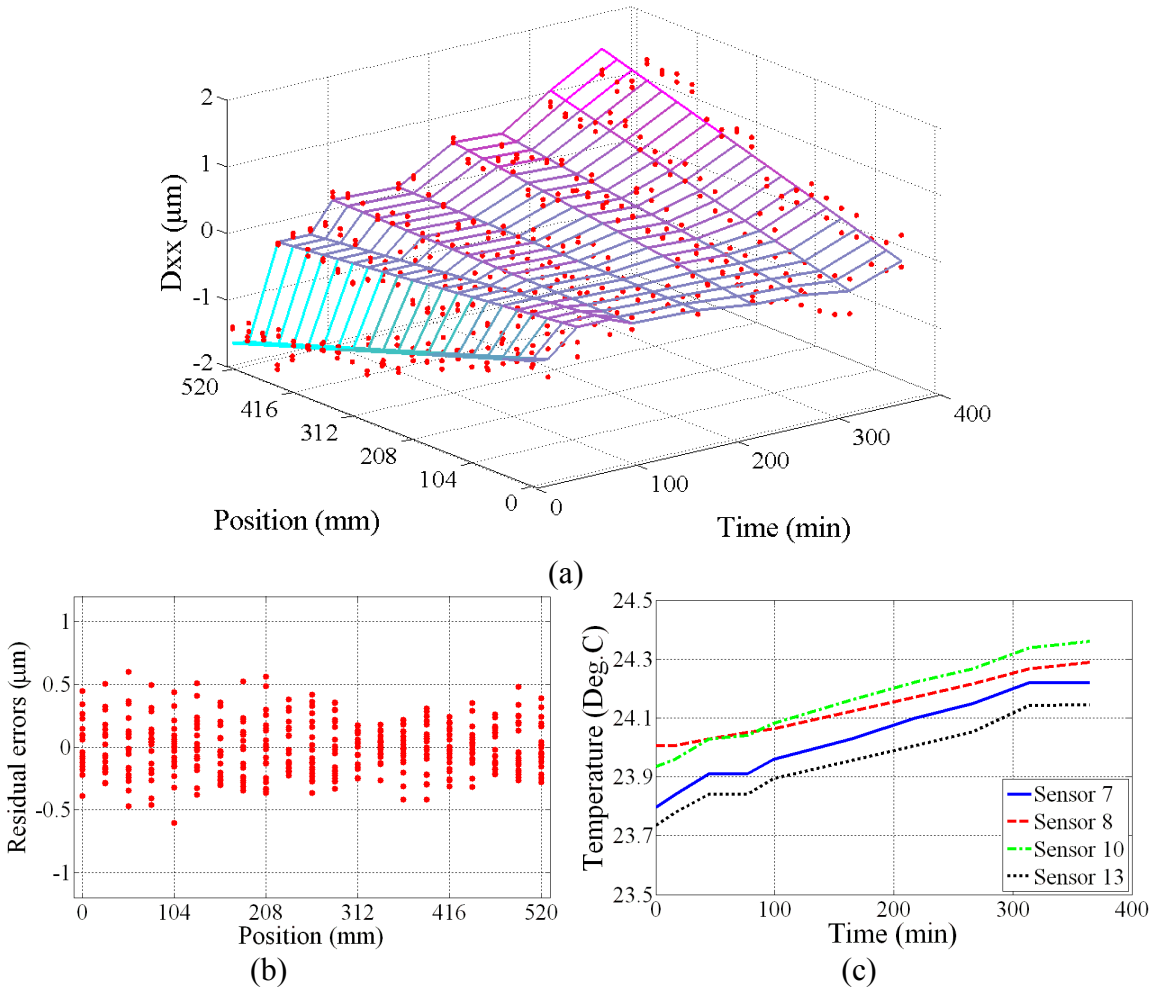

Figure 4.25 Thermal error model training for *X*-axis unit. (a) Thermal error model, (b) residual errors, and (c) temperature vairations.

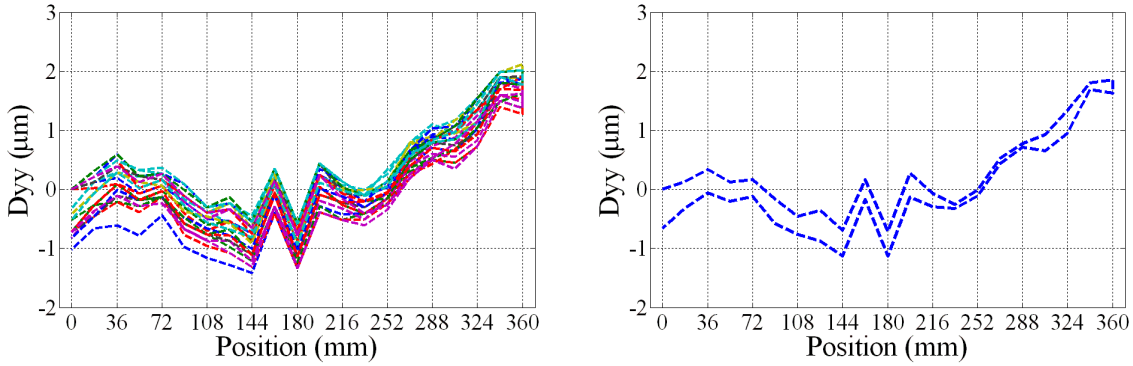

Figure 4.26 Geometrie and thermal errors of *Y*-axis unit. (a) Geometric and thermal errors and (b) Geometric errors.

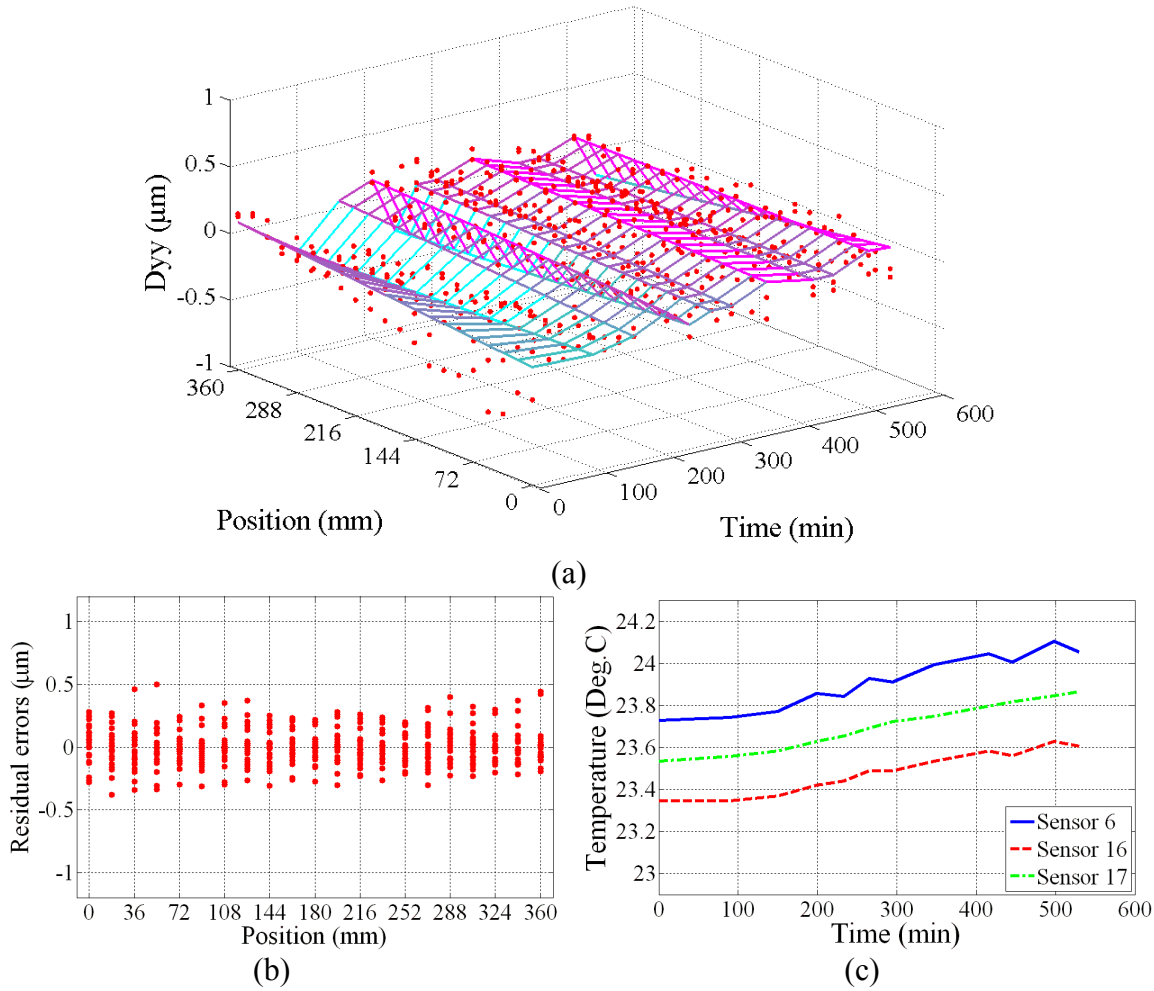

Figure 4.27 Thermal error model training for *Y*-axis unit. (a) Thermal error model, (b) residual errors, and (c) temperature vairations.

The mathematical models for thermal errors, $D_z(z)$, $D_x(x)$ and $D_y(y)$, are shown in Equations (4.3) to (4.5).

$$D_z^T(z,t) = [-3.35 + 0.40T_1(t) - 0.11T_3(t) - 0.15T_5(t)] + [-0.12 + 0.01T_1(t) - 0.01T_5(t)]P(z) \quad (4.3)$$

$$D_x^T(x,t) = [103.68 - 13.08T_7(t) - 12.48T_8(t) + 27.77T_{10}(t) - 6.64T_{13}(t)] + [-0.18 - 0.17T_7(t) - 0.02T_8(t) + 0.26T_{10}(t) + 0.02T_{13}(t)]P(x) \quad (4.4)$$

$$D_y^T(y,t) = [28.01 - 7.64T_6(t) - 10.20T_{16}(t) + 1.22T_{17}(t)] + [-0.05 - 0.01T_6(t) + 0.03T_{16}(t) - 0.19T_{17}(t)]P(y) \quad (4.5)$$

where the superscript T denote the thermal errors, $T_i(t)$ are the readings collected by the mounted temperature sensors, and $P(j)$ represents the nominal positions of each axis as indicated by the machine controller.

In the model training and verification plots, the dots and the surface denote the measured and modeled thermal errors, respectively. It can be seen from the plots of the residual errors that the linear positioning accuracy can be reduced to $-0.5 \sim 0.5$ μm range for the thermal errors of each axis. The advantage of the thermal modal analysis lies in the fact that thermal error models in compact forms are still capable of accurately and robustly accounting for the time variant thermal errors by capturing the essence of thermo-elastic relationship.

4.4.3 Thermal Loop Reassembly

The thermal error model for each thermal link is reassembled to predict the volumetric errors. In order to verify the results, the measurements of linear positioning accuracy along the face diagonal in the *XY*-plane and the body diagonal were compared with the predicted values by the thermal loop analysis. The results are shown in Figures 4.28 and 4.29.

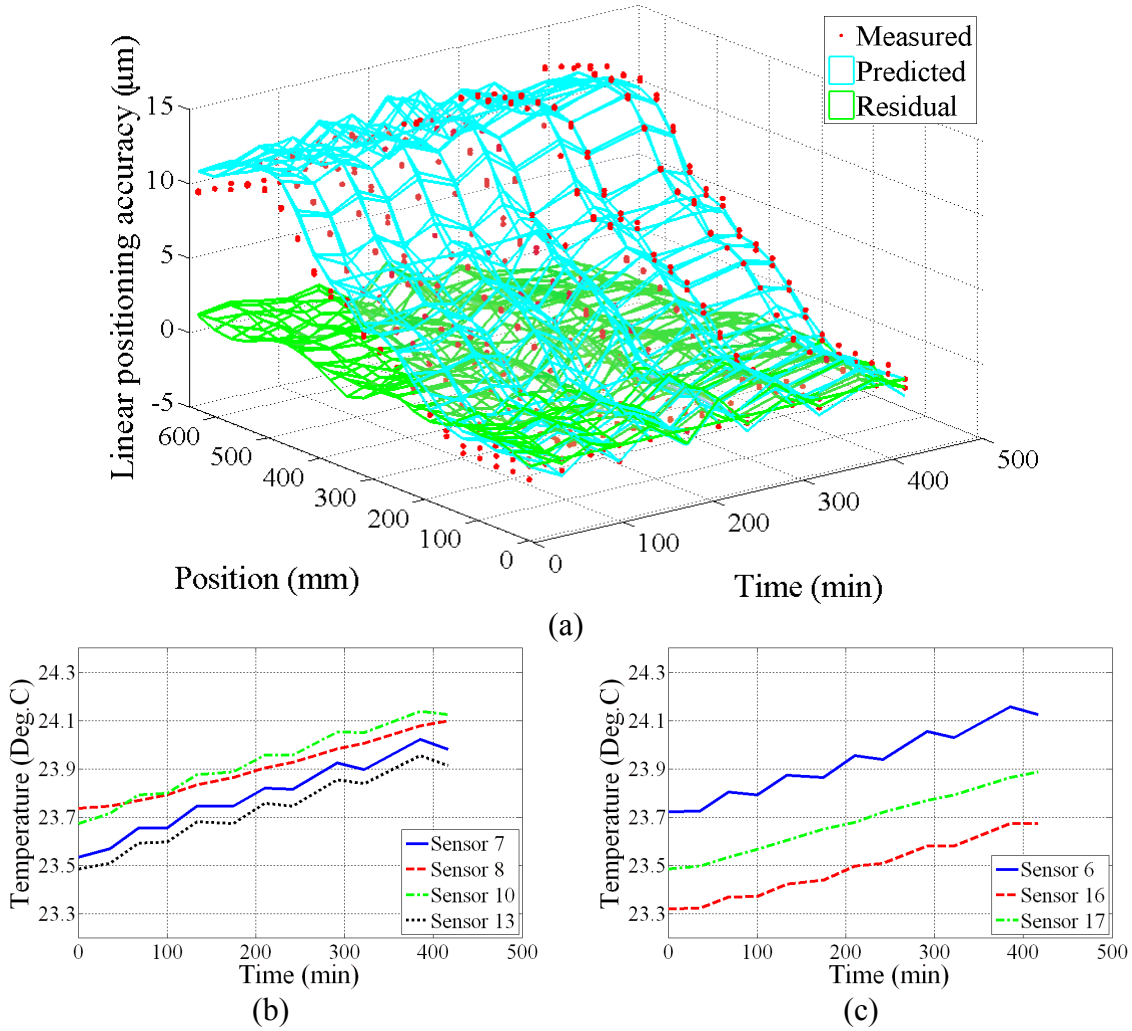

Figure 4.28 Modeling and measurement of linear positioning accuracy along *XY*-plane face diagonal. (a) Error modeling and verification, (b) temperature variation for *X*-axis, and (c) temperature variation for *Y*-axis.

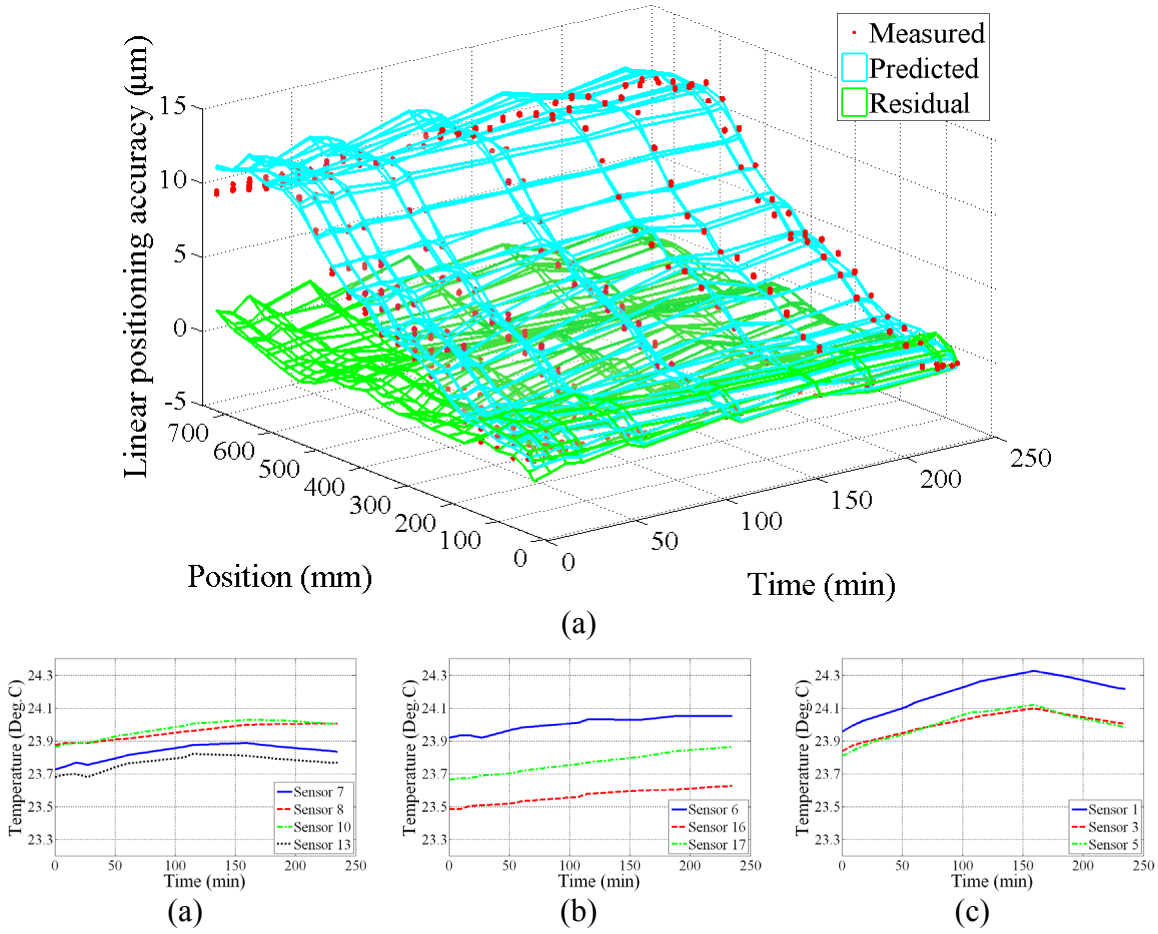

Figure 4.29 Modeling and measurement of linear positioning accuracy along body diagonal. (a) Error modeling and verification, (b) temperature variation for *X*-axis, (c) temperature variation for *Y*-axis, and (d) temperature variation for *Z*-axis.

In the plots of thermal error modeling and verification, the cyan surface, the red dots and green surface represent the predicted errors, measured errors and residual errors, respectively. The collected temperature sensor readings are divided according to the moving axis. As can be seen from the surfaces of residuals errors, the linear positioning accuracy along the face and body diagonal has been much enhanced in both temporal and spatial sense.

The measured errors and residual errors can be regarded as the linear positioning accuracy before and after implementing the error compensation. These errors are

collected and plotted in Figure 4.30, respectively for the face and body diagonal. Normal distributions are then fitted for the residual errors after compensation; the parameters, including mean and standard deviations, are summarized in Table 4.3.

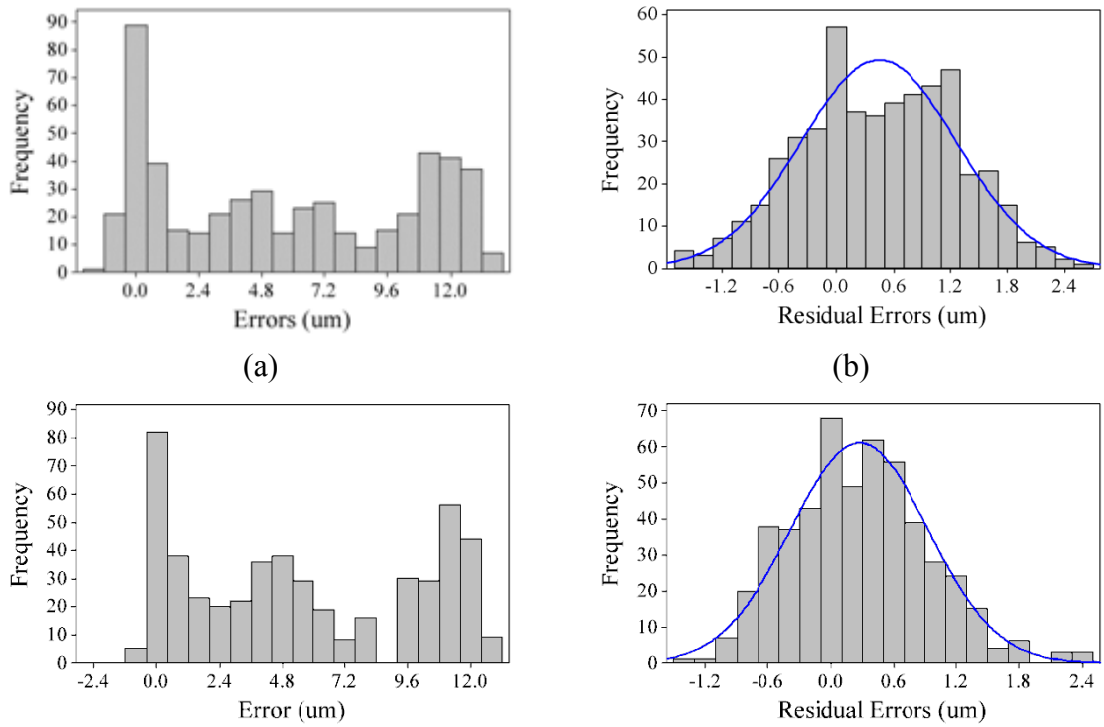

Figure 4.30 Histograms of linear positioning accuracy for (a) face diagonal before compensation (b) face diagonal after compensation, (c) body diagonal before compensation, and (d) body diagonal after compensation.

Table 4.3 Parameters of normal distribution for residual errors.

	Face diagonal	Body diagonal
Mean (μm)	0.45	0.27
Standard Deviation (μm)	0.82	0.66

Before compensation, the errors, shown in Figures 4.30(a) and (c), are relatively uniformly distributed due to the effects of position upon both geometric and thermal

errors. After compensation, however, the apparent evident of systematic errors have been removed, according to the normal distributions shown in Figure 4.30(b) and (d). Through the generalized thermal error compensation strategy, most of the geometric and thermal errors are accurately predicted and accounted for, the machining accuracy, therefore, can be significantly improved.

4.5 Summary

In this Chapter, the thermal loop analysis was proposed to describe the thermal behavior of an entire machine tool. The machine tool is first decomposed into several thermal links along the thermal loop; for each thermal link, thermal error models are developed based on the thermal modal analysis. These thermal links are finally reassembled to relate the thermal errors of each thermal link to the volumetric errors. A numerical example was used to illustrate the procedures of thermal loop analysis. This methodology was also applied for the thermal error modeling of an EDM machine; the effectiveness was validated through the comparison of the linear positioning accuracy prediction and measurement along the face and body diagonals.

Unlike the conventional FEA for a whole machine tool system, which is usually conducted at the nominal axis positions, the proposed thermal loop analysis is capable of modeling the positioning dependent thermal errors, which is usually coupled with geometric/kinematic errors. The thermal deformation inherent in each thermal link is also taken into account in the thermal loop analysis, which is sometimes ignored providing that the kinematic modeling based on the structural loop is utilized.

CHAPTER 5

ASSESSMENT OF ROTARY AXIS GEOMETRIC ERRORS BY USING TELESCOPIC MAGNETIC BALL BAR

5.1 Introduction

Traditional methods for machining complex surfaces on three-axis machine tools use ball-end cutters, and require long machining time, multiple setups and finishing process. Alternatively, five-axis machine tools have been utilized to reduce machining time and enhance machining accuracy during fabricating complex surfaces. The main advantages of five-axis machine tools over their three-axis counterparts are good geometric accommodation of the cutter to the surface of the workpiece, technically correct alignment of the cutter to the surface of the workpiece, small amount of jigs and fixtures, shorter machining time, and better surface finish (Takeuchi and Watanabe, 1992).

The consistent performance of any machine depends on the degree of its ability to position the tool tip at the required workpiece locations. This task is, however, largely constrained by the geometric errors either inherent in the machine or occurring during the machining process. Thompson (1989) stated that the availability of modern computational tools makes the application of active and pre-calibrated error compensation an economical alternative to designing and building for absolute accuracy.

In the past few decades, a large number of researches have been carried out to demonstrate the feasibility of geometric error measurement and compensation in three-axis machine tools. Based on an established error model, a compensation algorithm is adopted to eliminate the geometric errors, thus improving the machine accuracy. The error compensation in three-axis machines has delivered satisfactory results as long as the machine's operating conditions are well-defined and the geometric errors are repeatable.

Although geometric error measurement and compensation have been successfully implemented on three-axis machine tools, some barriers still exist, preventing this promising technique from being applied to five-axis machine tools. Relevant studies on the accuracy of five-axis machine tools are mainly confined to the theoretical simulation. One crucial barrier is the difficulty of measuring or identifying error components in the rotary axis due to the lack of proper measurement devices and algorithms. The complex structure and large number of error components is another major difficulty. Furthermore, the addition of two rotary axes makes the error compensation algorithm of five-axis machine tools extremely different from conventional three-axis machine tools.

Some methods have been summarized in ASME 5.54-1992 to measure the angular positioning error, which is one of the six motion errors induced by the rotary axis. All the proposed methods therein, however, have unavoidable deficiencies. The calibration interval of autocollimator with polygon approach is restricted by the number of faces of the polygon. The calibration accuracy by using laser interferometer with rotary indexer approach is limited by the accuracy of the rotary indexer; moreover, the laser alignment and calibration process is very time-consuming and labor-intensive. In

addition, these methods are not able to measure the error components other than the angular positioning error.

A Telescopic Magnetic Ball Bar (TMBB) and circular tests are exploited in this Chapter for the calibration of rotary axis. The TMBB was initially designed to collect the positioning inaccuracy of coordinate measuring machines and machine tools by Bryan (1982a and 1982b). Knapp (1983) developed a circular test method, utilizing a circular plate and a bi-directional displacement sensor. Kakino et al. (1987) applied the TMBB to the diagnosis of numerical controlled machine tools. Several similar measuring devices and methods were also developed by Ziegert and Mize (1994) and Lei and Hsu (2002a and 2002b).

The TMBB has been extensively explored for the measurement of error components of multi-axis machine tools. Hai (1995) developed a systematic approach to identify the error components of a machine tool. Wang and Ehmann (1999a and 1999b) developed two measurement methods to measure the total positioning errors at the tool tip of a multi-axis machine tool without the use of an error model. Abbaszadeh-Mir et al. (2002) presented a calibration algorithm identify link errors in a five-axis machine tool. A method based on the mathematical analysis of singularities of linear systems was used to assist in selecting a minimal but sufficient set of link error parameters. The effectiveness of this method was validated through numerical simulations. Lei and Hsu (2003) designed a 3D probe ball for the measurement of the link errors by moving each axes along some specific test paths and thus enhanced the accuracy of a five-axis machine. Tsutusmi and Saito (2003 and 2004) proposed two methods for identifying eight deviations inherent in a five-axis machine tool by means of a TMBB. One method

required four measurements by moving two linear axes and one rotary axis simultaneously, while the other required two measurements by moving two linear and two rotary axes simultaneously. But only numerical simulation was presented.

Though both the TMBB and the laser interferometer have been used for the rotary axis calibration, the TMBB is considered comparatively more appropriate than the laser interferometer under certain circumstances when the calibration accuracy is not the major concern. First of all, circular tests, as the main measurement approach for the TMBB, are completely compatible with the rotational motion of a rotary axis. In contrast, the laser alignment is always an issue for rotary table calibration using the laser interferometer, even though the precise rotary indexer has been employed. Moreover, the limited calibration range of the TMBB for linear axis calibration is no longer an issue for rotary axis calibration; on the other hand, the rotary indexer might be either too large or too heavy for the rotary axis to support, especially for those horizontally oriented rotary tables. Lastly, the TMBB is much easier to setup, providing more efficient assessment of the rotary axis.

In this Chapter, a quick assessment of rotary table by using the TMBB is proposed. The calibration algorithm based on the mathematical derivation is developed and further modified taking into consideration the setup errors and eccentricity. The feasibility and restriction are evaluated through the sensitivity analysis. Two estimation methods are separately utilized and compared for the error components estimation. The entire calibration procedures are demonstrated by measuring a commercially available rotary table, and the calibration results are compared with the pre-known values.

5.2 Rotary Axis Calibration Strategy

A Telescoping Magnetic Ball Bar (TMBB) is a measuring device consisting of two high precision spherical tooling balls of the same diameter connected by a rod, which is held by a socket at both ends and contains a displacement transducer allowing accurate measurement of the length variation of the ball bar as one socket moves with respect to the other.

When a TMBB is used to assess the accuracy of a rotary axis, one end of the TMBB is mounted on the rotary table, while the other end is attached to the spindle. The rotary axis, sometimes with linear axes as well, is programmed to following certain paths, mostly circular paths, while maintaining the nominal length of the ball bar. However, due to the errors induced by the rotational motion, the variation of the length would show certain error patterns. As a result, the associated error components can thus be estimated by an inverse kinematics analysis.

The calibration methods proposed in this Section are able to measure the error components induced by the movement of a rotary axis. The restriction of this method is discussed based on the analysis of the setup errors, particularly eccentricity.

5.2.1 Algorithm Derivation

There are six error components induced by the movement of a rotary axis. For a rotary axis, C, revolving around Z-direction, as depicted in Figure 5.1, three linear errors are two radial errors, $D_x(c)$ and $D_y(c)$, and one axial error $D_z(c)$, whereas three angular errors are two tilt errors, $E_x(c)$ and $E_y(c)$, and one angular positioning error, $E_z(c)$.

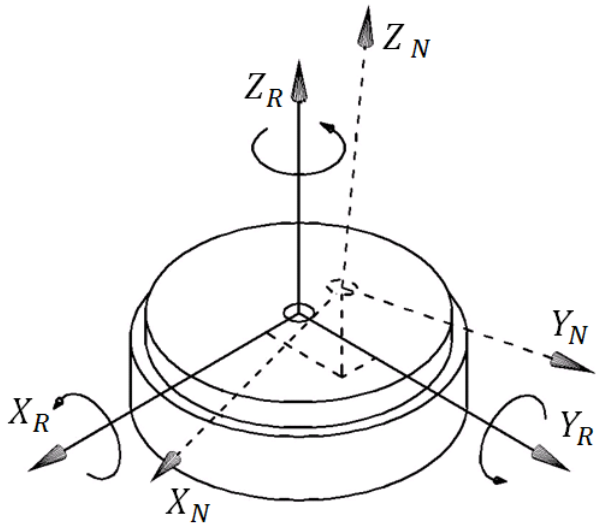

Figure 5.1 Error components induced by the rotational motion.

The schematic calibration setup is shown in Figure 5.2, where point O represents the center of the rotary table and points A and B represent the two ends of the TMBB. The nominal length of the TMBB is assumed to be equal to L. One stationary reference coordinate system, R, and one moving coordinate system, N, are assigned to the rotary table, respectively, for the derivation of the calibration model.

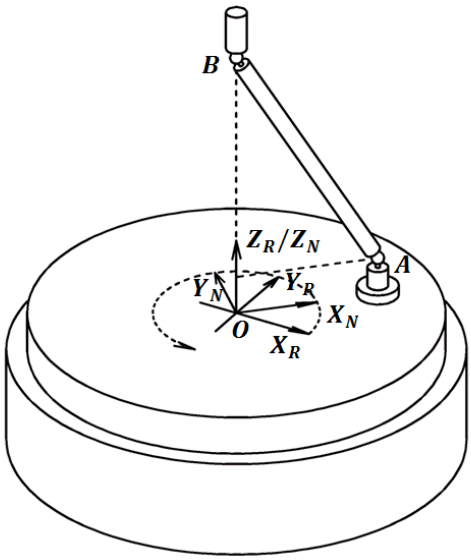

Figure 5.2 Schematic setup for rotary table calibration.

The homogeneous transformation matrices, $\boldsymbol{M_C}$ and $\boldsymbol{M_C^{Error}}$, describing the ideal and actual rotational motions of the rotary axis from moving coordinate system N to the reference coordinate system R are given in Equations (5.1) and (5.2),

$$\boldsymbol{M_C} = \begin{bmatrix} cos(c) & -sin(c) & 0 & 0 \\ sin(c) & cos(c) & 0 & 0 \\ 0 & 0 & 1 & 0 \\ 0 & 0 & 0 & 1 \end{bmatrix} \tag{5.1}$$

$$\boldsymbol{M_C^{Error}} \tag{5.2}$$

$$= \begin{bmatrix} cos(c) & -sin(c) & E_y(c) & D_x(c) \\ sin(c) & cos(c) & -E_x(c) & D_y(c) \\ E_x(c)sin(c) - E_y(c)cos(c) & E_x(c)cos(c) + E_y(c)sin(c) & 1 & D_z(c) \\ 0 & 0 & 0 & 1 \end{bmatrix}$$

where c is the angular positions of the rotary axis, C.

As shown in Figure 5.2, one end of the TMBB, A, is fixed at the rotary table, and its coordinates, $\overrightarrow{A_N}$, in the moving coordinate system N are

$$\overrightarrow{A_N} = \begin{bmatrix} R_x \\ 0 \\ R_z \\ 1 \end{bmatrix} \tag{5.3}$$

where R_x and R_z are the radial and axial distances from point A to point O in the moving coordinate system N. By using the transformation matrices in Equations (5.1) and (5.2), the ideal and actual coordinates of A in the reference coordinate system R, $\overrightarrow{A_R}$ and $\overrightarrow{A_R^E}$, are obtained

$$\overrightarrow{A_R} = \boldsymbol{M_C} \cdot \overrightarrow{A_N} = \begin{bmatrix} R_x \cos(c) \\ R_x \sin(c) \\ R_z \\ 1 \end{bmatrix} \tag{5.4}$$

$$\overrightarrow{A_R^E} = \boldsymbol{M_C^{Error}} \cdot \overrightarrow{A_N} = \begin{bmatrix} R_x \cdot [\cos(c) - E_z(c)\sin(c)] + R_z \cdot E_y(c) + D_x(c) \\ R_x \cdot [E_z(c)\cos(c) + \sin(c)] - R_z \cdot E_x(c) + D_y(c) \\ R_x \cdot [-E_y(c)\cos(c) + E_z(c)\sin(c)] + R_z + D_z(c) \\ 1 \end{bmatrix} \tag{5.5}$$

The other end of TMBB, B, is attached to the spindle, and its coordinates, $\overrightarrow{B_N}$, in the coordinate system N are

$$\overrightarrow{B_N} = \begin{bmatrix} 0 \\ 0 \\ H \\ 1 \end{bmatrix} \tag{5.6}$$

where H is the vertical distance from point B to point O in the moving coordinate system N. Because point B is stationary, independent of the rotation of the rotary axis, the real and actual coordinates of B in the reference coordinate system R, $\overrightarrow{B_R}$ and $\overrightarrow{B_R^E}$, are same as

$$\overrightarrow{B_R} = \overrightarrow{B_R^E} = \begin{bmatrix} 0 \\ 0 \\ H \\ 1 \end{bmatrix} \tag{5.7}$$

Based on the coordinates of two ends of the TMBB, points A and B, in the reference coordinate system R, the ideal and actual length of the TMBB during the movement of the rotary axis is expressed as

$$\vec{L} = \overrightarrow{A_R} - \overrightarrow{B_R} = \begin{bmatrix} R_x \cdot \cos(c) \\ R_x \cdot \sin(c) \\ R_z - H \\ 0 \end{bmatrix} \tag{5.8}$$

$$\overrightarrow{L^E} = \overrightarrow{A_R^E} - \overrightarrow{B_R^E} = \begin{bmatrix} R_x \cdot [\cos(c) - E_z(c)\sin(c)] + R_z \cdot E_y(c) + D_x(c) \\ R_x \cdot [E_z(c)\cos(c) + \sin(c)] - R_z \cdot E_x(c) + D_y(c) \\ R_x \cdot [-E_y(c)\cos(c) + E_z(c)\sin(c)] + R_z + D_z(c) - H \\ 0 \end{bmatrix} \tag{5.9}$$

where $\vec{L}$ and $\overrightarrow{L^E}$ are the ideal and actual length vectors of the TMBB, and three corresponding components indicate the magnitudes in the X, Y and Z-direction in the reference coordinate system R.

During a typical circular test, the length variation of the ball bar collected at a set of prescribed angular positions is the difference between the ideal and actual length

$$\Delta_1 = |\overrightarrow{L^E}| - |\vec{L}| \tag{5.10}$$

where $|\vec{L}|$ and $|\overrightarrow{L^E}|$ are the absolute magnitude of the ideal and actual length of the ball bar.

In order to estimate the error components, the difference between the square of the ideal and actual length of TMBB is explored

$$\begin{aligned}\Delta_2 = |\overrightarrow{L^E}|^2 - |\vec{L}|^2 \\ = -2R_x H \sin(c)\, E_x(c) + 2R_x H \cos(c)\, E_y(c) \\ + 2R_x \cos(c)\, D_x(c) + 2R_x \sin(c)\, D_y(c) + 2(R_z - H) \cdot D_z(c)\end{aligned} \tag{5.11}$$

As can be seen in Equation (5.11), Δ_2 is a function of both angular position, c, and five error components, $D_x(c)$, $D_y(c)$, $D_z(c)$, $E_x(c)$ and $E_y(c)$. Angular positioning error, $E_z(c)$, is not observable because it represents the difference between the actual angular position and the reference position, which is not able to be tracked by a TMBB. An external reference source, such as laser interferometer or autocollimator, must be utilized for the measurement of $E_z(c)$.

It is noted that rotary table is always axial symmetric, therefore, $D_x(c)$ and $D_y(c)$, and $E_x(c)$ and $E_y(c)$ can be assumed to be equivalent. This assumption is usually adopted by the rotary table vendors as well. $D_x(c)$ and $D_y(c)$ are regarded as the radial

runouts and $E_x(c)$ and $E_y(c)$ are regarded as the axial wobbles. In addition, these five error components are assumed to be constant during the rotational motion.

Error components induced by the rotary axis can be theoretically estimated based on Equation (5.11). However, setup errors have to be taken into account for the practical application of the proposed calibration approach. Eccentricity, due to the imperfect alignment of rotation axis between the rotary table and the ball bar, is always the critical factor influencing the circular test results. If assuming there exist eccentricity errors when locating point B right above the center point O, the coordinates of point B' in the moving coordinate system N, $\overrightarrow{B'_N}$, is therefore

$$\overrightarrow{B'_N} = \begin{bmatrix} H_x \\ H_y \\ H \\ 1 \end{bmatrix} \tag{5.12}$$

where H_x and H_y are the eccentricity errors along the X and Y-direction. Following the same derivation procedures above, the difference between the square of the ideal and actual length of the ball bar is attained

$$\begin{aligned} \Delta'_2 = |\overrightarrow{L^{E'}}|^2 - |\overrightarrow{L'}|^2 \qquad (5.13) \\ = -2R_x H \sin(c)\, E_x(c) + 2R_x H \cos(c)\, E_y(c) \\ + 2R_x \cos(c)\, D_x(c) + 2R_x \sin(c)\, D_y(c) + 2(R_z - H) \cdot D_z(c) \\ - 2R_x \cos(c)\, H_x - 2R_x \sin(c)\, H_y + H_x^2 + H_y^2 \end{aligned}$$

In Equation (5.13), additional terms have been introduced due to the eccentricity, $-2R_x \cos(c)\, H_x - 2R_x \sin(c)\, H_y + H_x^2 + H_y^2$, which are several orders larger than the remaining terms in magnitude; therefore, the eccentricity must be eliminated.

In order to remove the effects of the eccentricity errors, the proposed calibration procedures are correspondingly modified. Two setups with ball bars of different lengths, shown in Figure 5.3, are necessary for the isolation of the eccentricity. In the first setup, the two ends of the short ball bar with length $L1$ are located at the rotary table at point A and the spindle at point $B1$. In the second setup, the long ball bar with length $L2$ is used. The one end on the rotary table at point A maintains the same position; while the other end on the spindle is moving vertically up to point $B2$. But due to the eccentricity errors, the actual positions of points $B1$ and $B2$ are $B1'$ and $B2'$, respectively.

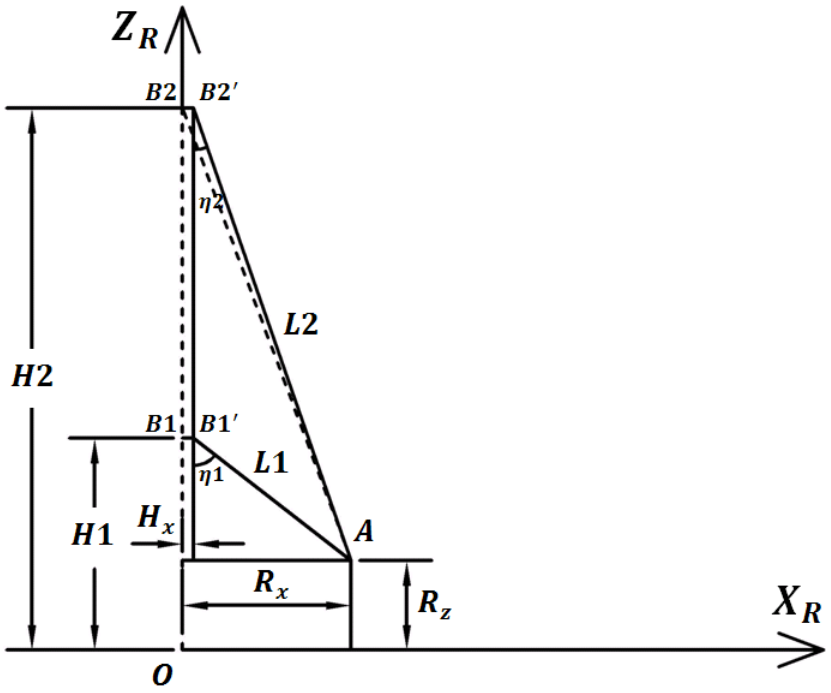

Figure 5.3 Modified rotary axis calibration setups.

According to Equation (5.13), the differences between the square of the ideal and actual length of the two ball bars with regard to the two setups are

$$\Delta_2'(L1) = -2R_x \cdot H1 \cdot \sin(c)\, E_x(c) + 2R_x \cdot H1 \cdot \cos(c)\, E_y(c) \tag{5.14}$$
$$+ 2R_x \cdot \cos(c)\, D_x(c) + 2R_x \cdot \sin(c)\, D_y(c) + 2(R_z - H1) \cdot D_z(c)$$
$$- 2R_x \cdot \cos(c)\, H_x - 2R_x \cdot \sin(c)\, H_y + H_x^2 + H_y^2$$

$$\Delta_2'(L2) = -2R_x \cdot H2 \cdot \sin(c)\, E_x(c) + 2R_x \cdot H2 \cdot \cos(c)\, E_y(c) \tag{5.15}$$
$$+ 2R_x \cdot \cos(c)\, D_x(c) + 2R_x \cdot \sin(c)\, D_y(c) + 2(R_z - H2) \cdot D_z(c)$$
$$- 2R_x \cdot \cos(c)\, H_x - 2R_x \cdot \sin(c)\, H_y + H_x^2 + H_y^2$$

where $H1$ and $H2$ are the height of point $B1$ and $B2$ from the surface of the rotary table.

Subtracting $\Delta_2'(L1)$ by $\Delta_2'(L2)$ yields

$$\Delta_2'(L1) - \Delta_2'(L2) \tag{5.16}$$
$$= 2R_x \cdot (H2 - H1) \cdot \sin(c)\, E_x(c) - 2R_x \cdot (H2$$
$$- H1) \cdot \cos(c)\, E_y(c) + 2(H2 - H1) \cdot D_z(c)$$

It can be seen from Equation (5.16) that the modified calibration method is capable of measuring only three error components, one axial error $D_z(c)$ and two tilt errors $E_x(c)$ and $E_y(c)$. Though eccentricity errors of H_x and H_y have been removed, two radial errors $D_x(c)$ and $D_y(c)$ also vanish. The reason for this is that H_x and $D_x(c)$, or H_y and $D_y(c)$ are coupled in their corresponding directions. Therefore, classic reversal techniques (Evans et al., 1996) have to be utilized to separate these errors.

5.2.2 Estimation Methods

In order to estimate the error components in Equation (5.16), certain estimation methods must be employed. The least squares (l_2 norm) estimation is widely used for solving such equation; however, it does not always provide the most suitable solutions for particular applications (Tajbakhsh et al., 1997). Two performance measures of parameter estimation are utilized and compared in this study.

l_2 norm estimation method measures the goodness of the fit by the average squared errors. This is the most commonly used method for parameter estimation as well as for measuring model performance. l_∞ norm method measures the goodness of the fit by the worst errors. This method is less convenient mathematically, but it is capable of guaranteeing the maximum error does not exceed the specification, which is desired in the acceptance tests of machine tools and finished parts. The mathematical expression for l_2 norm and l_∞ norm are shown in the following

$$l_2 = \frac{1}{n}\sum_{i=1}^{n} e_i^2 \tag{5.17}$$

$$l_\infty = max|e_i| \tag{5.18}$$

where n is the number of samples and e_i is the residual errors. The estimation results by using these two methods are compared in terms of the maximum errors and root-mean-square (RMS) errors for the sake of illustration.

5.3 Numerical Simulation

In this Section, the sensitivity analysis of the proposed calibration algorithm is carried out by numerically simulating the measurement procedures. The rotary table to

be calibrated, shown in Figure 5.4, is driven by a brushless servomotor with a precision gear and matched worm. This table is preloaded to reduce the backlash. Oil is also filled to assure long gear life at high continuous table speeds. The capability of continuous 360 Deg rotary positioning is provided. The accuracy specifications are listed in Table 5.1.

Figure 5.4 Rotary table to be calibrated (Courtesy of Aerotech. Inc.).

Table 5.1 Accuracy specifications of the rotary table.

Basic model	ART330
Table diameter	300 mm
Drive system	Precision worm gear
Accuracy	0.15 mrad (0.5 arcmin)
Repeatability (Unidirectional)	29.1 μrad (6 arcsec)
Axis wobble	24.3 μrad (5 arcsec)
Axis runout – Radial	15.0 μm (600 μin)
Axis runout – Axial	2.0 μm (80 μin)

There are two alternative lengths for the TMBB system, $L1 = 90.850$ mm and $L2 = 217.952$ mm. Figure 5.5 displays the socket with known dimensions used to fix one end of the ball bar onto the rotary table during the calibration process.

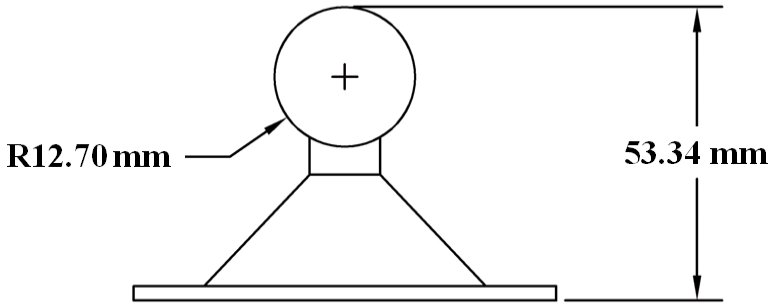

Figure 5.5 Socket with known dimensions for the calibration setup.

5.3.1 Sensitivity Analysis of R_x

Because two lengths of the TMBB, $L1$ and $L2$, and the height of the artifact R_z are specified, the position of the artifact on the rotary table along the X_R-direction, R_x, is the only adjustable parameter and thus plays an important role of deciding the accuracy of calibration results.

When estimating the error components, $E_x(c)$, $E_y(c)$ and $D_z(c)$, based on Equation (5.16), Equation (5.19) must be solved

$$\overrightarrow{\Delta_2} = \boldsymbol{J} \cdot \begin{bmatrix} E_x(c) \\ E_y(c) \\ D_z(c) \end{bmatrix} \tag{5.19}$$

where

$$\overrightarrow{\Delta_2} = \begin{bmatrix} \Delta_2'(L1, c_1) - \Delta_2'(L2, c_1) \\ \Delta_2'(L1, c_2) - \Delta_2'(L2, c_2) \\ \vdots \\ \Delta_2'(L1, c_n) - \Delta_2'(L2, c_n) \end{bmatrix}$$

$$\boldsymbol{J} = \begin{bmatrix} 2R_x \cdot (H2 - H1) \cdot \sin(c_1) & -2R_x \cdot (H2 - H1) \cdot \cos(c_1) & 2(H2 - H1) \\ 2R_x \cdot (H2 - H1) \cdot \sin(c_2) & -2R_x \cdot (H2 - H1) \cdot \cos(c_2) & 2(H2 - H1) \\ & \vdots & \\ 2R_x \cdot (H2 - H1) \cdot \sin(c_n) & -2R_x \cdot (H2 - H1) \cdot \cos(c_n) & 2(H2 - H1) \end{bmatrix}$$

and n is the number of collected data sets. The condition number of $\boldsymbol{J}$, a measure of the singularity of a matrix, is defined as

$$cond(\boldsymbol{J}) = \frac{\sigma_{max}}{\sigma_{min}} \tag{5.20}$$

where σ_{min} and σ_{max} are the minimum and maximum singular values of $\boldsymbol{J}$, respectively. The effectiveness of various R_x is analyzed through the evaluation of $cond(\boldsymbol{J})$. The results of sensitivity analysis of R_x are shown in Figure 5.6.

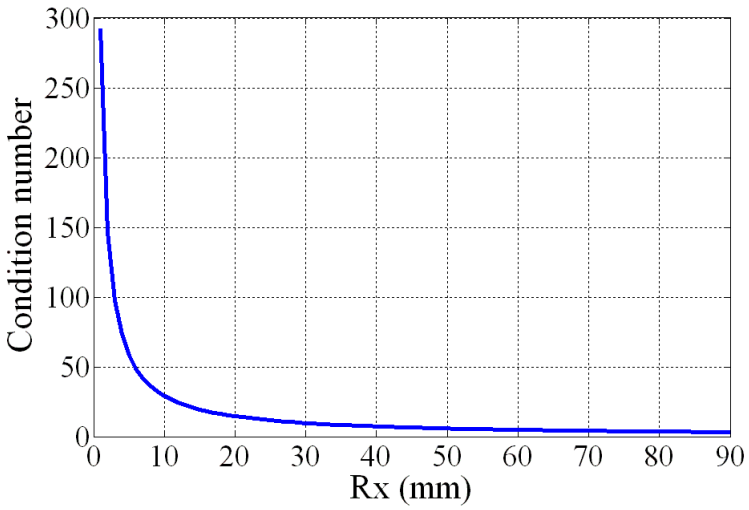

Figure 5.6 Sensitivity analysis of R_x.

Due to the limited length of the short TMBB, the range of R_x spreads merely from 0 mm to 90 mm. The condition number is correspondingly computed. As can be seen from Figure 5.6, larger R_x results in a smaller condition number, which is mathematically desired for the calculation of the inverse matrix of $\boldsymbol{J}$ if l_2 norm method is employed. The range in which $cond(\boldsymbol{J})$ is insensitive to the varying R_x is selected for the experimental

tests. Considering the screw layout of the rotary table, R_x is chosen to be 71.8420 mm. The corresponding angles between the ball bar and the vertical axis are $\eta 1 = 52.26$ Deg and $\eta 1 = 19.25$ Deg for calibration setups of the short and long ball bars, respectively.

5.3.2 Sensitivity Analysis of Dimensional Variations

Dimensional variations of setup parameters, R_x, R_z and H, are unavoidable. Deviations from nominal values may introduce unexpected factors, make the computation unstable and thus give rise to wrong results. The influences of dimensional variations are therefore investigated through the numerical simulation.

During the simulation, the error components are pre-assumed. The dimensional variation is purposely imposed from 0.1 mm to 1 mm for each setup parameter. The nominal value of each parameter, R_x, R_z and H, is decided in the previous Section. The deviation of the estimated error components, E_x, $E_y$and D_z, are finally computed based on Equation (5.19). The results are plotted in Figure 5.7.

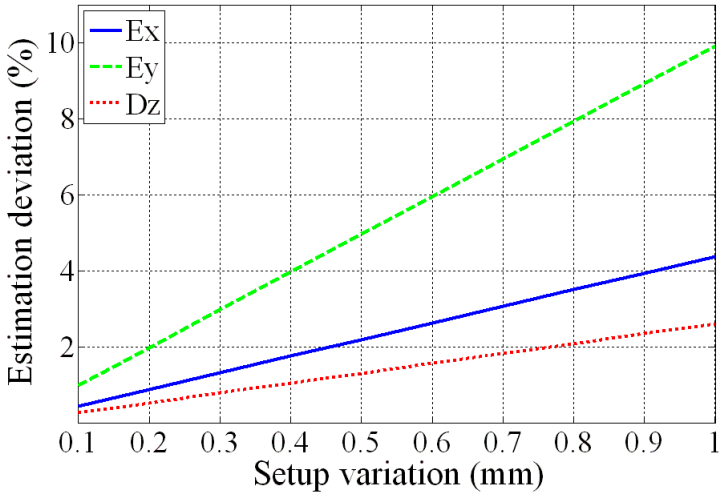

Figure 5.7 Sensitivity analysis of dimensional variation of setup parameters.

It can be seen from Figure 5.7 that the estimation deviation of each error component increases linearly with respect to the larger dimensional variations. E_y is more sensitive to the setup variation than E_x and D_z for the prescribed nominal setup parameters. However, the estimation deviations are still in the acceptable range when each setup parameter variation is less than $1\,\mathrm{mm}$, which can be easily achieved in practice.

Based on the above sensitivity analysis of setup parameters, the proposed rotary axis calibration algorithm is able to provide accurate results and is relatively robust to the setup errors, which are usually the most significant factors for a practically feasible calibration method.

5.4.3 Classification of Error Patterns

Error patterns directly indicate the existence and significance of certain error components in the circular tests. If the error patterns of two error components are similar to each other, these two error components cannot be distinguished mathematically. The error patterns of error components induced by rotational motion are illustrated in this Section to graphically clarify the restriction of the developed calibration algorithm by using the TMBB.

During the simulation, D_x and D_y, D_z, E_x and E_y, H_x and H_y are assumed to be specific values in turn while maintaining others zero. Figures 5.8 to 5.10 show the length variation, Δ_1, due to the error components D_x and D_y, D_z, E_x and E_y, respectively. In these figures, the continuous blue and dotted green lines represent the calibration results of different setups with the short and long ball bars, respectively.

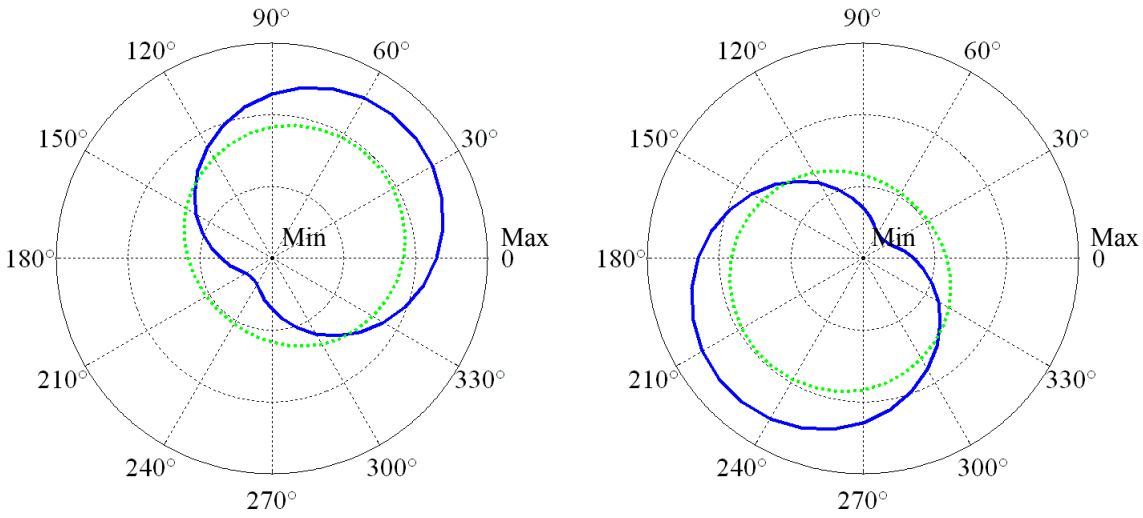

(a) (b)

Figure 5.8 Error patterns of error components D_x and D_y.
(a) Positive D_x and D_y and (b) negative D_x and D_y.

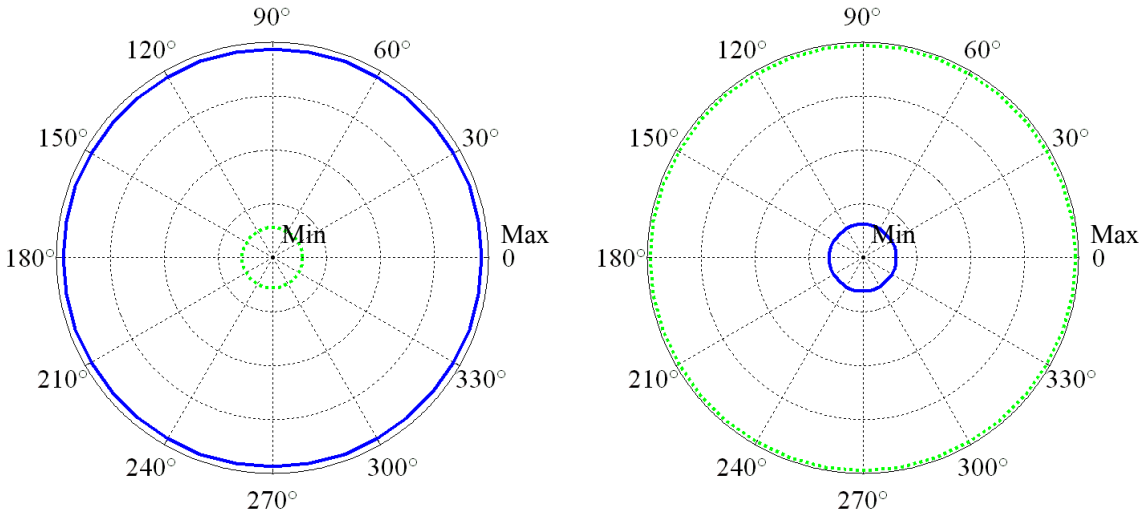

(a) (b)

Figure 5.9 Error patterns of error components D_z.
(a) Positive D_z and (b) negative D_z.

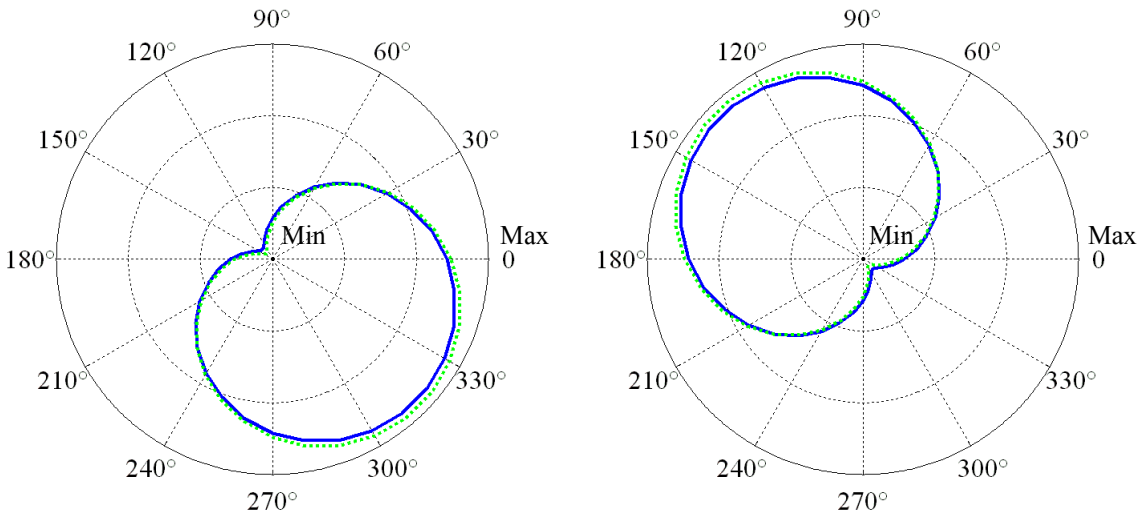

(a) (b)

Figure 5.10 Error patterns of error components E_x and E_y.
(a) Positive E_x and E_y and (b) negative E_x and E_y.

In Figures 5.8 to 5.10, the amount of radius in each plot is not straightly indicated due to the fact that the pattern shape is the only critical specification for each error pattern. The positive and negative values of each error component are separately simulated; and as can be seen, the sign (positive or negative) of these error components changes either the orientation, shown in Figures 5.8 and 5.10, or the size, shown in Figure 5.9, of the error patterns.

Figure 5.11 shows the error patterns of eccentricity errors, H_x and H_y. Only four possible sign combinations of H_x and H_y are illustrated, where the magnitude of H_x and H_y are assumed to be equal. For unequal H_x and H_y, the orientation of the error patterns would rotate correspondingly.

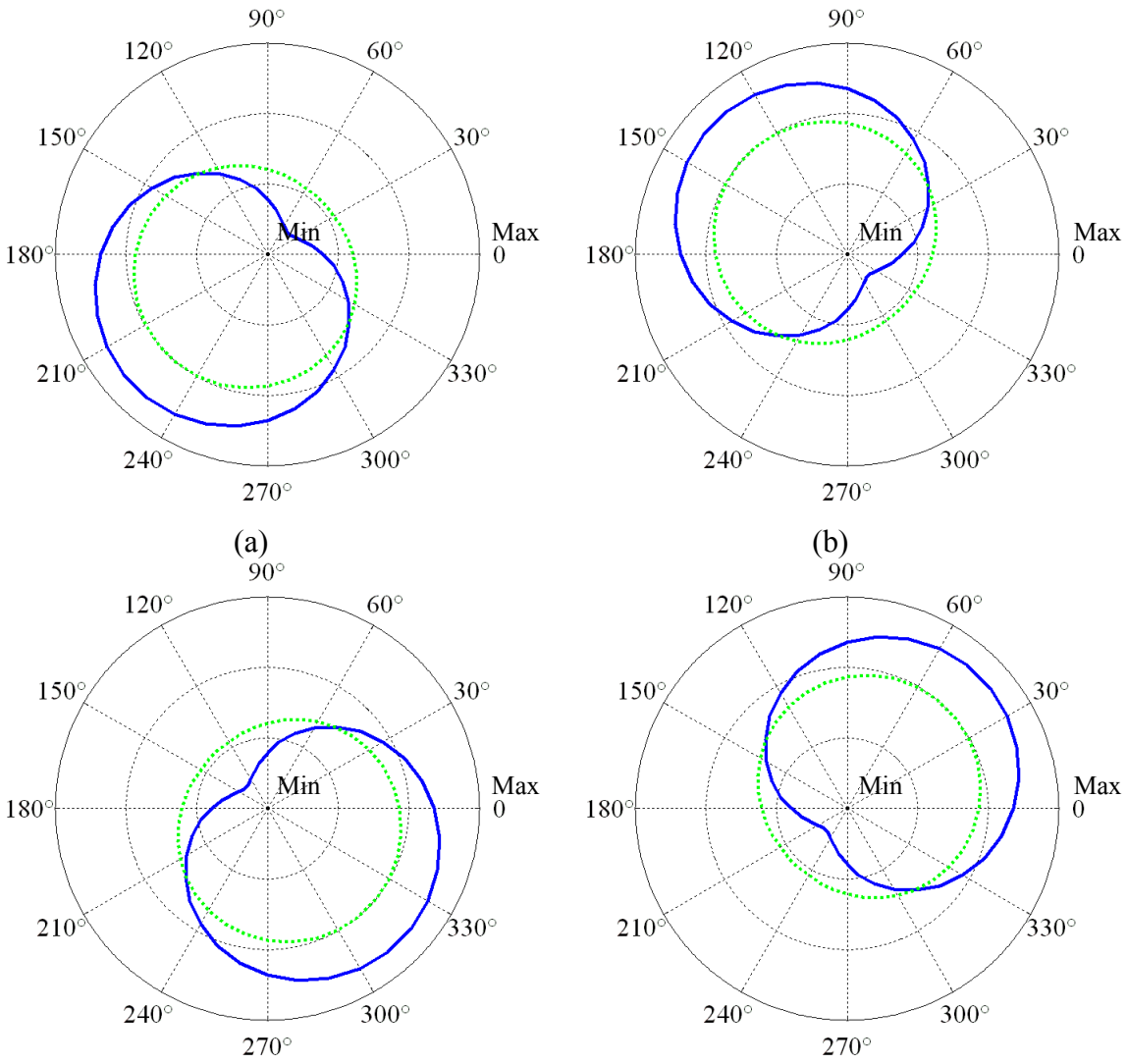

Figure 5.11 Error patterns of error components H_x and H_y.
(a) Positive H_x and positive H_y, (b) positive H_x and negative H_y, (c) negative H_x and positive H_y, and (d) negative H_x and negative H_y.

It is worth noting that the error patterns of D_x and D_y shown in Figure 5.8 and error patterns of H_x and H_y, shown in Figure 5.11, are close to each other in terms of the pattern shape and relative locations for both setups. This graphically reveals the coupling effects of D_x and D_y, and H_x and H_y, which as previously mentioned restrict the potentially full calibration of the rotary axis.

5.4 Experimental Demonstration

The experiments were conducted to illustrate the proposed rotary axis calibration approach. The calibration procedures described above were followed and the setup parameters were set according to the nominal values decided in the previous Section. During the data acquisition, the rotary table shown in Figure 5.4 was programmed to rotate 10 Deg and then dwell for several seconds, allowing the capture of length variation of the ball bar. Altogether 37 sets of data were captured for each rotation. Three replications were made for the two setups with the short and long ball bars, respectively.

The collected data are plotted in Figure 5.12. Figures 5.12(a) and 5.12(b) correspond to the two TMBB lengths. In both figures, the red dotted line and blue continuous line represent the nominal and actual length of the TMBB, respectively. The unit of the radius in both polar plots is mm.

The eccentricity is signified by the center offset of the actual plot from the ideal plot, compared with the eccentricity error pattern shown in Figure 5.11. The amount of the offset in the vertical direction is more severe than that in the horizontal direction, indicating the eccentricity is unequal in both directions. In addition, it is observed that the offset patterns for both setups are relatively similar. This implies that the eccentricity errors H_x and H_y do not change significantly during the vertical movement of the spindle between the two setups, which is desired for the elimination of the eccentricity according to the developed calibration method.

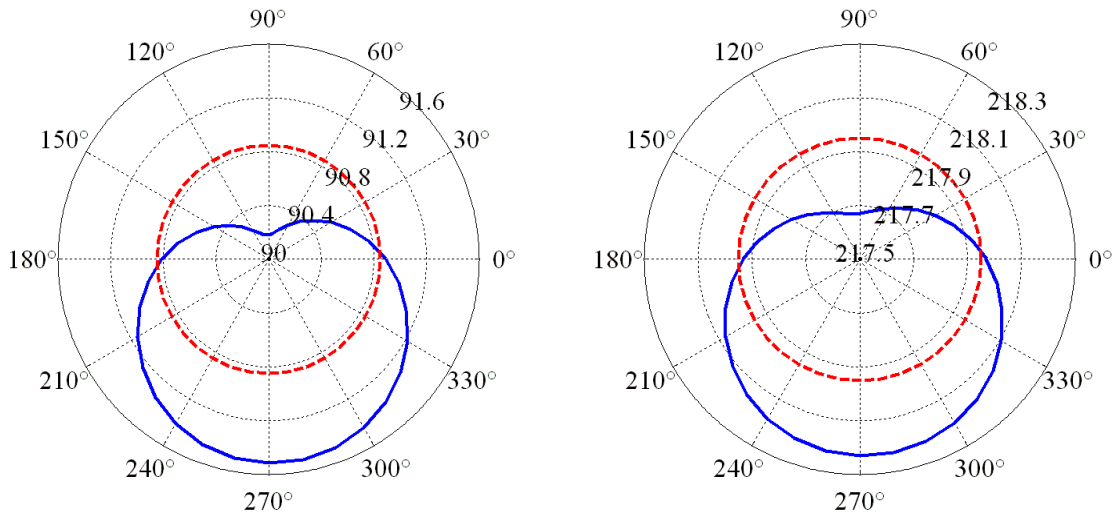

(a) (b)

Figure 5.12 Polar plots of the collected data for two calibration setups with (a) short TMBB and (b) long TMBB.

l_2 and l_∞ norm estimation methods based on Equation (5.16) are utilized to compute the error components E_x, E_y and D_z, respectively. The estimated results are summarized in Table 5.2. The estimated error components by using both estimation methods agree well with each other, and do not deviate significantly from the given values in Table 5.1. Moreover, the assumption of equivalent E_x and E_y are also verified.

Table 5.2 Error component estimation results.

	l_2 norm method	l_∞ norm method
E_x (arcsec)	7.93	6.54
E_y (arcsec)	7.38	8.70
D_z (μm)	2.68	2.55

The residual errors for both methods are shown in Figure 5.13. The unit of the radius in the polar plot is mm^2. The residual errors distribute tightly around the circle of

zero radius, indicating that most of the systematic errors have been eliminated. The discontinuity at 0 Deg signifies the existence of the backlash in the rotary table.

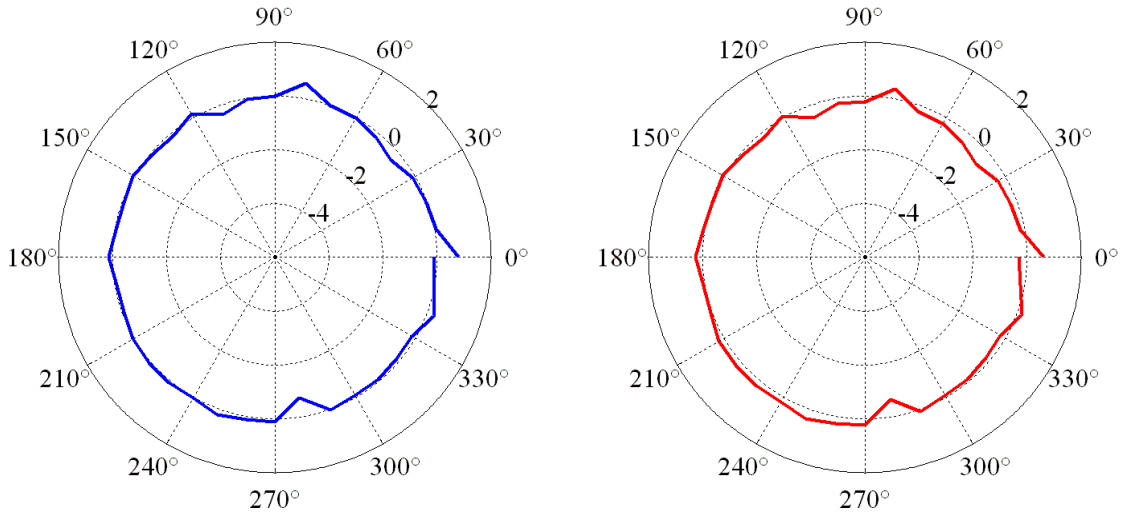

(a) (b)

Figure 5.13 Plots of residual errors by using (a) l_2 and (b) l_∞ norm methods.

Comparison of l_2 and l_∞ norm estimation methods are conducted and listed in Table 5.3 in terms of the measures of Max($|e_i|$), Range(e_i) and RMS(e_i). As can be seen from Table 5.3, the purpose of employing l_∞ or l_2 norm estimation methods has been attained considering the smaller maximum error or the RMS error for either estimation method.

Table 5.3 Comparison of the estimation results by using l_2 and l_∞ norm methods.

	l_2 norm method	l_∞ norm method
Max($\|e_i\|$)	0.807	0.632
Range(e_i)	1.520	1.263
RMS(e_i)	1.466	1.717

5.5 Summary

In this Chapter, a rotary table calibration algorithm by using the TMBB has been developed. The feasibility and restriction of this algorithm, accounting for the eccentricity, were presented based on the rigorous mathematical derivations. The sensitivity analysis of setup parameters was numerically simulated. The error pattern of each error component was separately generated, graphically clarifying the inherent constraints of this approach. The calibration procedures were carried out to measure a rotary table. Two different estimation methods were applied and compared for the error evaluation. The calibration results are close to the given values, verifying the effectiveness of the proposed calibration algorithm.

Though only three error components are measurable for this method, the quick setups and procedures still provide advantages over other approaches. In addition, the measurable wobble errors are usually more significant compared with the radial runouts due to the Abbe effects for rotary tables with large diameters.

CHAPTER 6

CONCLUSIONS AND FUTURE WORK

6.1 Conclusions

The major contributions of this research include: 1) Development of quick rotary axis calibration algorithm by using the Telescopic Magnetic Ball Bar for the geometric error compensation of five-axis machine tools; 2) Practical validation and utilization of thermal modal analysis for the temperature sensor placement determination and robust thermal error modeling; and 3) Development of a thermal loop analysis to relate the thermal deformation of machine elements and thermal errors between moving components to the volumetric errors.

The conclusions for this research are summarized as follows:

Thermal modal analysis is an important method for analyzing the machine tool thermal deformation errors. Time constant and temperature distribution field for each thermal mode can be computed through the finite element analysis and eigen-analysis. The mode weights based on the assumption of serial step heat flux input illustrate the existence of thermal modes and realize the application of thermal error modal analysis on the practical machine tool elements. Temperature sensor placement schemes with mode truncation are validated through the comparison with Gaussian integration method and exhaustive search method. Thermal error models thus derived are shown to be robust in

terms of both extrapolation and frequency sensitivity through both numerical simulation and practical experiments.

Thermal loop analysis is utilized for the thermal error prediction and compensation of an entire machine tool. The machine tool is decomposed into several thermal links along an identified thermal loop. The temperature sensor placement scheme and thermal error modeling are developed for each machine element based on the thermal modal analysis. The volumetric errors are then predicted and compensated through the reassembly of machine elements. The thermal loop analysis mitigates the inaccurate thermal modeling of machine joints, and extensively enhances the effectiveness of the finite element method in the thermal error modeling and compensation. In addition, both the thermal deformation of machine element and thermal error coupled with geometric and kinematic errors between moving axes can be embraced in the thermal error models for the volumetric errors.

The introduction of two rotary axes not only substantially facilitates the functionality of five-axis machine tools, but also necessitates the rotary axis calibration method for the assurance of five-axis machining accuracy. The Telescopic Magnetic Ball Bar is explored for its easy setup and quick assessment algorithm. The axial runout and two wobbles can be effectively estimated by two circles tests. Two radial runouts and angular position accuracy cannot be assessed due to the interconnection with the setup eccentricity and lack of angular reference, respectively.

6.2 Recommendations for Future Work

Recommendations for future work related to this research are as follow:

1. Development of efficient thermal error identification methods. Thermal error calibration by using the laser interferometer is able to result in accurate and repeatable measurement results. However, this approach is extremely time-consuming and labor-intensive; moreover, the calibration of certain thermal errors might not contribute to the dimensional accuracy of machined parts. Methods of identifying thermal errors from the measurement of dimensional deviations of machined parts have the potential to alleviate this issue. In addition, the continuous measurement of machined parts is capable of updating the estimated thermal error models, enabling the in-process compensation of the thermal errors.

2. Extension of the thermal modal analysis towards the virtual machine tool design. The current thermal modal analysis is performed for each individual machine element. The facilitation of finite element analysis for the whole machine tool would be realized if an efficient interface formulation between machine elements could be established. This interface formulation must have the capability of combining the intricate thermal mechanism and the existing thermal modal analysis of machine elements, without resorting to remeshing and recalculating the whole machine tool structure. By doing this, the lead time of machine tool design could be significantly shortened.

3. Application of thermal loop analysis to the evaluation of the modular machine tool design. The basic idea of thermal loop analysis is delivered from the decomposition of the thermal loop to the recombination of each thermal link. Each thermal link conceptually corresponds to a module. The thermal error model associated with each

thermal link can be assembled according to the specified configuration for the volumetric error prediction. The machining accuracy in terms of the amount of thermal errors can be therefore compared, similar to the dynamic analysis of the reconfigurable machine tools. The results would be helpful in the decision of the modular machine tool design and the configuration determination of the reconfigurable machine tools for a certain part family.

4. Derivation of quick assessment of the complete geometric errors for five-axis machine tools. The calibration algorithm for rotary axis provides an opportunity of fully assessing the geometric errors of a five-axis machine tool. However, such geometric errors between the moving axes as squareness and parallelism are still difficult to measure, in that several axes are required to move simultaneously. Moreover, these errors are usually interconnected with the geometric errors inherent in each axis. The five-axis machining accuracy would not be ultimately assured without the correct identification of all the geometric errors.

APPENDICES

APPENDIX A
Kinematic Error Synthesis Modeling

Kinematic error synthesis models play a pivotal role in the performance assessment of machine tools. The formulation of synthesis model is usually dependent on the assumptions of rigid body and small errors (Yuan and Ni, 1998). Rigid body assumption means that the error components of one axis are merely the function of that axis and not affected by the motion of other axis. Small error assumption neglects the higher order errors. The kinematic chain and the homogeneous transformation matrix (HTM) are usually combined to develop kinematic models.

A kinematic chain, K_C, is used to synthesize the feasible configurations of all kinds of machine tools and their corresponding kinematic characteristics. One generic kinematic chain for a typical machine configuration is displayed in Figure A.1 by arranging each machine component, K_i, $i = -m, \cdots, -1, 1, \cdots n$, according to the machine structure from workpiece, P_T, through the ground, G_R, and to tool, T_L. For this configuration, there are m and n machine elements in the part branch (from P_T to G_R) and the tool branch (from G_R to T_L), respectively.

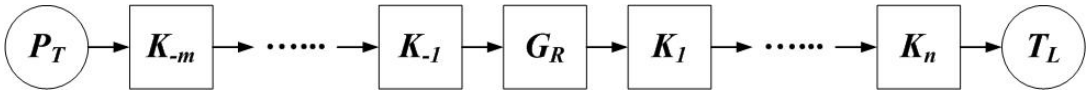

Figure A.1 A representative kinematic chain for multi-axis machine tools.

The simplified mathematical form based on this chain is expressed as

$$K_C = P_T K_{-m} \cdots K_{-1} G_R K_1 \cdots K_n T_L \tag{A.1}$$

Particularly, $K_i = X, Y, Z$ denotes translation, T_R, and $K_i = A, B, C$ denotes rotation, R_O. T_R and R_O are sometimes used to represent a set of machine configurations for the general purpose. Because workpiece, P_T, and tool, T_L, are always at the two ends of a kinematic chain, they are usually not presented to avoid confusion.

Based on the kinematic chain, coordinate systems are then placed to describe the axis motion and the induced error components. Three coordinate systems, the world coordinate system (WCS), the tool coordinate system (TCS), and the part coordinate system (PCS) are individually assigned. The HTM from the TCS to the PCS is expressed by Equation (A.2)

$$\boldsymbol{M_{PCS}^{TCS}} = \boldsymbol{M_{PCS}^{0}} \cdot \boldsymbol{M_{0}^{TCS}} = \left(\boldsymbol{M_{-0}^{-1}} \cdot \cdots \cdot \boldsymbol{M_{-m}^{PCS}}\right)^{-1} \cdot \left(\boldsymbol{M_{0}^{1}} \cdot \cdots \cdot \boldsymbol{M_{n}^{TCS}}\right) \tag{A.2}$$

where $\boldsymbol{M_{PCS}^{O}}$ is the HTM from WCS to PCS, and $\boldsymbol{M_{O}^{TCS}}$ is the HTM from TCS to WCS. The relative motion of components K_i with respect to K_{i-1} in three-dimensional space can be generally described by a transformation matrix as follows

$$\boldsymbol{M_{i-1}^{i}} = \begin{bmatrix} O_{ix} & O_{iy} & O_{iz} & P_x \\ O_{jx} & O_{jy} & O_{jz} & P_y \\ O_{kx} & O_{ky} & O_{kz} & P_z \\ 0 & 0 & 0 & 1 \end{bmatrix} \tag{A.3}$$

where the first three columns are direction cosines representing the orientation of the machine component and the last column represents the position of the machine component (Slocum, 1992).

For each moving component, there are two corresponding HTMs depending on the motion types and directions, one for ideal motion and the other for actual motion. Theoretically, the actual motion differs slightly from the ideal motion with six error components, three translational and three rotational errors. These errors can be defined as occurring along and about the assigned coordinate system.

For a linear axis moving in the X-direction, as shown in Figure A.2(a), the three translational errors are one linear displacement error, $D_x(x)$, and two straightness errors, $D_y(x)$ and $D_z(x)$, while the three rotational errors are roll, $E_x(x)$, pitch, $E_y(x)$, and yaw, $E_z(x)$. For a rotary axis revolving around Z-direction, as shown in Figure A.2(b), the three translational errors are two radial errors, $D_x(c)$ and $D_y(c)$, and one axial error $D_z(c)$, while the three rotational errors are two tilt errors, $E_x(c)$ and, $E_y(c)$, and one angular displacement error $E_z(c)$. The corresponding HTMs describing the ideal and actual motions of the linear axis, X-axis, and the rotary axis, C-axis, are summarized in Equations (A.4) to (A.7).

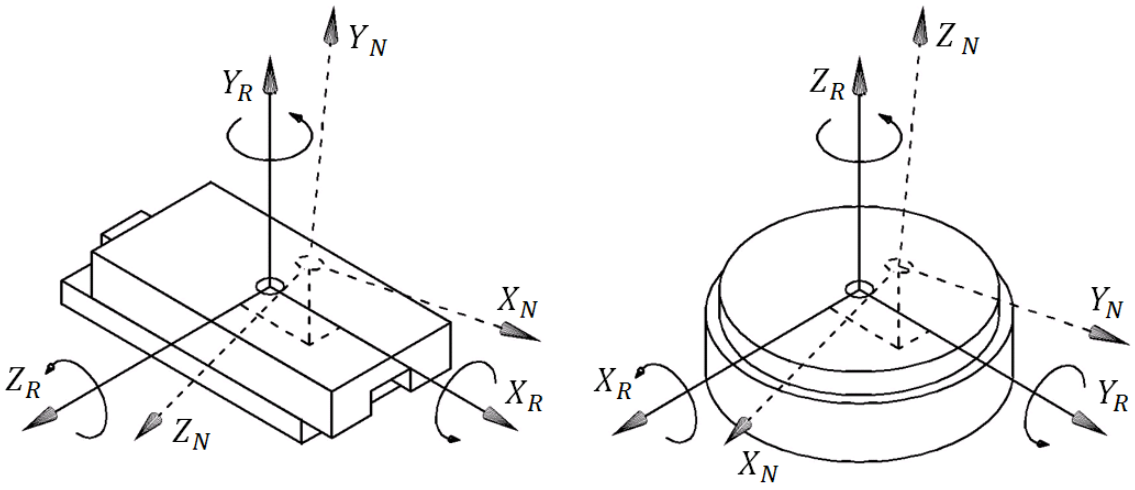

(a) (b)

Figure A.2 Motion errors induced by translational and rotational motions.
(a) Linear axis: *X*-axis and (b) Rotary axis: *C*-axis.

$$\boldsymbol{M_X} = \begin{bmatrix} 1 & 0 & 0 & x \\ 0 & 1 & 0 & 0 \\ 0 & 0 & 1 & 0 \\ 0 & 0 & 0 & 1 \end{bmatrix} \tag{A.4}$$

$$\boldsymbol{M_X^{Error}} = \begin{bmatrix} 1 & -E_z(x) & E_y(x) & D_x(x)+x \\ E_z(x) & 1 & -E_x(x) & D_y(x) \\ -E_y(x) & E_x(x) & 1 & D_z(x) \\ 0 & 0 & 0 & 1 \end{bmatrix} \tag{A.5}$$

$$\boldsymbol{M_C} = \begin{bmatrix} cos(c) & -sin(c) & 0 & 0 \\ sin(c) & cos(c) & 0 & 0 \\ 0 & 0 & 1 & 0 \\ 0 & 0 & 0 & 1 \end{bmatrix} \tag{A.6}$$

$$\boldsymbol{M_C^{Error}} \tag{A.7}$$

$$= \begin{bmatrix} cos(c) & -sin(c) & E_y(c) & D_x(c) \\ sin(c) & cos(c) & -E_x(c) & D_y(c) \\ E_x(c)sin(c) - E_y(c)cos(c) & E_x(c)cos(c) + E_y(c)sin(c) & 1 & D_z(c) \\ 0 & 0 & 0 & 1 \end{bmatrix}$$

where $\boldsymbol{M_X}$ and $\boldsymbol{M_X^{Error}}$ represent the ideal and actual motion of X-axis, and $\boldsymbol{M_C}$ and $\boldsymbol{M_C^{Error}}$ represent the ideal and actual motion of C-axis.

Besides these position dependent motion errors, there is another kind of errors, which is induced by the relative movement between axis and machine structure imperfection. There errors, commonly referred to as link errors, including squareness errors between linear axes, S_{xy}, S_{yz} and S_{zx}, and parallelism errors between linear and rotary axes, S_{ya}, S_{za}, S_{xb}, S_{yb} , S_{xc} and S_{yc} (ASME B5.54-1992).

For the purpose of error compensation, the volumetric errors in PCS must be computed depending on the tool position and orientation in TCS. Let the position and orientation vectors of the central tip of the tool in TCS be

$$\vec{T}_{L\_P} = [0, 0, l, 1]^T \tag{A.8}$$

$$\vec{T}_{L\_O} = [0, 0, 1, 0]^T \tag{A.9}$$

where $\vec{T}_L$ represents the tool; subscript P and O denotes the position and orientation in

TCS, and l is the length of the tool. Volumetric errors, as the difference between ideal and actual position and orientation of the tool in PCS can be calculated by using the following equations

$$\overrightarrow{VE_P} = \boldsymbol{M}_{\boldsymbol{PCS\_actual}}^{\boldsymbol{TCS}} \cdot \vec{T}_{L\_P} - \boldsymbol{M}_{\boldsymbol{PCS\_ideal}}^{\boldsymbol{TCS}} \cdot \vec{T}_{L\_P} = \left(\boldsymbol{M}_{\boldsymbol{PCS\_actual}}^{\boldsymbol{TCS}} - \boldsymbol{M}_{\boldsymbol{PCS\_ideal}}^{\boldsymbol{TCS}} \right) \cdot \vec{T}_{L\_P} \quad \text{(A.10)}$$

$$\overrightarrow{VE_O} = \boldsymbol{M}_{\boldsymbol{PCS\_actual}}^{\boldsymbol{TCS}} \cdot \vec{T}_{L\_O} - \boldsymbol{M}_{\boldsymbol{PCS\_ideal}}^{\boldsymbol{TCS}} \cdot \vec{T}_{L\_O} = \left(\boldsymbol{M}_{\boldsymbol{PCS\_actual}}^{\boldsymbol{TCS}} - \boldsymbol{M}_{\boldsymbol{PCS\_ideal}}^{\boldsymbol{TCS}} \right) \cdot \vec{T}_{L\_O} \quad \text{(A.11)}$$

where $\mathrm{M}_{\mathrm{PCS\_ideal}}^{\mathrm{TCS}}$ and $\mathrm{M}_{\mathrm{PCS\_actual}}^{\mathrm{TCS}}$ are the ideal and actual HTMs from TCS to PCS.

Both of them can be obtained based on Equation (A.2) with proper substitutions of different motion transformation matrices shown in Equations (A.10) and (A.11). $\overrightarrow{VE_P}$ and $\overrightarrow{VE_O}$ are, respectively, the position and orientation errors, which are the function of both error components and the spatial positions of translational and rotational axes in the workspace.

APPENDIX B
Machine Tool Error Budget and Its Application

Manufacturers all over the world are pursuing the methodology of increasing part accuracy while reducing manufacturing cost to maintain their competence nowadays. Part accuracy, defined as the degree of conformance of the finished workpiece to dimensional and geometric specifications (Hocken, 1980), is highly dependent on the performance of machine tools. Machine tool errors, accumulating and propagating through the machine tool kinematic structure, finally manifest themselves in the part dimensional variations.

Quasi-static errors, such as geometric and kinematic errors, and thermal errors, etc., are the main contributors to the machine tool errors (Yuan and Ni, 1998). The interaction between these errors must be modeled, controlled and predicted to guarantee that the part dimensions meet the required specifications. Machine tool error budget is such an efficient tool to control the machine tool errors and predict the part dimensional accuracy (Treib, 1987; Thompson, 1989; Steinmetz, 1990; Homann and Thornton, 1998).

Broadly speaking, tolerance analysis and synthesis in assembly and mechanism, accuracy and variation analysis of parallel machine tools and robots also fall into the category of error budgeting. The basis for rational tolerance specification in the assembly is to create an analytical model to predict the accumulation of tolerances in a mechanical assembly (Chase and Parkinson, 1991). Tolerance accumulation is usually analyzed through vectors chains or loops, and common models such as the worst case (WC) method, the root-sum-squares (RSS) method and Monte Carlo simulation. Further modifications to RSS model have also been proposed to adopt a more general form

(Spotts, 1978) or to consider mean shifts or biased distributions (Chase and Greenwood, 1988). Sensitivity analysis is also performed to evaluate the significance of component dimensional variation to the assembly tolerance. Tolerance allocation is to assign the tolerances for an assembly based on certain performance requirements. Minimum-cost tolerance allocation is one of the most commonly used methods. Optimization algorithms are explored to systematically search the most appropriate combination of component tolerance, which would result in the least overall production cost based on the assigned empirical cost-tolerance function (Wu et al., 1988; Chase et al., 1990).

Variation analysis is necessary for the robust mechanism design. A mechanism generally has one or more kinematic variables as a prescribed input. The nonlinear kinematic equations, relating the input variables to the motion outputs, have to be solved for the proper function of the specified mechanism. Sensitivity of mechanism system to variations has been studied be means of robustness index and sensitivity ellipsoid (Faik and Erdman, 1991; Zhu and Ting, 2001; Zhang and Porchet, 1993).

Accuracy analysis of parallel machine tools has also been investigated by considering the effects of manufacturing and actuation errors. Kinematic models relating various kinds of error sources to the pose accuracy are first developed based on D-H conventions (Wang and Masory, 1993; Ropponen and Arai, 1995). Accuracy in terms of variation transmission is then described by using different approaches, such as plotting the error gain sensitivity (Patel and Ehmann, 1997), evaluating norms of Jacobian matrix (Xi and Mechefske, 2000), or applying the Monte Carlo simulation (Pasek, 2000).

The abovementioned methodology can be modified to deal with the machine tool error budget from different perspectives. There are two basic sub-problems inherent in

error budgeting; one is the mapping of the machine element errors to volumetric errors and part dimensional accuracy, and the other is the allocation of the total volumetric errors into machine element levels. Though machine tool error budgeting methods have been investigated (Shen, 1993) and applied to the conventional machine tool design (Treib, 1987; Thompson, 1989), there does not exist systematic formulation to address and resolve both forward and reverse machine tool error budgeting problems.

B.1 Machine Tool Error Budget

Machine tool error budget is a systematic tool used for the prediction and control of the total errors of a machine tool and accuracy of machined workpieces such that any error component does not exceed its allowed specification. The performance of machine tools is highly dependent on the errors in the machine components and their combined effects on the accuracy, repeatability, and resolution of the interaction between tool and workpiece. It is of primary importance to ensure that these requirements be achieved during the design stage. This can be demonstrated by using the error budget.

Two basic issues exist for an error budget analysis, as shown in Figure B.1. One is error budget analysis and the other is error budget synthesis. Error budget analysis, as a forward problem, is to predict the overall volumetric errors of a machine tool and machined part accuracy with known or assumed error distributions of the machine components. Error budget synthesis, as a backward problem, is to allocate the overall part dimensional variations, particularly volumetric errors, into each machine component.

In this research, geometric and kinematic errors are considered to be the major contributors to the machined workpieces. The derived error budgeting method, however,

is applicable to other errors sources if they are properly included in the kinematic models. In addition, the part dimensional deviation is assumed to be equivalent to the volumetric errors of the machine tool. The error components are assumed to follow certain statistical distributions with zero means and independent of each other, which underlines the stochastic nature of error sources. This zero-mean assumption is reasonable once error compensation technique is appropriately applied.

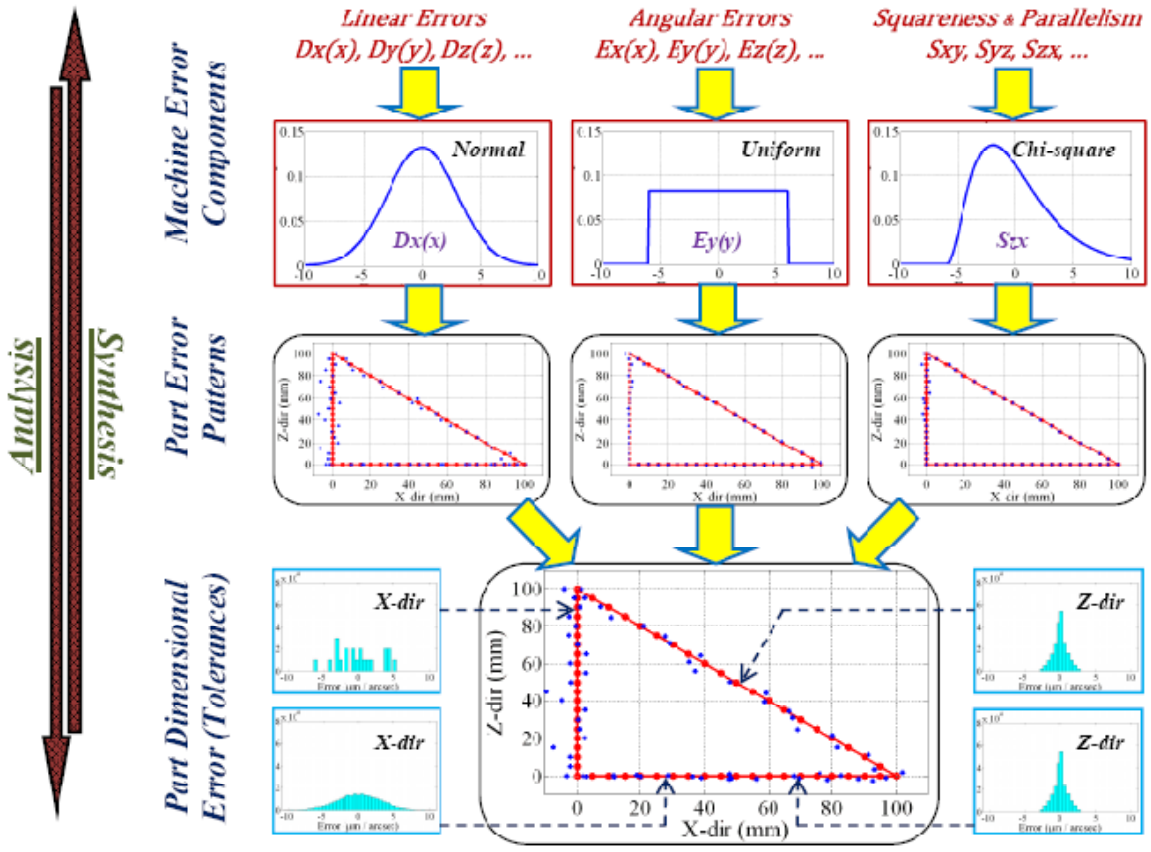

Figure B.1 Machine tool error budget analysis and synthesis.

Machine Tool Error Budget Analysis

The forward problem is mainly about the analysis of propagation properties of the kinematic model that transmits the error sources to the volumetric errors and part

dimensional accuracy. Sensitivities of each error type to the volumetric errors are used to describe the variation propagation and indicate the dominant errors (Slocum, 1992).

In general, kinematic error synthesis model can be compactly expressed as

$$\overrightarrow{VE} = \boldsymbol{SE} \cdot \vec{e} \tag{B.1}$$

where

$$\overrightarrow{VE} = \begin{bmatrix} VE_x \\ VE_y \\ VE_z \end{bmatrix} \text{ and } \vec{e} = \begin{bmatrix} D_i(j) \\ E_i(j) \\ S_{ij} \end{bmatrix}$$

$\overrightarrow{VE}$ represents the volumetric errors in three orthogonal directions, and $\vec{e}$ represents the error components, including linear errors, $D_i(j)$, angular errors, $E_i(j)$, and squareness errors, S_{ij}. $\boldsymbol{SE}$ is the sensitivity matrix (sometime called error gain matrix as well). For a certain volumetric error VE_i,

$$VE_i = \sum_{j=1}^{n} SE_{ij} \cdot e_j \tag{B.2}$$

where SE_{ij} indicates the sensitivity or amplification factor of the error component e_j to the volumetric errors VE_i; n is the number of error components.

In order to make the sensitivity matrix, $\boldsymbol{SE}$, is dimensionally homogeneous, the linear errors are transformed through the division by their corresponding axis length. For instance, a linear error of 1 μm for an axis with the total length of 1 m is henceforth regarded as 1 μm/m. In practice, 1 μm linear error over 1 m axis is approximately equivalent to 1 μm/m angular error in terms of manufacturing difficulty and cost.

The advantage of sensitivity analysis is that there is no need to know the error source distributions in advance. The sensitivity matrix can be characterized mainly by singular values. Two commonly used measures are the maximum singular value and the

condition number. The maximum singular value is a measure of the largest error sensitive direction. The condition number is a measure of the relative error amplification ratio. Both measures can be illustrated through the design sensitivity ellipsoid (Zhu and Ting, 2001), as shown in Figure B.2, where only two error components, e_1 and e_2, are taken into account and the ellipsoid represents the constant value of $\left\|\overrightarrow{VE}\right\|_2$. The longer principal axis corresponds to the less sensitive direction to the error variation; while the shorter principal axis corresponds to the larger sensitive direction to the error variation.

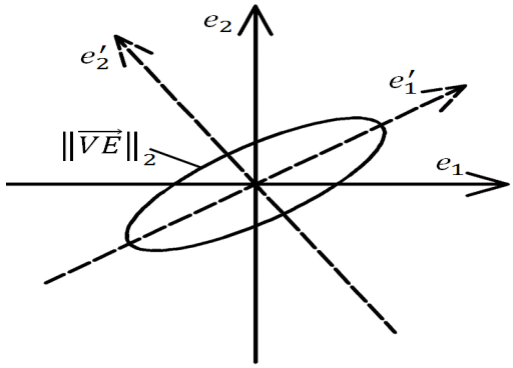

Figure B.2 Design sensitivty ellipoid.

Once the distributions of error sources are obtained, the volumetric errors and machined workpiece dimensional accuracy can be computed based on either the root-sum-squares (RSS) method, Equation (B.3), or the worst-case method, Equation (B.4).

$$VE_i = \sqrt{\sum_{j=1}^{n} \left(SE_{ij} \cdot e_j\right)^2} \tag{B.3}$$

$$VE_i = \sum_{j=1}^{n} \left|SE_{ij}\right| \cdot e_j \tag{B.4}$$

In the RSS model, the probability of each error component is assumed to follow the Gaussian distribution. Equation (B.3) can be further modified to accommodate the assumption of various statistical distributions. The range of the resultant error components spreads wider if the RSS model is adopted compared with the worst-cast model, which assumed that each error component occurs at its worst limit simultaneously.

Machine Tool Error Budget Synthesis

The reverse error budget problem deals with the allocation of the volumetric errors or the machined workpiece dimensional variations to each error component based on a set of specific criteria. Error components are stochastic variables following certain distributions; cost is correspondingly assigned for different distributions. The exponential cost function, Equation (B.5), is employed to describe the cost-error relationship of each error component.

$$Cost(e_i) = \frac{A_i}{e_i^k} \tag{B.5}$$

where $Cost(e_i)$ is the cost for each error component e_i, and A_i is unit cost which has to be adjusted according to the practical applications. The cost-error trend could be approximately captured by tuning the index, k.

Based on the RSS model, Equation (B.3), and the assigned cost function, Equation (B.5), the optimal error allocation problem with the objective function and constraints is arranged in the following:

$$\text{Minimize: } \sum_{i}^{n} Cost(e_i) \tag{B.6}$$

$$\text{Subject to: } \sqrt{\sum_{j=1}^{n} \left(S_{ij} \cdot e_j\right)^2} \leq VE_{i\_R} \tag{B.7}$$

$$e_j^l \leq e_j, j = 1, \cdots, n \tag{B.8}$$

where VE_{i_R} is the required specification for volumetric errors, VE_i; e_j^l represents the lower limit for each error component, which is imposed to eliminate unexpectedly small allocated error.

Conventionally, the method of Lagrange multipliers is widely used to solve the abovementioned optimal machine tool error budgeting problem (Chase et al, 1990). The method of Lagrange multipliers is able to provide a closed-form solution through the iterative process, especially efficient to solve simple problem with one inequality constraint like Equation (B.7). However, it has certain limitations. It cannot treat cost-error functions for which preferred variation limits are specified, such as Equation (B.8). In addition, it is difficult to handle the problems which are described by more than one dimensional accuracy requirements with shared error components, because this requires the simultaneous solution of a set of nonlinear equations.

A hybrid Genetic Algorithm (GA) and sequential quadratic programming (SQP) is thus proposed. This hybrid GA/SQP method shows an advantage over the method of Lagrange multipliers in the abovementioned two aspects. This method is applicable not only to the machine tool error budgeting, but 2D or 3D assembly tolerance allocation as well. GA is a search and optimization procedure that arrives at an optimal solution by mimicking the principles of natural genetics (Holland, 1975; Goldberg, 1989). GA is

able to quickly reach the region of global optimal solution compared with other optimization algorithms, but it is relatively slow in convergence to the optimum solution; therefore SQP is employed to identify the optimum solution with the outputs of the GA as the initial values.

- **Genetic Algorithm (GA)**

GA operates on the principles of the "survival of the fittest", where weak individuals die before reproducing, while stronger ones survive and bear many offspring and breed children who often inherit the quantities that enabled their parents to survive.

The flowchart of GA is shown in Figure B.3. GA relies on the process of reproduction, crossover and mutation to improve the fitness of population generation by generation, and finally reach the global or near-global optimum. The initial population is constructed randomly from the gene pool with precautions taken to avoid redundant genes in solutions. Reproduction is a process simulating natural selection by judging individual solutions according to their fitness through a fitness function and a roulette wheel. Rank order method is commonly adopted for reproduction process. Crossover involves random mating of solutions in the mating pool. Two new solutions (children) are created from two old solutions (parents) by exchanging partial information. Mutation is the occasional random partial alternation of a solution. Mutation is necessary because it introduces new information to the gene pool.

For optimal variation allocation problem, every gene represents an error component, and the length of the chromosome indicates the total number of error components after Jacobian sensitivity analysis. In order to accommodate multiple constraints imposed on the overall volumetric errors, a penalty is assigned once the

generated volumetric errors cannot reach the satisfactory level.

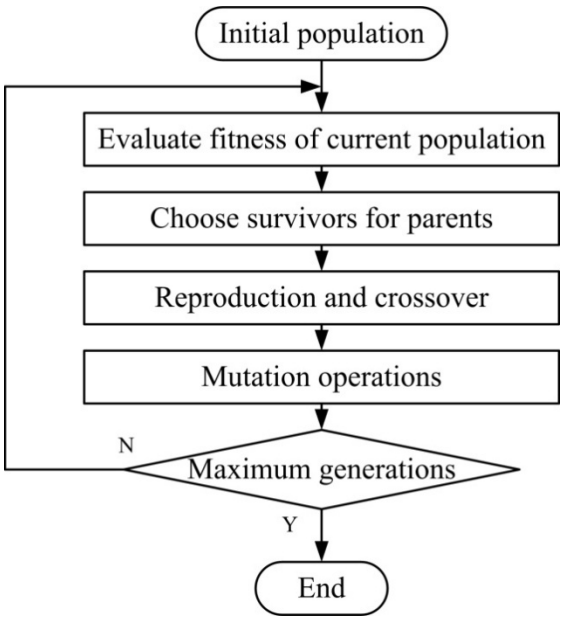

Figure B.3 Flowchart of the Genetic Algorithm.

The disadvantage of GA is that it lacks efficiency in reaching local optima. When a near local optimum solution is reached, GA has difficulties finding the local optimum due to its ignorance of neighborhood structures.

- **Sequential Quadratic Programming (SQP)**

SQP attempts to solve a nonlinear program directly rather than convert it to a sequence of unconstrained minimization problems. SQP (Vanderplaats, 1984) is a generalization of Newton's method for unconstrained optimization in that it finds a step away from the current point by minimizing a quadratic model of the problem. At each step, an approximation is made of the Hessian of the Lagrangian function using a quasi-Newton updating method. This is then used to generate a quadratic programming (QP) sub-problem whose solution is used to form a search direction for a line search procedure.

The local convergence properties of the SQP approach are well understood when the second-order sufficiency conditions are satisfied. The generated sequence search converges to the optimal solution at a second-order rate. These assurances cannot be made in other optimization methods. The convergence properties of the basic SQP algorithm can be further improved by using a line search. The choice of distance to move along the direction generated by the sub-problem is not as clear as in the unconstrained case, where a step length is simply chosen to approximately minimize along the search direction. For constrained problems the next iteration is preferred not only to decrease, but also to come closer to satisfying the constraints. Often these two aims conflict, so it is necessary to weigh their relative importance and define a merit function, which is used as a criterion for determining whether or not one point is better than another.

In this study, the Genetic Algorithm toolbox in MATLAB is utilized. Parameters, such as population size, maximum generations, crossover probability, etc. are tuned to improve the computation efficiency. The solutions generated by the GA are employed as the set of feasible initial values to start the SQP program, which is also written in MATLAB. The implementation of SQP consists of updating of the Hessian matrix of the Lagrangian function, quadratic programming problem solution, and line search and merit function calculation.

B.2 Application of Error Budget for Three-Axis Machine Tool Miniaturization

The current trend for the miniature workpieces requires the design guidelines for the scaling-down of machine tools. The physical realization of size reduction of a machine, while retaining the original functions, is challenging. Micro/meso-scale

machine tools (mMTs), as the counterparts of the conventional machine tools, have been designed and reported by many researchers (Lu and Yoneyama, 1999; Kussul et al., 2002; Chen et al., 2004; Kurita and Hattori, 2005). The scaling effects on the miniaturization of machine tools have also been studied (Kussul et al., 1996; Lee, 2004; Chen, 2005; Kussul et al., 2006; Liang, 2006). Miniaturization of machine tools would cause scaling effects of acting forces, machine stiffness, surface properties, manufacturing accuracy, and traveling speed (Vogler et al., 2002).

As far as the accuracy is concerned, many error sources that are present in machine tools scale favorably with miniaturization, allowing simplification of the design to meet the accuracy requirements, resulting in a less expensive machine tool. Vogler et al. (2002) pointed out that shorter Abbe offsets in mMTs result in less amplification of angular errors, which allows for the use of components with less stringent geometric tolerances. Slocum (1992) mentioned that the lower mass/size ratio for micro-machines makes them reach thermal equilibrium more quickly. Several methods have been proposed to measure, calibrate and analyze the error sources in mMTs. Lee et al. (2005) presented a six-degree-of-freedom geometric error measurement system for the simultaneous measurement of six geometric error components of the moving axes of mMTs. Honegger et al. (2006) developed a trigger probe measurement system and measurement methodology for kinematic self-calibration of mMTs. Caballero-Ruiz et al. (2007) proposed to use two-ball gauges to identify the geometric errors in mMTs.

However, quantitative methods are still needed for variation analysis in the design of mMTs. The relationship between the quasi-static errors and the part dimensional accuracy has not yet been addressed for the miniaturization of machine tools. How to

distribute the error variations among the machine tool elements in the design stage, which error sources should be emphasized, and how the errors are amplified and propagated through mMTs have to be clarified theoretically. The proposed machine tool error budgeting methods in the previous Section will be employed herein to investigate the scaling effects of part sizes on the variation propagation properties of a three-axis machine tool. The size of the parts is assumed to correspond to the size of the machine tools.

For a three-axis machine tool, there are, theoretically, 21 error components (i.e., three linear and three angular errors for each axis, and three squareness errors between each axes). The scaling effects of part sizes are analyzed from two aspects, conceptually similar to the forward and reverse problems of machine tool error budgeting. Two sets of measures are also defined from part-oriented and machine-oriented aspects.

Error Budget Analysis for the Miniaturization of Machine Tools

From the part perspective, the magnitude of the dimensional accuracy along each direction is of primary concern. Therefore, the sensitivities of part dimensional accuracy with respect to the error components in the machine element level are defined as:

$$SP_x = \frac{\|VE_x\|_2}{\|\vec{e}\|_2} \tag{B.9}$$

$$SP_y = \frac{\|VE_y\|_2}{\|\vec{e}\|_2} \tag{B.10}$$

$$SP_z = \frac{\|VE_z\|_2}{\|\vec{e}\|_2} \tag{B.11}$$

where $\|\cdot\|_2$ is the Euclidean norm. VE_x, VE_y and VE_z are the dimensional tolerances (volumetric errors) along X, Y and Z directions of the machined parts; and $\vec{e}$ is the error vector including all the error components of the machine tool elements.

In addition, the most sensitive direction of machined part and the ratio of the part dimensional accuracy between each direction are also important. The following two robustness indices are defined as

$$RI_1 = \frac{\sigma_{max}}{\sigma_{min}} = cond\left(\frac{\left\|\overrightarrow{VE}\right\|_2}{\|\vec{e}\|_2}\right) \tag{B.12}$$

$$RI_2 = \sigma_{max} = \frac{\left\|\overrightarrow{VE}\right\|_2}{\|\vec{e}\|_2} \tag{B.13}$$

where RI_1 and RI_2 are the condition number and the Euclidean norm of the sensitivity matrix, respectively.

From the machine perspective, it is always the machine tool designers' concern to understand the variation contribution of each axis and each error type. The sensitivities of part dimensional accuracy with respect to each axis and error component types are thus defined:

$$SM_x = \frac{\left\|\overrightarrow{VE}\right\|_2}{\|\vec{e}(\vec{e} \in X\text{-}axis)\|_2} \tag{B.14}$$

$$SM_y = \frac{\left\|\overrightarrow{VE}\right\|_2}{\|\vec{e}(\vec{e} \in Y\text{-}axis)\|_2} \tag{B.15}$$

$$SM_z = \frac{\left\|\overrightarrow{VE}\right\|_2}{\|\vec{e}(\vec{e} \in Z\text{-}axis)\|_2} \tag{B.16}$$

$$SM_L = \frac{\left\|\overrightarrow{VE}\right\|_2}{\left\|\vec{e}(\vec{e} \in Linear)\right\|_2} \tag{B.17}$$

$$SM_A = \frac{\left\|\overrightarrow{VE}\right\|_2}{\left\|\vec{e}(\vec{e} \in Angular)\right\|_2} \tag{B.18}$$

$$SM_S = \frac{\left\|\overrightarrow{VE}\right\|_2}{\left\|\vec{e}(\vec{e} \in Squareness)\right\|_2} \tag{B.19}$$

where $\overrightarrow{VE}$ is the total volumetric errors, and error components, $\vec{e}$, are divided into different groups depending on the machine axis or error types.

These measures defined above are exemplified through a three-axis machine tool with the kinematic chain of $K_C = P_T G_R XYZT_L$ is considered. Each axis is assumed to be equal in terms of errors. Only the variation of error components are considered, therefore, the location of G_R makes no difference. The part is assumed to be a cube with equal length in every direction. The length of 10, 20, 50, 100, 200, and 300 mm are utilized; 10, 20 and 50 mm are considered to be the parts for meso-scale machine tools, while 100, 200, and 300 mm are for conventional machine tools.

Figure B.4(a) shows the part dimensional sensitivities, SP_x, SP_y and SP_z, with respect to the machine tool error variations. With the increase of part size, the dimension along the axis which is farther away from the tool of the machine, in this case *X*-dir, becomes more sensitive to the variation of the error components. Figure B.4(b) shows the trend of robustness indices. For larger parts, both indices, RI_1 and RI_2, increase. The results indicate that for fabricating larger parts, certain direction should have lower error variation in order to make the part variations in each direction balanced; otherwise, the dimensional deviation of the machined parts would differ.

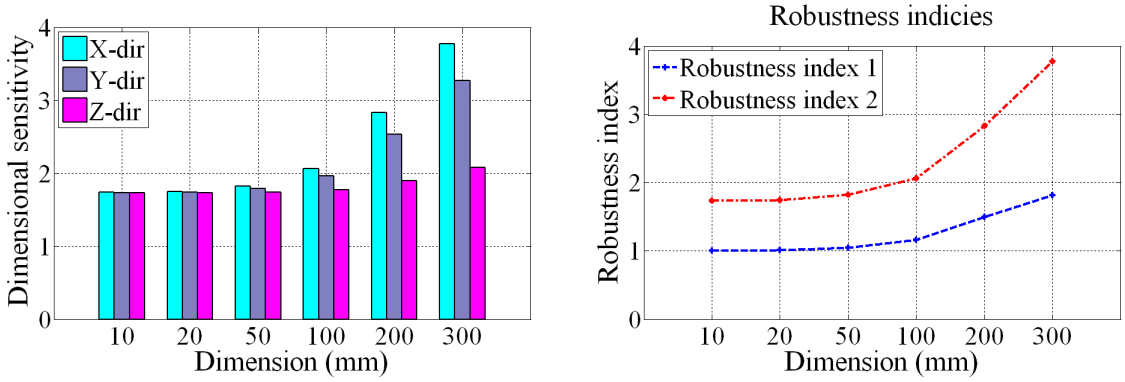

(a) (b)

Figure B.4 Part-oriented measures with respect to the part size variations. (a) Dimensional sensitivities and (b) robustness indices.

Figure B.5 shows the change of machine-oriented sensitivity measures. In terms of machine tool axes, with the increase of part size, the axis away from the tool in the kinematic chain contribute more variations. In term of error types, for larger parts, angular and squareness errors become more dominant compared with the constant linear errors. These results illustrate the well-recognized Abbe effects, the angular errors would be amplified by the effective lever arms, and the static nature of linear errors (Slocum, 1992).

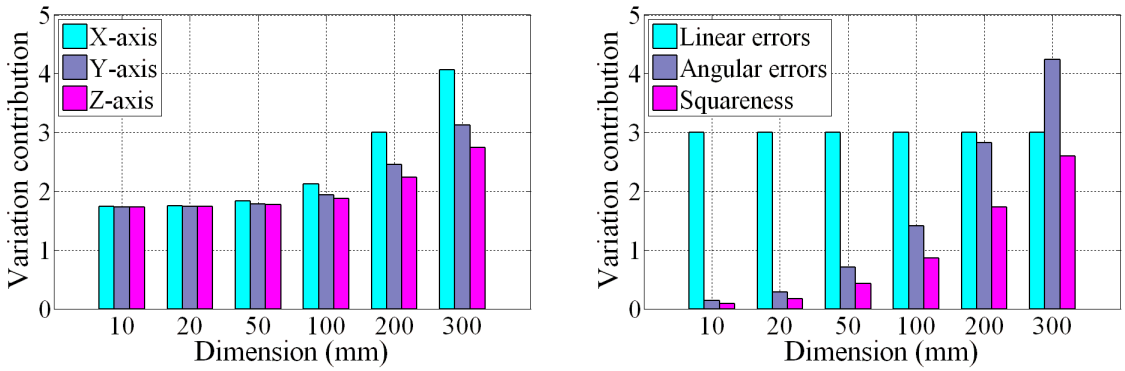

(a) (b)

Figure B.5 Machine-oriented measures with respect to the part size variations depending on (a) Machine tool axes and (b) error types.

Error Budget Synthesis for the Miniaturization of Machine Tools

The proposed hybrid GA/SQP method is utilized to solve the reverse machine tool error budgeting. In order to allocate the part dimensional variations to error components in the machine element level, the required volumetric errors along each direction, $\overrightarrow{VE}_{i\_R}$, must be assumed. The concept of relative accuracy, defined as the ratio of the attainable tolerance-to-workpiece size (Vogler et al., 2002) is employed. The relative accuracy, as shown in Figure B.6, is assumed to be constant for various part sizes.

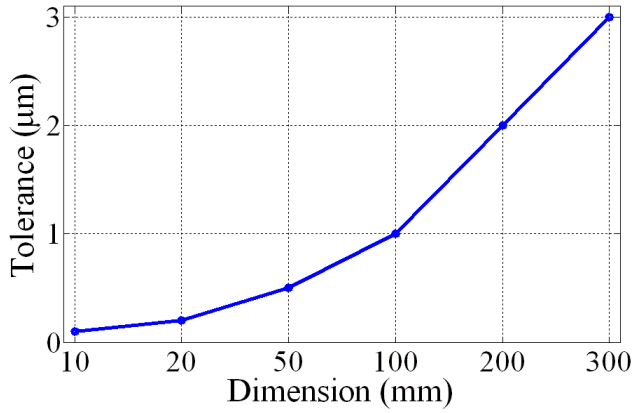

Figure B.6 Relative accuracy with respect to the part size variations.

The hybrid GA/SQP method was then utilized to solve the optimal allocation problem. The parameters for the GA are listed in Table B.1. The results of the GA were then used as the initial values for the SQP. The allocated error variations are summarized in Figure B.7. In Figure B.7, the units for linear and angular errors are μm and arcsec, respectively. Only those error components affecting the volumetric errors are shown. From the allocation results, the ratio between the linear and angular errors obviously changes with the decrease of the part sizes.

Table B.1 Parameters for the GA in the optimal error allocation application.

Population size	10	Maximum generations	5000
Crossover probability	0.9	Mutation probability	0.1

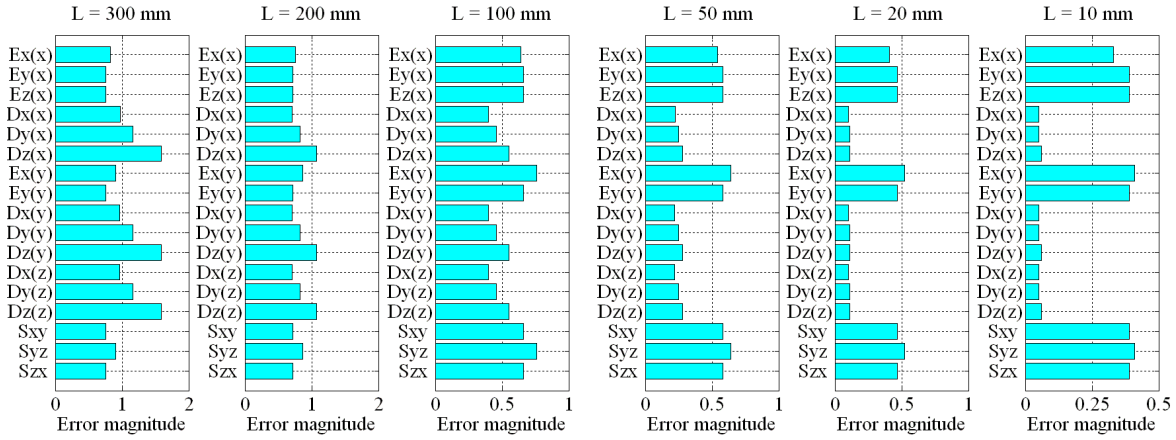

Figure B.7 Error components of machine elements allocated through the hybrid GA/SQP method with respect to the part size variations.

Figure B.8 summarizes the allocation results in terms of the machine tool axis and error types. In calculating the percentage of variation contribution, the angular and squareness errors are converted into linear errors by multiplying the length of the parts and each error component is taken into account in the RSS sense. Therefore, the percentage variation in terms of machine tool axis and error type is defined as

$$(Variation\ contribution\_axis)\% = \frac{\|\vec{e}(\vec{e} \in i\text{-}axis)\|_2}{\|\vec{e}\|_2} \tag{B.20}$$

$$(Variation\ contribution\_error\ type)\% = \frac{\|\vec{e}(\vec{e} \in error\ type)\|_2}{\|\vec{e}\|_2} \tag{B.21}$$

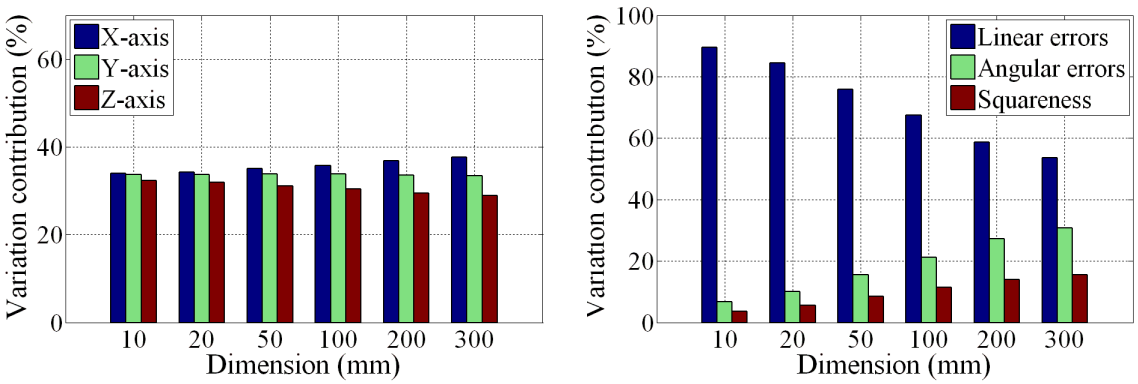

Figure B.8 Comparison of the allocation results in terms of (a) machine tool axis and (b) error types.

These results show the same trend as in the machine tool error budget analysis. In terms of machine tool axis, with the increase of part size, the axis away from the tool becomes more sensitive to the error variations; therefore, more error variations are allocated to that axis. In terms of error types, with the decrease of the part sizes, the linear errors become more dominant.

For a meso-scale machine tool design, if the quasi-static errors are considered as the main contributor, the linear errors should be placed more attention. The underlying reason is that the decrease of the machine tool size alleviates the Abbe effects. In addition, the miniaturization of machine tools balances the influence of each axis in the kinematic chain. Conventionally, the moving axis away from the tool should have better accuracy and repeatability. However, for the meso-scale machine tool, each axis shows relatively similar contribution to the machined part dimensional variations. Therefore, it is not necessary to make those moving axis away from the tool more robust in terms of repeatability.

The results provide some new guidelines about the design of mMTs. First, the position of moving axis in the kinematic chain becomes equal in terms of variation

contribution to the volumetric errors due to the miniaturization of machine tools. This increases the flexibility of mMTs because configurations could be adjusted without considering the issue of potential accuracy deterioration.

In addition, the linear errors become dominant for mMTs comparing with angular and squareness errors. Error reduction should be applied to decrease the linear errors. Compensation of linear errors is usually easier to realize because the coupling effects of angular errors are significantly reduced. Therefore, the accuracy of mMTs could be guaranteed with less effort than the conventional machine tools.

APPENDIX C
Five-Axis Machine Tool Classification

Classification and comparison of five-axis machine configurations have been investigated by a few researchers (Sakamoto and Inasaki, 1993) The addition of two rotary axes, making both tool position and orientation crucial for precision machining, is the basic difference between three-axis and five-axis machine tool. Bohez (2002) categorized the possible conceptual designs of five-axis machine tools based on the theoretically possible combinations of linear and rotary axes. Some useful quantitative parameters, such as the workspace utilization factor, machine tool space efficiency, orientation space index and orientation angle index were defined. Tutunea-Fatan and Feng (2004) proposed a generic model for the analysis of practical machine configuration designs. The importance of effective tool length was stressed based on the minimization of the total translational movement. This research could be further extended to the optimal tool length determination and workpiece placement for five-axis machine tools.

Following the discussion in the Appendix A, if axes are selected from X, Y, Z and A, B, C for configuration codes of five-axis machine tools without considering the location of machine bed in the kinematic chain, there are $6 \times 5! = 720$ possible combinations (Bohez, 2002). If only five-axis machines with three linear axes are taken into account, only $3 \times 5! = 360$ combinations are still possible. These possible five-axis machine tools can be further classified based on the location where the rotary axes are distributed: (a) rotary axes are on the tool side; (b) rotary axes are separated; (c) rotary axes are on the workpiece side. Each category has 120 possible configurations. By employing kinematic chains, the three categories can be denoted as: $R_o R_o T_R T_R T_R$,

$R_o T_R T_R T_R R_o$ and $T_R T_R T_R R_o R_o$. If substituting T_R and R_o with X, Y, Z and A, B, C, and placing G_R in the appropriate position in the kinematic chain, there will be 144 for each category and altogether 432 configurations, as long as there is no repetition of any axis.

For the sake of illustration, it is assumed that the sequence of linear axes in the kinematic chain is always XYZ and the effects of the ground, G_R, is ignored. Therefore, the configuration number is down to 6 for each category, as summarized in Table C.1, where the corresponding ideal kinematic models are also listed.

In a broad sense, any machines with five axes, no matter how many translational or rotational axes, can be regarded as five-axis machine tools. However, a real five-axis machine must be able to provide five DOF in order to position and orient the tool and workpiece under any angle relative to each other during machining. Hence, two rotary axes are the minimum requirement for a real five-axis machine tool. Moreover, almost all the five-axis machine tools have three translational and two rotational axes in practice due to the fact that the sequence of kinematic chain for a five-axis machine must satisfy some specific geometric and kinematic constraints imposed by the machining process (Tutunea-Fatan and Feng, 2004).

Table C.1 Ideal kinematic models for five-axis machine tools

Kinematic chain		Position	Orientation
$R_oR_oT_RT_RT_R$	$ABXYZ$	$l = \sin(b)\cdot p + \sin(b)\cdot z + \cos(b)\cdot x$ $m = -\sin(a)\cos(b)\cdot p - \sin(a)\cos(b)\cdot z + \cos(a)\cdot y + \sin(a)\sin(b)\cdot x$ $n = \cos(a)\cos(b)\cdot p + \cos(a)\cos(b)\cdot z + \sin(a)\cdot y - \cos(a)\sin(b)\cdot x$	$u = \sin(b)$ $v = -\sin(a)\cos(b)$ $w = \cos(a)\cos(b)$
	$ACXYZ$	$l = -\sin(c)\cdot y + \cos(\ \ )\cdot x$ $m = -\sin(a)\cdot p - \sin(a)\cdot z + \cos(a)\cos(c)\cdot y + \cos(a)\sin(c)\cdot x$ $n = \cos(a)\cdot p + \cos(a)\cdot z + \sin(a)\cos(c)\cdot y + \sin(a)\sin(c)\cdot x$	$u = 0$ $v = -\sin(a)$ $w = \cos(a)$
	$BAXYZ$	$l = \cos(a)\sin(b)\cdot p + \cos(a)\sin(b)\cdot z + \sin(a)\sin(b)\cdot y + \cos(b)\cdot x$ $m = -\sin(a)\cdot p - \sin(a)\cdot z + \cos(a)\cdot y$ $n = \cos(a)\cos(b)\cdot p + \cos(a)\cos(b)\cdot z + \sin(a)\cos(b)\cdot y + \sin(b)\cdot x$	$u = \cos(a)\sin(b)$ $v = -\sin(a)$ $w = \cos(a)\cos(b)$
	$BCXYZ$	$l = \sin(b)\cdot p + \sin(b)\cdot z - \cos(b)\sin(c)\cdot y + \cos(b)\cos(c)\cdot x$ $m = \cos(c)\cdot y + \sin(c)\cdot x$ $n = \cos(b)\cdot p + \cos(b)\cdot z + \sin(b)\sin(c)\cdot y - \sin(b)\sin(c)\cdot x$	$u = \sin(b)$ $v = 0$ $w = \cos(b)$
	$CAXYZ$	$l = \sin(c)\sin(a)\cdot p + \sin(a)\sin(c)\cdot z - \cos(a)\sin(c)\cdot y + \cos(c)\cdot x$ $m = -\cos(c)\sin(a)\cdot p - \sin(a)\cos(c)\cdot z + \cos(a)\cos(c)\cdot y + \sin(c)\cdot x$ $n = \cos(a)\cdot p + \cos(a)\ \cdot z + \sin(a)\ \cdot y$	$u = \sin(a)\sin(c)$ $v = -\sin(a)\cos(c)$ $w = \cos(a)$
	$CBXYZ$	$l = \sin(b)\cos(c)\cdot p + \cos(c)\sin(b)\cdot z + \sin(c)\cdot y + \cos(c)\cos(b)\cdot x$ $m = \sin(b)\sin(c)\cdot p + \sin(c)\sin(b)\cdot z + \cos(c)\cdot y + \sin(c)\cos(b)\cdot x$ $n = \cos(b)\cdot p + \cos(b)\ \cdot z - \sin(b)\ \cdot y$	$u = \cos(c)\sin(b)$ $v = \sin(c)\sin(b)$ $w = \cos(b)$
$R_oT_RT_RT_RR_o$	$AXYZB$	$l = \sin(b)\cdot p + x$ $m = -\sin(a)\cos(b)\cdot p - \sin(a)\cdot z + \cos(a)\cdot y$ $n = \cos(a)\cos(b)\cdot p + \cos(a)\cdot z + \sin(a)\cdot y$	$u = \sin(b)$ $v = -\sin(a)\cos(b)$ $w = \cos(a)\cos(b)$
	$AXYZC$	$l = x$ $m = -\sin(a)\cdot p - \sin(a)\cdot z + \cos(a)\cdot y$ $n = \cos(a)\cdot p + \cos(a)\cdot z + \sin(a)\cdot y$	$u = 0$ $v = -\sin(a)$ $w = \cos(a)$
	$BXYZA$	$l = \cos(a)\sin(b)\cdot p + \sin(b)\cdot z + \cos(b)\cdot x$ $m = -\sin(a)\cdot p + y$ $n = \cos(a)\cos(b)\cdot p + \cos(b)\cdot z + \sin(b)\cdot x$	$u = \cos(a)\sin(b)$ $v = -\sin(a)$ $w = \cos(a)\cos(b)$
	$BXYZC$	$l = \sin(b)\cdot p + \sin(b)\cdot z + \cos(b)\cdot x$ $m = y$ $n = \cos(b)\cdot p + \cos(b)\cdot z - \sin(b)\cdot x$	$u = \sin(b)$ $v = 0$ $w = \cos(b)$
	$CXYZA$	$l = \sin(c)\sin(a)\cdot p - \sin(c)\cdot y + \cos(c)\cdot x$ $m = -\cos(c)\sin(a)\cdot p + \cos(c)\cdot y + \sin(c)\cdot x$ $n = \cos(a)\cdot p + z$	$u = \sin(a)\sin(c)$ $v = -\sin(a)\cos(c)$ $w = \cos(a)$
	$CXYZB$	$l = \sin(b)\cos(c)\cdot p + \sin(c)\cdot y + \cos(c)\cdot x$ $m = \sin(b)\sin(c)\cdot p + \cos(c)\cdot y + \sin(c)\cdot x$ $n = \cos(b)\cdot p + z$	$u = \cos(c)\sin(b)$ $v = \sin(c)\sin(b)$ $w = \cos(b)$
$T_RT_RT_RR_oR_o$	$XYZAB$	$l = \sin(b)\cdot p + x$ $m = -\sin(a)\cos(b)\cdot p + y$ $n = \cos(a)\cos(b)\cdot p + z$	$u = \sin(b)$ $v = -\sin(a)\cos(b)$ $w = \cos(a)\cos(b)$
	$XYZAC$	$l = x$ $m = -\sin(a)\cdot p + y$ $n = \cos(a)\cdot p + z$	$u = 0$ $v = -\sin(a)$ $w = \cos(a)$
	$XYZBA$	$l = \cos(a)\sin(b)\cdot p + x$ $m = -\sin(a)\cdot p + y$ $n = \cos(a)\cos(b)\cdot p + z$	$u = \cos(a)\sin(b)$ $v = -\sin(a)$ $w = \cos(a)\cos(b)$
	$XYZBC$	$l = x$ $m = -\sin(a)\cdot p + y$ $n = z$	$u = \sin(b)$ $v = 0$ $w = \cos(b)$
	$XYZCA$	$l = \sin(c)\sin(a)\cdot p + x$ $m = -\cos(c)\sin(a)\cdot p + y$ $n = \cos(a)\cdot p + z$	$u = \sin(a)\sin(c)$ $v = -\sin(a)\cos(c)$ $w = \cos(a)$
	$XYZCB$	$l = \sin(b)\cos(c)\cdot p + x$ $m = \sin(b)\sin(c)\cdot p + y$ $n = \cos(b)\cdot p + z$	$u = \cos(c)\sin(b)$ $v = \sin(c)\sin(b)$ $w = \cos(b)$

However, even a machine equipped with three linear axes and two rotary axes does not necessarily provide five-axis machining. For a real five-axis machine tool, all five axes should be incorporated in the form shaping function. But form shaping functions of some configurations, as highlighted in Table C.1, merely include four axis. This means these configurations can only provide four degree-of-freedom machining. Therefore, the number of possible conceptual configurations of five-axis machine tools reduces to 288, and 96 configurations for each category.

In order to compare the five-axis machine tools in the three categories, volumetric utility (Vogler et al., 2003) defined as the ratio of the machine and workpiece volumes, is exploited to analyze different configurations because the volume of workspace is one of the basic concerns when designing a new machine, which directly determines the traveling ranges of each axis and the size of the final machine. The volume of workspace is basically relevant to the size of the workpiece and the length of the tool. For a three axis machine, the floor space of the machine tool is about twenty times as large as the workpiece size (Sakamoto and Inasaki, 1993). It is, therefore, worthwhile to investigate the effects of workpiece size on the workspace of five-axis machines, so that the most appropriate machine structure could be chosen to minimize the workspace of the machine in the design stage.

The ideal kinematic models are utilized herein to relate the workpiece size to the workspace volume. The workpiece size is assumed to be $l \times m \times n$, whereas the required workspace is the multiplication of each axis travel range, obtained by solving form shaping functions. The maximum required travel range for illustrated five-axis configurations in Table C.1 are summarized in Table C.2. If the workpiece is cubic, that

is, $l = m = n$, required workspace for each category is same, in other words, the space utility of five-axis machine tools, defined as the volume ratio of the workpiece to the workspace, is basically dependent on the distribution of two rotary axes and the tool length, p.

Table C.2 Maximum required workspace for conceptual five-axis machine configurations.

Kinematic chains		Maximum required workspace		
		X-dir	Y-dir	Z-dir
$R_o R_o T_R T_R T_R$	$ABXYZ$	$\sqrt{l^2+m^2+n^2}$	$\sqrt{m^2+n^2}$	$p+\sqrt{l^2+m^2+n^2}$
	$BAXYZ$	$\sqrt{l^2+n^2}$	$\sqrt{l^2+m^2+n^2}$	$p+\sqrt{l^2+m^2+n^2}$
	$CAXYZ$	$\sqrt{l^2+m^2}$	$\sqrt{l^2+m^2+n^2}$	$p+\sqrt{l^2+m^2+n^2}$
	$CBXYZ$	$\sqrt{l^2+m^2+n^2}$	$\sqrt{l^2+m^2}$	$p+\sqrt{l^2+m^2+n^2}$
$R_o T_R T_R T_R R_o$	$AXYZB$	$p+l$	$\sqrt{m^2+n^2}$	$\sqrt{p^2+m^2+n^2}$
	$BXYZA$	$\sqrt{l^2+n^2}$	$p+m$	$\sqrt{p^2+l^2+n^2}$
	$CXYZA$	$\sqrt{l^2+m^2}$	$\sqrt{p^2+l^2+m^2}$	$p+n$
	$CXYZB$	$\sqrt{p^2+l^2+m^2}$	$\sqrt{l^2+m^2}$	$p+n$
$T_R T_R T_R R_o R_o$	$XYZAB$	$p+l$	$p+m$	$p+n$
	$XYZBA$	$p+l$	$p+m$	$p+n$
	$XYZCA$	$p+l$	$p+m$	$p+n$
	$XYZCB$	$p+l$	$p+m$	$p+n$

Consequently, the space utility for three five-axis machine categories with respect to the length ratio of the workpiece to the tool, l/p, is plotted in Figure C.1. It is obvious that $R_o R_o T_R T_R T_R$ configuration provides better space utility when the workpiece is small; while when the workpiece size is large, $T_R T_R T_R R_o R_o$ configuration becomes more space-saving. Figure C.1 analytically validates the statement mentioned by Bohez (2002) that the useful workspace is usually much smaller than the product of the travel in X, Y, Z-axis for five-axis machines with $R_o R_o T_R T_R T_R$ configurations for large workpieces. Five-axis machines with $T_R T_R T_R R_o R_o$ configuration can machine very large workpieces. For

$R_o T_R T_R T_R R_o$ configuration, the application range of these machines is about the same as $R_o R_o T_R T_R T_R$ configuration.

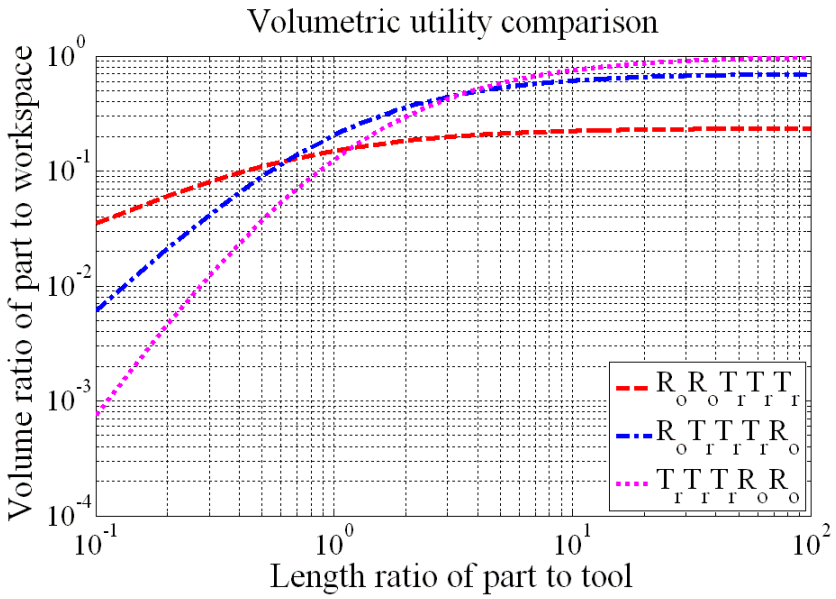

Figure C.1 Comparison of volumetric utility of five-axis machine configurations.

APPENDIX D
Temperature Sensor Locations for the Sodick AQ55L EDM Machine

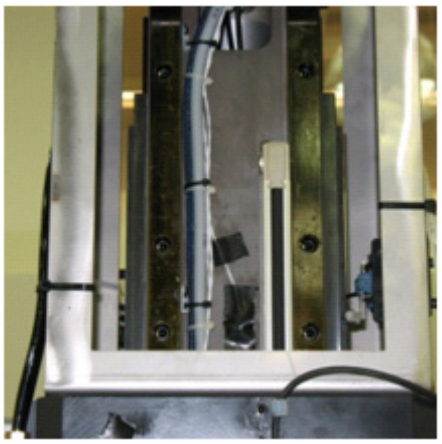

(a)

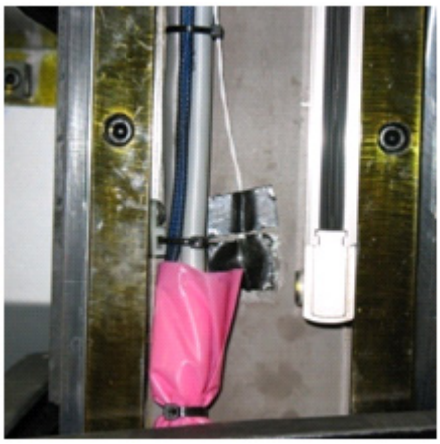

(b)

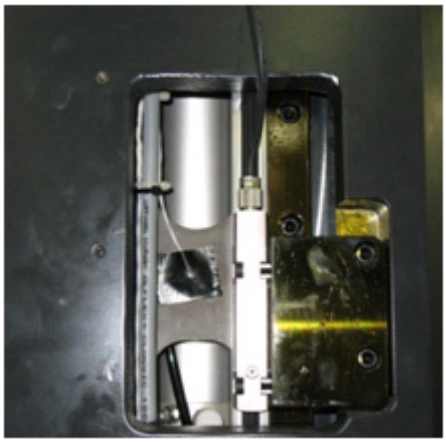

(c)

(d)

(e)

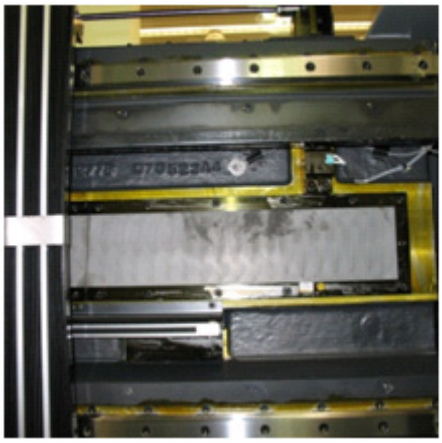

(f)

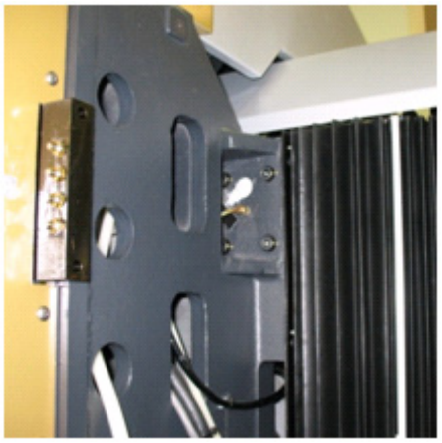

(g)

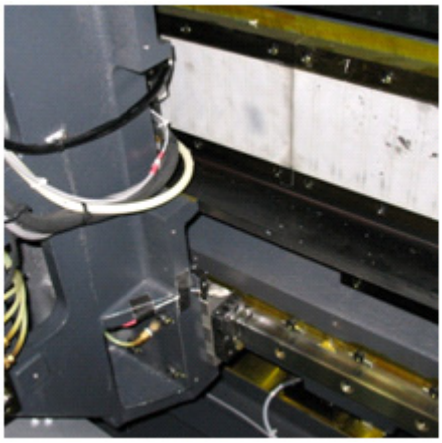

(h)

(i)

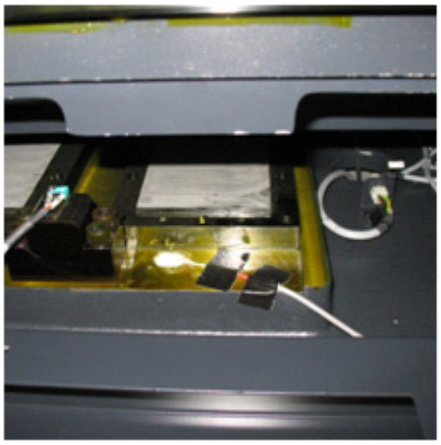

(j)

Figure D.1 Detailed temperature sensor locations on the Sodick AQ55L EDM Machine, and their purpose for the corresponding thermal error models. (a) Ch1 (*Z*-axis), (b) Ch3 (*Z*-axis), (c) Ch5 (*Z*-axis), (d) Ch6 (*Y*-axis), (e) Ch7 (*X*-axis), (f) Ch8 (*X*-axis), (g) Ch10 (*X*-axis), (h) Ch13 (*X*-axis), (i) Ch16 (*Y*-axis), and (j) Ch17 (*Y*-axis).

BIBLIOGRAPHY

BIBLIOGRAPHY

Abbaszadeh-Mir, Y., Mayer, J., Cloutier, G. and Fortin, C., 2002, "Theory and Simulation for the Identification of the Link Geometric Errors for a Five-Axis Machine Tool Using a Telescoping Magnetic Ball-Bar," International Journal of Production Research, Vol. 40, No. 18, pp. 4781-4797.

Alejandre, I. and Artes, M., 2006, "Thermal Non-Linear Behaviour in Optical Linear Encoders," International Journal of Machine Tools and Manufacture, Vol. 46, No. 12-13, pp. 1319-1325.

Attia, M. and Fraser, S., 1999a, "A Generalized Modelling Methodology for Optimized Real-Time Compensation of Thermal Deformation of Machine Tools and CMM Structures," International Journal of Machine Tools and Manufacture, Vol. 39, No. 6, pp. 1001-1016.

Attia, M. and Fraser, S., 1999b, "A Generalized Modeling Methodology for Optimized Real-Time Compensation of Thermal Deformation of Machine Tools and CMM Structures," International Journal of Machine Tools and Manufacture, Vol. 39, No. 6, pp. 1001-1016.

Attia, M. and Kops, L., 1979a, "Nonlinear Thermoelastic Behaviour of Structural Joints – Solution to a Missing Link for Prediction of Thermal Deformation of Machine Tools," Journal of Engineering for Industry, Vol. 101, No. 3, pp. 348–354.

Attia, M. and Kops, L., 1979b, "Computer Simulation of Nonlinear Thermoelastic Behaviour of a Joint in Machine Tool Structure and Its Effect on Thermal Deformation," Journal of Engineering for Industry Vol. 101, No. 3, pp. 355–361.

Attia, M. and Kops, L., 1980, "Importance of Contact Pressure Distribution on Heat Transfer in Structural Joints of Machines," Journal of Engineering for Industry Vol. 102 No. 2, pp. 159–167.

Attia, M. and Kops, L., 1981a, "System Approach to the Thermal Behavior and Deformation of Machine Tool Structures in Response to the Effect of Fixed Joints," Journal of Engineering for Industry, Vol. 103, No. 1, pp. 67-72.

Attia, M. and Kops, L., 1981b, "A New Method for Determining the Thermal Contact Resistance at Machine Tool Joints," CIRP Annals, Vol. 30, No. 1, pp. 259–264.

Attia, M. and Kops, L., 1993, "Thermometric Design Considerations for Temperature Monitoring in Machine Tools and CMM Structures," International Journal of Advanced Manufacturing Technology, Vol. 8, No. 5, pp. 311–319.

Balsamo, A., Franke, M., Trapet, E., Waldele, F., De Jonge, L. and Vanherck, P., 1997, "Results of the CIRP - Euromet Intercomparison of Ball Plate-Based Techniques for Determining CMM Parametric Errors," CIRP Annals, Vol. 46, No. 1, pp. 463-466.

Balsamo, A., Marques, D. and Sartori, S., 1990, "A Method for Thermal Deformation Corrections of CMMs," CIRP Annals, Vol. 39, No. 1, pp. 557-560.

Barakat, N., Elbestawi, M. and Spence, A., 2000, "Kinematic and Geometric Error Compensation of a Coordinate Measuring Machine," International Journal of Machine Tools and Manufacture, Vol. 40, No. 6, pp. 833-850.

Belforte, G., Bona, B., Canuto, E., Donati, F., Ferraris, F., Gorini, I., Morei, S., Peisino, M. and Sartori, S., 1987, "Coordinate Measuring Machines and Machine Tools Selfcalibration and Error Correction," CIRP Annals, Vol. 36, No. 1, pp. 359-364.

Bohez, E., 2002, "Compensating for Systematic Errors in 5-Axis NC Machining," Computer Aided Design, Vol. 34, No. 5, pp. 391-403.

Bossmanns, B. and Tu, J., 1999, "A Thermal Model for High Speed Motorized Spindles" International Journal of Machine Tools and Manufacture, Vol. 39, No. 9, pp. 1345-1366.

Buchanan J. and Turner, P. 1992, Numerical Methods and Analysis, McGraw-Hill College.

Bryan, J., 1982a, "Simple Method for Testing Measuring Machines and Machine Tools. Part I: Principles and Applications," Precision Engineering, Vol. 4, No. 2, pp. 61-69.

Bryan, J., 1982b, "Simple Method for Testing Measuring Machines and Machine Tools. Part II: Construction details," Precision Engineering, Vol. 4, No. 3, pp. 125-138.

Bryan, J., 1990, "International Status of Thermal Error Research (1990)," CIRP Annals, Vol. 39, No. 2, pp. 645-656.

Caballero-Ruiz, A., Ruiz-Huerta, L., Baidyk, T. and Kussul, E., 2007, "Geometric Error Analysis of a CNC Micro-Machine Tool," Mechatronics, Vol. 17, No. 4-5, pp. 231-243.

Carne, T. and Dohrmann, C., 1995, "A Modal Test Design Strategy for Model Correlation," Proceedings of 13th International Modal Analysis Conference, pp. 927-933.

Chapman, M., 2003, "Limitations of Laser Diagonal Measurements," Precision Engineering, Vol. 27, No. 4, pp. 401-406.

Chase, K. and Greenwood, W., 1988, "Design Issues in Mechanical Tolerance Analysis," Manufacturing Review, Vol. 1, No. 1, pp. 50-59.

Chase, K., Greenwood, W., Loosli, B. and Hauglund, L., 1990, "Least Cost Tolerance Allocation for Mechanical Assemblies with Automated Process Selection," Manufacturing Review, Vol. 3, No. 1, pp. 49-59.

Chase, K. and Parkinson, A., 1991, "A Survey of Research in the Application of Tolerance Analysis to the Design of Mechanical Assemblies," Research in Engineering Design, Vol. 3, No. 1, pp. 23-37.

Chen, G., Yuan, J. and Ni, J., 2001, "A Displacement Measurement Approach for Machine Geometric Error Assessment," International Journal of Machine Tools and Manufacture, Vol. 41, No. 1, pp. 149-161.

Chen, H., 2005, Generation and Evaluation of Meso-Scale Machine Tool Designs for Micro-Machining Applications, Ph.D. Dissertation, the University of Michigan.

Chen, H., Mayor, R. and Ni, J., 2004, "A Virtual Machine Tool (VMT) Integrated Design Environment and its Application to Meso-Scale Machine Tool Development," Transactions of the North American Manufacturing Research Institute of SME, Vol. 32, pp. 327-334.

Chen, J., 1995, "Computer Aided Accuracy Enhancement for Multi-Axis CNC Machine Tool," International Journal of Machine Tools and Manufacture, Vol. 35, No. 4, pp. 593-605.

Chen, J., 1996a, "A Study of Thermally Induced Machine Tool Errors in Real Cutting Conditions," International Journal of Machine Tools and Manufacture, Vol. 36, No. 12, pp. 1401-1411.

Chen, J., 1996b, "Fast Calibration and Modeling of Thermally-Induced Machine Tool Errors in Real Machining," International Journal of Machine Tools and Manufacture, Vol. 37, No. 2, pp. 159-169.

Chen, J. and Chiou, G., 1995, "Quick Testing and Modeling of Thermally-Induced Errors of CNC Machine Tools," International Journal of Machine Tools and Manufacture, Vol. 35, No. 7, pp. 1063-1074.

Chen, J., Kou, T. and Chiou, S., 1999, "Geometric Error Calibration of Multi-Axis Machines Using an Auto-Alignment Laser Interferometer," Precision Engineering, Vol. 23, No. 4, pp. 243-252.

Chen, J. and Ling, C., 1996, "Improving the Machine Accuracy through Machine Tool Metrology and Error Correction," International Journal of Advanced Manufacturing Technology, Vol. 11, No. 3, pp. 198-205.

Chen, J., Yuan, J. and Ni, J., 1996, "Thermal Error Modeling for Real-Time Error Compensation", International Journal of Advanced Manufacturing Technology, Vol. 12, No. 4, pp. 266-275.

Chen, J., Yuan, J., Ni, J. and Wu, S., 1993, "Real-Time Compensation for Time-Variant Volumetric Error on a Machining Center," Journal of Engineering for Industry, Vol. 115, No. 4, pp. 472-479.

Cho M., Kim, G., Seo, T., Hong, Y. and Cheng, H., 2006, "Integrated Machining Error Compensation Method Using OMM Data and Modified PNN Algorithm," International Journal of Machine Tools and Manufacture, Vol. 46, No. 12-13, pp. 1417-1427.

Choi, J., Min, B. and Lee, S., 2004, "Reduction of Machining Errors of a Three-Axis Machine Tool by On-Machine Measurement and Error Compensation System," Journal of Materials Processing Technology, Vol. 155-156, No. 1-3, pp. 2056-2064.

Coutinho, A., Landau, L., Wrobel, L. and Ebecken, F., 1989, "Modal Solution of Transient Heat Conduction Utilizing Lanczos Algorithm," International Journal for Numerical Methods in Engineering, Vol. 28, No. 1, pp. 13-25.

De Aquino Silva, J. and Burdekin, M., 2002, "A Modular Space Frame for Assessing the Performance of Co-ordinate Measuring Machines (CMMs)," Precision Engineering, Vol. 26, No. 1, pp. 37-48.

Delbressine, F., Florussen, G., Schijvenaars, L. and Schellekens, P., 2006, "Modelling Thermomechanical Behaviour of Multi-Axis Machine Tools," Precision Engineering, Vol. 30, No. 1, pp. 47-53.

Denavit, J. and Hartenberg, R., 1954, "A Kinematic Notation for Lower-Pair Mechanism Based on Matrices," Journal of Applied Mechanics, Vol. 22, No. 77, pp. 215-221.

Donaldson, R., 1980, "Error Budgets," Technology of Machine Tools, Vol. 5: Machine Tool Accuracy, Lawrence Livermore Laboratories, University of California, UCRL-52960-5, Livermore, CA.

Donaldson, R. and Thompson, D., 1986, "Design and Performance of a Small Precision CNC Turning Machine," CIRP Annals, Vol. 35, No. 1, pp. 373-376.

Donmez, M., Blomquist, D., Hocken, R., Liu, C. and Barash, M., 1986, "A General Methodology for Machine Tool Accuracy Enhancement by Error Compensation," Precision Engineering, Vol. 8, No. 4, pp. 187-196.

Dos Santos, F., Coutinho, A., and Landau, L., 1990, "New Load Dependent Methods for Modal Solution of Transient Heat Conduction," Proceedings of the International Conference on Advanced Computational Methods in Heat Transfer, Vol. 1, pp. 51-59.

Duffie, N. and Malmberg, S., 1987, "Error Diagnosis and Compensation Using Kinematic Models and Position Error Data," CIRP Annals, Vol. 36, No. 1, pp. 355-358.

El Ouafi, A., Guillot, M. and Bedrouni, A., 2000, "Accuracy Enhancement of Multi-Axis CNC Machines Through On-Line Neurocompensation," Journal of Intelligent Manufacturing, Vol. 11, No. 6, pp. 535-545.

Evans, C., Hocken, R. and Estler, W., 1996, "Reversal, Redundancy, Error Separation, and 'Absolute Testing'," CIRP Annals, Vol. 45, No. 2, pp. 617-634.

Faik, S. and Erdman, A., 1991, "Sensitivity Distribution in Synthesis Space of Four-Bar Linkage," Journal of Mechanical Design, Vol. 113, No. 1, pp. 3-9.

Ferreira, P. and Liu, C., 1986, "An Analytical Quadratic Model for the Geometric Error of a Machine Tool," Journal of Manufacturing Systems, Vol. 5, No. 1, pp. 51-63.

Franse, J., 1990, "Manufacturing Techniques for Complex Shapes with Submicron Accuracy," Reports on Progress in Physics, Vol. 53, No. 8, pp. 1049-94.

Fraser, S., Attia, M. and Osman, M., 1998a, "Modelling, Identification and Control of Thermal Deformation of Machine Tool Structure. Part 1: Concept of Generalized Modeling," Journal of Manufacturing Science and Engineering, Vol. 120, No. 3, pp. 623-631.

Fraser, S., Attia, M. and Osman, M., 1998b, "Modelling, Identification and Control of Thermal Deformation of Machine Tool Structure. Part 2: Generalized Transfer Functions," Journal of Manufacturing Science and Engineering, Vol. 120, No. 3, pp. 632-639.

Fraser, S., Attia, M. and Osman, M., 1999a, "Modelling, Identification and Control of Thermal Deformation of Machine Tool Structure. Part 3: Real-Time Estimation of Heat Sources," Journal of Manufacturing Science and Engineering, Vol. 121, No. 3, pp. 501-508.

Fraser, S., Attia, M. and Osman, M., 1999b, "Modelling, Identification and Control of Thermal Deformation of Machine Tool Structure. Part 4: A Multi-Variable Closed-Loop Control System," Journal of Manufacturing Science and Engineering, Vol. 121, No. 3, pp. 509-516.

Fraser, S., Attia, M. and Osman, M., 1999c, "Modelling, Identification and Control of Thermal Deformation of Machine Tool Structure. Part 5: Experimental Verification," Journal of Manufacturing Science and Engineering, Vol. 121, No. 3, pp. 517-523.

Goldberg, D., 1989, Genetic Algorithms in Search, Optimization, and Machine Learning, Addison-Wesley Professional.

Hai, N., 1995, Machine Tool Accuracy Enhancement by Inverse Kinematic Analysis and Real Time Error Compensation, Ph.D. Dissertation, the University of Michigan

Harris, J. and Spence, A., 2004, "Geometric and Quasi-Static Thermal Error Compensation for a Laser Digitizer Equipped Coordinate Measuring Machine," International Journal of Machine Tools and Manufacture, Vol. 44, No. 1, pp. 65-77.

Hatamura, Y., Nagao, T., Mitsuishi, M., Kato, K., Taguchi, S., Okumura, T., Nakagawa, G. and Sugishita, H., 1993, "Development of an Intelligent Machining Center Incorporating Active Compensation for Thermal Distortion," CIRP Annals, Vol. 42, No. 1, pp. 549-552.

Hocken, R., 1980, Technology of Machine Tools, Volume 5: Machine Tool Accuracy, Lawrence Livermore Laboratories, University of California, UCRL-52960-5, Livermore, CA.

Hocken, R., Simpson, J., Borchardt, B., Lazar, J., Reeve, C. and Stein, P., 1977, "Three Dimensional Metrology," CIRP Annals, Vol. 26, No. 2, pp. 403-408.

Holland, J., 1975, Adaptation in Natural and Artificial Systems, University of Michigan Press, Ann Arbor.

Homann, B. and Thornton, A., 1998, "Precision Machine Design Assistant: a Constraint-Based Tool for the Design and Evaluation of Precision Machine Tool Concepts," Artificial Intelligence for Engineering Design, Analysis and Manufacturing, Vol. 12, No. 5, pp. 419-429.

Honegger, A., Kapoor, S. and DeVor, R., 2006, "A Hybrid Methodology for Kinematic Calibration of Micro/Meso-Scale Machine Tools (mMTs)," Journal of Manufacturing Science and Engineering, Vol. 128, No. 2, pp. 513-522.

Huo, D., Cheng, K., Webb, D. and Wardle, F., 2004, "A Novel FEA Model for the Integral Analysis of a Machine Tool and Machining Processes," Key Engineering Materials, Vol. 257-258, pp. 45-50.

Huang, P. and Ni, J., 1995, "On-Line Error Compensation of Coordinate Measuring Machines," International Journal of Machine Tools and Manufacture, Vol. 35, No. 5, pp. 725-738.

Janeczko, J., 1989, "Machine-Tool Thermal Compensation," Tooling and Production, Vol. 55, No. 5, pp. 60-65.

Janeczko, J., Griffin, B. and Wang, C., 2000, "Laser Vector Measurement Technique for the Determination and Compensation of Volumetric Positioning Errors. Part II: Experimental Verification," Review of Scientific Instruments, Vol. 71, No. 10, pp. 3938-3941.

Jedrzejewski, I., Kaczmarek, J., Kowal, Z. and Winiarski, Z., 1990, "Numerical Optimization of Thermal Behavior of Machine Tools," CIRP Annals, Vol. 39, No. 1, pp. 109-112.

Jedrzejewski, I. and Modrzycki, W., 1992, "A New Approach to Modeling Thermal Behavior of a Machine Tool under Service Condition," CIRP Annals, Vol. 41, No. 1, pp. 455-458.

Juang, J. and Pappa, R., 1985, "Eigensystem Realization Algorithm for Modal Parameter Identification and Model Reduction," Journal of Guidance, Control, and Dynamics, Vol. 8, No. 5, pp. 620-627.

Kakino, Y., Ihara, Y. and Nakatsu, Y., 1987, "The Measurement of Motion Errors of NC Machine Tools and Diagnosis of Their Origins by Using Telescoping Magnetic Ball Bar Method," CIRP Annals, Vol. 36, No. 1, pp. 377-380.

Kakino, Y., Ihara, Y., Shinohara, A., Heidenhain, J., Knapp, W., Chok, L. and Del Grosso, F., 1993, Accuracy Inspection of NC Machine Tools by Double Ball Bar Method, Hanser/Gardner Publications.

Kang, Y., Chang, C., Huang, Y., Hsu, C. and Nieh, I., 2007, "Modification of a Neural Network Utilizing Hybrid Filters for the Compensation of Thermal Deformation in Machine tools," International Journal of Machine Tools and Manufacture, Vol. 47, No. 2, pp. 376-387.

Kim, J., Jeong, H. and Cho, D., 2004, "Thermal Behavior of a Machine Tool Equipped with Linear Motors," International Journal of Machine Tools and Manufacture, Vol 44, No. 7-8, pp. 749-758.

Kim, K. and Chung, S., 2004, "Synthesis of the 3D Artefact for Quick Identification of Thermal Errors in Machine Tools," International Journal of Production Research, Vol. 42, No. 6, pp. 1167-1187.

Kim, K. and Kim, M., 1991, "Volumetric Accuracy Analysis Based on Generalized Geometric Error Model in Multi-Axis Machine Tools," Mechanism and Machine Theory, Vol. 26, No. 2, pp. 207-219.

Kim, S. and Cho, D., 1997, "Real-Time Estimation of Temperature Distribution in a Ball-Screw System," International Journal of Machine Tools and Manufacture, Vol. 37, No. 4, pp. 451-464.

Kammer, D., 1991, "Sensor Placement for On-Orbit Modal Identification and Correlation of Large Space Structures," Journal of Guidance, Control, and Dynamics, Vol. 14, No. 2, pp. 251-259.

Kiridena, V. and Ferreira, P., 1993, "Mapping the Effects of Positioning Errors on the Volumetric Accuracy of Five-Axis CNC Machine Tools," International Journal of Machine Tools and Manufacture, Vol. 33, No. 3, pp. 417-437.

Knapp, W., 1983, “Circular Test for Three-Coordinate Measuring Machines and Machine Tools,” Precision Engineering, Vol. 5, No. 3, pp. 115-124.

Kodera, T., Yokoyama, K., Miyaguchi, K., Nagai, Y., Suzuki, T., Masuda, M. and Yazawa, T., 2004, “Real-Time Estimation of Ball-Screw Thermal Elongation Based upon Temperature Distribution of Ball-Screw,” JSME International Journal, Series C: Mechanical Systems, Machine Elements and Manufacturing, Vol. 47, No. 4, pp. 1175-1181.

Koren, Y., Heisel, U., Jovane, F., Moriwaki, T., Pritschow, G., Ulsoy, G. and Van Brussel, H., 1999, “Reconfigurable Manufacturing Systems,” CIRP Annals, Vol. 48, No. 2, pp. 527-540.

Krulewich, D., 1998, “Temperature Integration Model and Measurement Point Selection for Thermally Induced Machine Tool Errors,” Mechatronics, Vol. 8, No. 4, pp. 395-412.

Kruth, J., Vanherck, P. and De Jonge, L., 1994, “Self-Calibration Method and Software Error Correction for Three-Dimensional Coordinate Measuring Machines Using Artefact Measurements,” Measurement, Vol. 14, No. 2, pp. 157-167.

Kunzmann, H. and Waldele,.F., 1983, “On Testing Coordinate Measuring Machines (CMM),” CIRP Annals, Vol. 32, No. 1, pp. 465-468.

Kurita, T. and Hattori, M., 2005, “Development of New-Concept Desk Top Size Machine Tool,” International Journal of Machine Tools and Manufacture, Vol. 45, No. 7-8, pp. 959-965.

Kurtoglu, A., 1990, “The Accuracy Improvement of Machine Tools,” CIRP Annals, Vol. 39, No. 1, pp. 417-419.

Kussul, E., Baidyk, T., Ruiz-Huerta, L., Caballero-Ruiz, A. and Velasco, G., 2006, “Scaling Down of Microequipment Parameters,” Precision Engineering, Vol. 30, No. 2, pp. 211-222.

Kussul, E., Baidyk, T., Ruiz-Huerta, L., Caballero-Ruiz, A., Velasco, G. and Kasatkina, L, 2002, “Development of Micromachine Tool Prototypes for Microfactories,” Journal of Micromechanics and Microengineering, Vol. 12, No. 6, pp. 795-812.

Kussul, E., Rachkovskij, D., Baidyk, T. and Talayev, S., 1996, “Micromechanical Engineering: a Basis for the Low-Cost Manufacturing of Mechanical Microdevices Using Microequipment,” Journal of Micromechanics and Microengineering, Vol. 6, No. 4, pp. 410-425.

KwonY., Jeong, M. and Omitaomu, O., 2006, “Adaptive Support Vector Regression Analysis of Closed-Loop Inspection Accuracy,” International Journal of Machine Tools and Manufacture, Vol. 46, No. 6, pp. 603-610.

Lee, J. and Yang, S., 2002, "Statistical Optimization and Assessment of a Thermal Error Model for CNC Machine Tools," International Journal of Machine Tools and Manufacture, Vol. 42, No. 1, pp. 147-155.

Lee, S., 2004, Development and Characterization of Meso-Scale Machine Tool Systems, Ph.D. Dissertation, the University of Michigan.

Lee, S., Mayor, R. and Ni, J., 2005, "Development of a Six-Degree-of-Freedom Geometric Error Measurement System for a Meso-Scale Machine Tool," Journal of Manufacturing Science and Engineering, Vol. 127, No. 4, pp. 857-865.

Leete, D., 1961, "Automatic Compensation of Alignment Errors in Machine Tools," International Journal of Machine Tool Design and Research, Vol. 1, No. 4, pp. 293-324.

Lei, W. and Hsu, Y., 2002a, "Accuracy Test of Five-Axis CNC Machine Tool with 3D Probe-Ball. Part I: design and modeling," International Journal of Machine Tools and Manufacture, Vol. 42, No. 10, pp. 1153-1162.

Lei, W. and Hsu, Y., 2002b, "Accuracy Test of Five-Axis CNC Machine Tool with 3D Probe-Ball. Part II: errors estimation," International Journal of Machine Tools and Manufacture, Vol. 42, No. 10, pp. 1163-1170.

Lei, W. and Hsu, Y., 2003, "Accuracy Enhancement of Five-Axis CNC Machines through Real-Time Error Compensation," International Journal of Machine Tools and Manufacture, Vol. 43, No. 9, pp. 871-877.

Li, S., Zhang, Y. and Zhang, G., 1997, "A Study of Pre-Compensation for Thermal Errors of NC Machine Tools," International Journal of Machine Tools and Manufacture, Vol. 37, No. 12, pp. 1715-1719.

Liang, S., 2006, "Mechanical Machining and Metrology at Micro/Nano Scale," Proceedings of SPIE – the International Society for Optical Engineering, Vol. 6280 I, pp. 628002.

Lim, E. and Meng, C.,1997, "Error Compensation for Sculptured Surface Productions by the Application of Control-Surface using Predicted Machining Errors," Journal of Manufacturing Science and Engineering, Vol. 119, No. 3, pp. 402-9.

Lim, H., Son, S., Wong, Y. and Rahman, M., 2007, "Development and Evaluation of an On-Machine Optical Measurement Device," International Journal of Machine Tools and Manufacture, Vol. 47, No. 10, pp. 1556-1562.

Lin, P. and Ehmann, K., 1993, "Direct Volumetric Error Evaluation for Multi-Axis Machines," International Journal of Machine Tools and Manufacture, Vol. 33, No. 5, pp. 675-693.

Lingard, P., Purss, M., Sona, C., Thwaite, E. and Mariasson, G., 1991, "Temperature Perturbation Effects in a High Precision CMM," Precision Engineering, Vol. 13, No. 1, pp. 41-51.

Lo, C., 1994, Real-Time Error Compensation on Machine Tools through Optimal Thermal Error Modeling, Ph.D. Dissertation, the University of Michigan.

Lo, C., Yuan, J. and Ni, J., 1995, "An Application of Real-Time Error Compensation on a Turning Center," International Journal of Machine Tools and Manufacture, Vol. 35, No. 12, pp. 1669-1682.

Lo, C., Yuan, J. and Ni, J., 1999, "Optimal Temperature Variable Selection by Grouping Approach for Thermal Error Modeling and Compensation," International Journal of Machine Tools and Manufacture, Vol. 39, No. 9, pp. 1383-1396.

Lu, Z. and Yoneyama, T., 1999, "Micro Cutting in the Micro Lathe Turning System," International Journal of Machine Tools and Manufacture, Vol. 39, No. 7, pp. 1171-1183.

Ma, Y., 2001, Sensor Placement Optimization for Thermal Error Compensation on Machine Tools, Ph.D. Dissertation, the University of Michigan.

Ma, Y., Yuan, J. and Ni, J., 1999, "A Strategy for the Sensor Placement Optimization for Machine Thermal Error Compensation," American Society of Mechanical Engineers, Manufacturing Engineering Division, Vol. 10, pp. 629-637.

Matsuo, M., Yasui, T., Inamura, T. and Matsumura, M., 1986, "High-Speed Test of Thermal Effects for a Machine-Tool Structure Based on Modal Analysis," Precision Engineering, Vol. 8, No. 2, pp. 72-78.

Mico, V., Molina-Jimenez, M., Caballero-Aroca, J., Simon-Martin, S., Perez-Picazo, E.,Jimenez, A., Calderon, L., Calvache, M., Seco, F. and Bueno, R., 2005, "3D Interferometric Measurement System for Machine Tool On-Line Control," Proceedings of SPIE – the International Society for Optical Engineering, Vol. 5948 II, pp. 1-8.

Moriwaki, T., 1988, "Thermal Deformation and its Online Compensation of Hydrostatically Supported Precision Spindle," CIRP Annals, Vol. 37, No. 1, pp. 283-286.

Moriwaki, T. and Shamoto, E., 1998, "Analysis of Thermal Deformation of an Ultra Precision Air Spindle System," CIRP Annals, Vol. 47, No. 1, pp. 283-286.

Mou, J., 1997, "A Method of Using Neural Networks and Inverse Kinematics for Machine Tools Error Estimation and Correction," Journal of Manufacturing Science and Engineering, Vol. 119, No. 2, pp. 247-254.

Mou, J., Donmez, M. and Cetinkunt, S., 1995a, "An Adaptive Error Correction Method Using Feature-Based Analysis Techniques for Machine Performance Improvement. Part I: Theory Derivation," Journal of Engineering for Industry, Vol. 117, No. 4, pp. 584-590.

Mou, J., Donmez, M. and Cetinkunt, S., 1995b, "An Adaptive Error Correction Method Using Feature-Based Analysis Techniques for Machine Performance Improvement. Part II: Experimental Verification," Journal of Engineering for Industry, Vol. 117, No. 4, pp. 591-600.

Ni, J., Huang, P. and Wu, S., 1991, "Multi-Degree-Of-Freedom Measuring System for CMM Geometric Errors," American Society of Mechanical Engineers, Production Engineering Division, Vol. 55, pp. 255-269.

Ni, J. and Wu, S., 1993, "An On-Line Measurement Technique for Machine Volumetric Error Compensation," Journal of Engineering for Industry, Vol. 115, No. 1, pp. 85-92.

Ni, J., 1997, "CNC Machine Accuracy Enhancement through Real-Time Error Compensation", Journal of Manufacturing Science and Engineering, Vol. 119, No. 4B, pp. 717-725.

Pahk, H., Kim, J. and Lee, K., 1996, "Integrated Real Time Compensation System for Errors Introduced by Measurement Probe and Machine Geometry in Commercial CMMs," International Journal of Machine Tools and Manufacture, Vol. 36, No. 9, pp. 1045-1058.

Papadimitriou, C., Beck, J. and Au, S., 2000, "Entropy-Based Optimal Sensor Location for Structural Model Updating," Journal of Vibration and Control, Vol. 6, No. 5, pp. 781-800.

Pasek, Z., 2000, "Statistical Approach to PKM Accuracy Analysis," Proceeding of PKM 2000 International Conference, pp. 42-49.

Patel, A. and Ehmann, K., 1997, "Volumetric Error of a Stewart Platform-Based Machine Tool," CIRP Annals, Vol. 46, No. 1, pp. 287-290.

Paul, R., 1981, Robot Manipulators: Mathematics, Programming, and Control, the MIT Press.

Raksir, C. and Parnichkun, M., 2004, "Geometric and Force Errors Compensation in a 3-Axis CNC Milling Machine," International Journal of Machine Tools and Manufacture, Vol. 44, No. 12-13, pp. 1283-1291.

Ramesh, R., Mannan, M. and Poo, A., 2000a, "Error Compensation in Machine Tools – a Review. Part I: Geometric, Cutting-Force Induced and Fixture-Dependent Errors," International Journal of Machine Tools and Manufacture, Vol. 40, No. 9, pp. 1235-1256.

Ramesh, R., Mannan, M. and Poo, A., 2000b, "Error Compensation in Machine Tools – a Review. Part II: Thermal Errors," International Journal of Machine Tools and Manufacture, Vol. 40, No. 9, pp. 1257-1284.

Ramesh, R., Mannan, M. and Poo, A., 2003a, "Thermal Error Measurement and Modelling in Machine Tools. Part I: Influence of Varying Operating Conditions," International Journal of Machine Tools and Manufacture, Vol. 43, No. 4, pp. 391-404.

Ramesh, R., Mannan, M., Poo, A. and Keerthi, S., 2003b, "Thermal Error Measurement and Modelling in Machine Tools. Part II: Hybrid Bayesian Network-Support Vector Machine Model," International Journal of Machine Tools and Manufacture, Vol. 43, No. 4, pp. 405-419.

Ropponen, T. and Arai, T., 1995, "Accuracy Analysis of Modified Steward Platform Manipulator," Proceedings of the IEEE International Conference on Robotics Automation, pp. 521-525.

Sakamoto, S. and Inasaki, I., 1993, "Analysis of Generating Motion for Five-Axis Machining Centers," Transactions of the North American Manufacturing Research Institute of SME, Vol. 21, pp. 287-293.

Salama, M., Rose, T. and Garba, J., 1987, "Optimal Placement of Excitations and Sensors for Verification of Large Dynamical Systems," Proceedings of the 28th Structures, Structural Dynamics, and Materials Conference, pp. 1024-1031.

Sartori, S. and Zhang, G., 1995, "Geometric Error Measurement and Compensation of Machines," CIRP Annals, Vol. 44, No.2, pp. 599-609.

Sata, T., Takeuchi, Y. and Okubo, N., 1975, "Control of the Thermal Deformation of a Machine tool," Proceedings of the 16th MTDR Conference, Vol. 16, pp. 203-208.

Schellekens, P., Rosielle, N., Vermeulen, H., Vermeulen, M., Wetzels, S. and Pril, W., 1998, "Design for Precision: Current Status and Trends," CIRP Annals, Vol. 47, No.2, pp. 557-586.

Schultschik, R., 1977, "The Components of Volumetric Accuracy," CIRP Annals, Vol. 26, No.1, pp. 223-228.

Shah, P. and Udwadia, F., 1978, "A Methodology for Optimal Sensor Location for Identification of Dynamic System," Journal of Applied Mechanics, Vol. 45, No. 1, pp. 188-196.

Shen, Y. and Duffie, N., 1993, "Comparison of Combinatorial Rules for Machine Error Budgets," CIRP Annals, Vol. 42, No.1, pp. 619-622.

Slocum, A., 1992, Precision Machine Design, Prentice Hall.

Slocum, A., 1992, “Precision Machine Design: Macromachine design philosophy and its applicability to the design of Micromachines,” Proceedings of the IEEE Micro Electro Mechanical Systems, pp. 37-42.

Soons, J., Theuws, F. and Schellekens, P., 1992, “Modeling the Errors of Multi-Axis Machines: a General Methodology,” Precision Engineering, Vol. 14, No. 1, pp. 5-19.

Spotts, M., 1978, “Dimensioning Stacked Assemblies,” Machine Design, Vol. 50, No. 9, pp. 60-63.

Spur, G., Hoffmann, E., Paluncic, Z., Benzinger, K. and Nymoen, H., 1988, “Thermal Behavior Optimization of Machine Tools,” CIRP Annals, Vol. 37, No.1, pp. 401-405.

Srivastava, A., Veldhuis, S. and Elbestawit, M., 1995, “Modelling Geometric and Thermal Errors in a Five-Axis CNC Machine Tool,” International Journal of Machine Tools and Manufacture, Vol. 35, No.9, pp. 1321-1337.

Srinivasa, N. and Ziegert, J., 1996, “Automated Measurement and Compensation of Thermally Induced Error Maps in Machine Tools,” Precision Engineering, Vol. 19, No. 2-3, pp. 112-132.

Srinivasa N. and Ziegert, J., 1997, “Prediction of Thermally Induced Time-Variant Machine Tool Error Maps Using a Fuzzy ARTMAP Neural Network,” Journal of Manufacturing Science and Engineering, Vol. 119, No. 4(A), pp. 623-630.

Steinmetz, C., 1990, “Sub-Micro Position Measurement and Control on Precision Machine Tools with Laser Interferometry,” Precision Engineering, Vol. 12, No. 1, pp. 12-24.

Suh, J. and Lee, D., 2004, “Thermal Characteristics of Composite Sandwich Structures for Machine Tool Moving Body Applications,” Composite Structures, Vol. 66, No. 1-4, pp. 429-438.

Suh, S. and Lee, E., 2000, “Contouring Performance Measurement and Evaluation of NC Machine Controller for Virtual Machining CAM System,” International Journal of Advanced Manufacturing Technology, Vol. 16, No. 4, pp. 271-276.

Svoboda, 2006, “Testing the Diagonal Measuring Technique,” Precision Engineering, Vol. 30, No. 2, pp. 132-44.

Oiwa, T., 2005, “Error Compensation System for Joints, Links and Machine Frame of Parallel Kinematics Machines,” International Journal of Robotics Research, Vol. 24, No. 12, pp. 1087-1102.

Tajbakhsh, H., Abadin, Z. and Ferreira, P., 1997, "L_∞ Parameter Estimates for Volumetric Error in Models of Machine Tools," Precision Engineering, Vol. 20, No. 3, pp. 179-187.

Takeuchi, Y. and Watanabe, T., 1992, "Generation of 5-Axis Control Collision-Free Tool Path and Postprocessing for NC Data," CIRP Annals, Vol. 41, No. 1, pp. 539-542.

Thompson, D., 1989, "The Design of an Ultra-Precision CNC Measuring Machine," CIRP Annals, Vol. 38, No. 1, pp. 501-504.

Treib, T., 1987, "Error Budgeting – Applied to the Calculation and Optimization of the Volumetric Error Field of Multiaxis Systems," CIRP Annals, Vol. 36, No. 1, pp. 365-368.

Tsutsumi, M. and Saito, A., 2003, "Identification and Compensation of Systematic Deviations Particular to 5-Axis Machining Centers," International Journal of Machine Tools and Manufacture, Vol. 43, No. 8, pp. 771-780.

Tsutsumi, M. and Saito, A., 2004, "Identification of Angular and Positional Deviations Inherent to 5-Axis Machining Centers with a Tilting-Rotary Table by Simultaneous Four-Axis Control Movements," International Journal of Machine Tools and Manufacture, Vol. 44, No. 12-13, pp. 1333-1342.

Tutunea-Fatan, O. and Feng, H., 2004, "Configuration Analysis of Five-Axis Machine Tools Using a Generic Kinematic Model," International Journal of Machine Tools and Manufacture, Vol. 44, No. 11, pp. 1235-1243.

Umetsu, K., Furutnani, R., Osawa, S., Takatsuji, T. and Kurosawa, T., 2005, "Geometric Calibration of a Coordinate Measuring Machine Using a Laser Tracking System," Measurement Science and Technology, Vol. 16, No. 12, pp. 2466-2472.

Vanderplaats, G., 1984, "Numerical Optimization Techniques for Engineering Design: with Applications," Mcgraw-Hill College.

Veldhuis, S. and Elbestawi, M., 1995, "A Strategy for the Compensation of Errors in Five-Axis Machining," CIRP Annals, Vol. 44, No. 1, 1995, pp. 373-377.

Vogler, M. Liu, X., Kapoor, S., DeVor, R. and Ehmann, K., 2002, "Development of Meso-Scale Machine Tool (mMT) Systems," Transactions of the North American Manufacturing Research Institute of SME, pp. 1-9.

Wang, C., 2000, "Laser Vector Measurement Technique for the Determination and Compensation of Volumetric Positioning Errors. Part I: Basic Theory," Review of Scientific Instruments, Vol. 71, No. 10, pp. 3933-3937.

Wang, J. and Masory, O., 1993, "On the Accuracy of a Steward Platform – Part I. The Effect of Manufacturing Tolerance," Proceedings of the IEEE International Conference on Robotics Automation, pp. 114-120.

Wang, K., Tseng, P. and Lin, K., 2006, "Thermal Error Modeling of a Machining Center Using Grey System Theory and Adaptive Network-Based Fuzzy Inference System," JSME International Journal, Series C: Mechanical Systems, Machine Elements and Manufacturing, Vol. 49, No. 4, pp. 1179-1187.

Wang, S. and Ehmann, K., 1999a, "Measurement Methods for the Position Errors of a Multi-Axis Machine. Part 1: Principles and Sensitivity Analysis," International Journal of Machine Tools & Manufacture, Vol. 39, No. 6, pp. 951-964.

Wang, S. and Ehmann, K., 1999b, "Measurement Methods for the Position Errors of a Multi-Axis Machine. Part 2: Applications and Experimental Results," International Journal of Machine Tools and Manufacture, Vol. 39, No. 9, pp. 1485-1505.

Wang, S., Liu, Y. and Kang, Y., 2002, "An Efficient Error Compensation System for CNC Multi-Axis Machines," International Journal of Machine Tools and Manufacture, Vol. 42, No. 11, pp. 1235-1245.

Wang, Y., Zhang, G., Moon, K. and Sutherland, J., 1998, "Compensation for the Thermal Error of Multi-Axis Machining Center," Journal of Materials Processing Technology, Vol. 75, No. 1-3, pp. 45-53.

Weck, M. and Bibring, H., 1984, Handbook of Machine Tools. Volume 4: Metrological Analysis and Performance Tests, Wiley.

Weck, M., Mckeown, P., Bonse, R. and Herbst, U., 1995, "Reduction and Compensation of Thermal Errors in Machine Tools," CIRP Annals, Vol. 44, No. 2, pp. 589-598.

Wu, C. and Kung, Y., 2003, "Thermal Analysis for the Feed Drive System of a CNC Machine Center," Journal of Machine Tools and Manufacture, Vol. 43, No. 15, pp. 1521-1528.

Wu, Z., Eimaraghy, W. and Eimaraghy, H., 1988, "Evaluation of Cost-Tolerance Algorithms for Design Tolerance Analysis and Synthesis," Manufacturing Review, Vol. 1, No. 3, pp. 168-179.

Xi, F. and Mechefske, C., 2000, "Modeling and Analysis of Errors in Hexapods with Fixed-Leg Lengths," Proceeding of PKM 2000 International Conference, pp. 236-244.

Xu, M., Jiang, S. and Cai, Y., 2007, "An Improved Thermal Model for Machine Tool Design," International Journal of Machine Tools and Manufacture, Vol. 47, No. 1, pp. l53-162.

Yandayan, T. and Burdekin, M., 1997, "In-Process Dimensional Measurement and Control of Workpiece Accuracy," International Journal of Machine Tools and Manufacture, Vol. 37, No. 10, pp. 1423-1439.

Yang, H., 2002, Dynamic Modeling for Machine Tool Thermal Error Compensation, Ph.D. Dissertation, the University of Michigan.

Yang, H. and Ni, J., 2003, "Dynamic Modeling for Machine Tool Thermal Error Compensation," Journal of Manufacturing Science and Engineering, Vol. 125, No. 2, pp. 245-254.

Yang, H. and Ni, J., 2005a, "Adaptive Model Estimation of Machine-Tool Thermal Errors Based on Recursive Dynamic Modeling Strategy," International Journal of Machine Tools and Manufacture, Vol. 45, No. 1, pp. 1-11.

Yang, H. and Ni, J., 2005b, "Dynamic Neural Network Modeling for Nonlinear, Nonstationary Machine Tool Thermally Induced Error," International Journal of Machine Tools and Manufacture, Vol. 45, No. 4-5, pp. 455-465.

Yang, J., Yuan, J. and Ni, J., 1999, "Thermal Error Mode Analysis and Robust Modeling for Error Compensation on a CNC Turning Center," International Journal of Machine Tools and Manufacture, Vol. 39, No. 9, pp. 1367-1381.

Yang, S., Yuan, J. and Ni, J., 1996, "The Improvement of Thermal Error Modeling and Compensation on Machine Tools by Neural Network," International Journal of Machine Tools and Manufacture, Vol. 36, No. 4, pp. 527-537.

Yoshioka, H., Matsumura, S., Hashizume, H. and Shinno, H., 2006, "Minimizing Thermal Deformation of Aerostatic Spindle System by Temperature Control of Supply Air," JSME International Journal, Series C: Mechanical Systems, Machine Elements and Manufacturing, Vol. 49, No. 2, pp. 606-611.

Yuan, J. and Ni, J., 1998, "The Real-Time Error Compensation Technique for CNC Machining Systems," Mechatronics, Vol. 8, No. 4, pp. 359-380.

Yun, W., Kim, S. and Cho, D., 1999, "Thermal Error Analysis for a CNC Lathe Feed Drive System," International Journal of Machine Tools and Manufacture, Vol. 39, No. 7, pp. 1087-1101.

Zhang, G. and Porchet, M., 1993, "Some New Developments in Tolerance Design in CAD," American Society of Mechanical Engineers, Design Engineering Division, Vol. 65, Pt. 2, pp. 175-185.

Zhang, G. and Fu, J., 2000, "A Method for Optical CMM Calibration Using a Grid Plate," CIRP Annals, Vol. 49, No. 1, pp. 399-402.

Zhang, G., Ouyang, R., Lu, B. and Hocken, R., 1988, "A Displacement Method for Machine Geometry Calibration," CIRP Annals, Vol. 37, No. 1, pp. 515-518.

Zhang, G., Veale, R., Charlton, T., Borchardt, B. and Hocken, R., 1985, "Error Compensation of Coordinate Measuring Machines," CIRP Annals, Vol. 34, No. 1, pp. 445-448.

Zhang, G. and Zang, Y., 1991, "A Method for Machine Geometry Calibration Using 1-D Array Ball," CIRP Annals, Vol. 40, No. 1, pp. 519-522.

Zhao, H., Yang, J. and Shen, J., 2007, "Simulation of Thermal Behavior of a CNC Machine Tool Spindle," International Journal of Machine Tools and Manufacture, Vol. 47, No. 6, pp. 1003-1010.

Zhu, J. and Ting, K., 2001, "Performance Distribution Analysis and Robust Design," Journal of Mechanical Design, Vol. 123, No. 1, pp. 11-17.

Ziegert. J. and Kalle, P., 1994, "Error Compensation in Machine Tools: a Neural Network Approach," Journal of Intelligent Manufacturing, Vol. 5, No. 3, pp. 143-51.

Ziegert, J. and Mize, C. 1994, "Laser Ball Bar: a New Instrument for Machine Tool Metrology," Precision Engineering, Vol. 16, No. 4, pp. 259-267.